Studies on Intermolecular Interactions, Crystallization Behavior and Highly Ordered/Intermediate Structures of Poly(3-hydroxybutyrate) in the Blends and Ultrathin Films by Infrared Spectroscopy and Grazing Incidence X-ray Diffraction

Studies on Intermolecular Interactions, Crystallization Behavior and Highly Ordered/Intermediate Structures of Poly(3-hydroxybutyrate) in the Blends and Ultrathin Films by Infrared Spectroscopy and Grazing Incidence X-ray Diffraction

March 2017

A Dissertation

by

Khasanah

Department of Chemistry

Graduate School of Science and Technology

Kwansei Gakuin University

Contents

List of Symbols and Abbreviations

φ	weight fraction
$(020)_H$	the (020) reflection at lower 2θ
$(020)_L$	the (020) reflection at lower 2θ
2D-GIXD	two-dimensional grazing incidence X-ray Diffraction
CAB	cellulose acetate butyrate
DSC	differential scanning calorimeter
FWHM	full-width at half maximum
GIXD	grazing incidence X-ray Diffraction
HBs	hydrogen bonds
HFIP	1,1,1,3,3,3-hexafluoro-2-propanol
I_{PHB}	integrated intensity of (020) peak of neat PHB
IR	infrared spectroscopy
IRRAS	infrared-reflection absorption spectroscopy
I_i	integrated intensity of (020) peak in the blends
M_w	molecular weight
PFA	perfluoroalkoxy
PHB	poly(3-hydroxybutyrate)
PLLA	poly(L-lactic acid)

PVPh	poly(4-vinyl phenol)
T_c	crystallization temperature
T_g	glass transition temperature
T_m	melting temperature
WAXD	wide-angle X-ray diffraction
X_c	degree of crystallinity
***free* C=O**	free C=O group of PHB (without HBs)
***inter* C=O**	intermolecularly HB(s) C=O group of PHB with chitin
***inter* C=O chitin**	intermolecularly C＝O···HN HBs within chitin
***intra* C=O**	intramolecularly HB(s) C=O group within PHB
***intra* C=O chitin**	intramolecularly C＝O···HO HBs within chitin
wt %	weight percentage
ΔH_m	measured enthalphy
$\Delta H°_{PHB}$	enthalphy of the neat 100% PHB
θ_c	critical angle for total reflection

GENERAL INTRODUCTION

1. Scope of This Thesis

This thesis is mainly concerned with the study of intermolecular hydrogen bonding interactions, crystallization behavior and crystal structures of poly(3-hydroxybutyrate) [PHB] and blends. These three aspects are closely interrelated in determining the final physical and mechanical properties of a polymer. Thus, they have been gaining much attention for a long time as very important research themes in polymer science. Moreover, controlling the crystallinity of such semicrystalline PHB is also crucial in order to fit the best condition for practical applications. One of the most simple and economic approaches to modify the properties of a polymer is blending. In this thesis, PHB was blended with two biodegradable polymers, chitin and poly(L-lactic acid) PLLA, to control the crystallinity of PHB. Several measurements were used in this thesis are differential scanning calorimetry (DSC), infrared spectroscopy (IR), and wide-angle X-ray diffraction (WAXD). Two surface sensitive techniques were specially employed to investigate the crystallization and crystal structure of PHB ultrathin films, i.e. infrared-reflection absorption spectroscopy (IRRAS) and grazing incidence X-ray diffraction (GIXD).

The novelty and originality of this thesis can be described as follows:

1. The existence of intermolecular hydrogen bondings between PHB and chitin in their

blends was revealed through the intensive analysis of various ratios of blends with the temperature dependence of IR spectroscopy combined with the results obtained from DSC and WAXD measurements. We systematically analyzed the IR spectra of PHB including the intensity change, full width at half maximum (FWHM), and wavenumber shift of C＝O bands with composition and temperature dependences. Similarly, the change of amide I and II bands of chitin is also discussed as well. The effect of intermolecular hydrogen bonding formation on crystallization and crystal structure of PHB also carefully discussed by monitoring the change of DSC and WAXD profiles of PHB.

2. Through the measurement and analysis of temperature-dependent IRRAS and GIXD, we proposed two different ordered of crystalline structures in PHB ultrathin films: less ordered and highly ordered structure. The existence of less ordered structure was obviously recognized in the intermediate state which generally difficult to find in bulk PHB. The transformation from intermediate state to highly ordered state was meticulously examined from the integrated intensity change of their corresponding IR bands as a function of temperature. Moreover, the nucleation site, growth and preferred orientation of crystallites PHB were elucidated from temperature-dependent of 2D-GIXD profiles.
3. The effect of a small addition of PLLA on the crystallization of PHB ultrathin films is

interpreted through investigating of various molecular weight of PLLA and two different film thicknesses using surface sensitive IRRAS and GIXD measurements. The results exposed that the inhibition of crystallization of PHB by PLLA strongly depends on the molecular weight of PLLA and thickness confinement. The crystallization behavior of PHB in the PHB/PLLA ultrathin films behaves relatively inverse from the PHB/PLLA bulk. The present of a very confined environment by reducing the film thickness seems to enhance the miscibility of PHB and PLLA in the blends. Apart from the molecular weight of PLLA and thickness confinement dependences, phase separation due to the presence of free surface effect, entanglement of PHB and aggregation of small molecules of PLLA are also found to be important factors that influence the ability of a small amount of PLLAs in inhibiting the crystallization of PHB.

2. Introduction of PHB, Chitin and PLLA

2.1 PHB

In recent years, biodegradable polymers have been gaining considerable attention along with increasing global concern over the harmful effects of plastic derived from petroleum in the environment. Biodegradable polymers can degraded naturally in the environment into water and carbon dioxide, thus, they are ideal alternative for replacing petrochemical based-plastics. One of the most studied biodegradable polymer is

poly(3-hydroxybutyrate) [PHB] that belong to polyhydroxyalkanoates (PHAs) class polyester. PHAs is produced from various bacteria in the storage granules as carbon and energy.[1-5] On the other hand, PHAs is very potential to use in the wide-range applications because of their advantageous characteristics, such as biodegradable, biocompatible, insoluble in water and impermeable to oxygen, nontoxic, piezoelectric, thermoplastic and/or elastomeric.[6-8]

PHB was firstly isolated and characterized from *Bacillus megaterium* bacteria by Maurice Lemoigne in 1925[9], however, its commercial production scale had wait until the early of 1960s.[1] The chemical structure of PHB is shown in Figure 1a. PHB is a semicrystalline polymer where the crystalline molecules are arranged in an orthorhombic structure. Yokouchi et al.[10] and Marchessault et al.[11] reported that the orthorhombic has two-left handed helices along the antiparallel orientation in accordance with the $P2_12_12_1$-D^4_2 space group. The crystal lattice parameters are determined with a = 5.76 Å, b = 13.20 Å and c = 5.96 Å (fiber axis).[10-12] Figure 2 is depicted the crystal structure of PHB reproduced from Ref. 10.

In the PHB crystalline, there was found weak hydrogen bonds between methyl and carbonyl groups ($CH_3\cdots O{=}C$). The formation of $CH_3\cdots O{=}C$ hydrogen bond was firstly proposed by Sato et al.[13] on the basis of IR spectra study of an antisymmetric C−H stretching band at anomalously high frequency position. This finding was further

reinforced by WAXD study and chemical quantum analysis.[14-16] Recently, Tashiro et al.[17] reinvestigated the existence of this hydrogen bonding in the PHB α-form crystal through the advance X-ray approach. It was reported that the abnormally short distance of methyl group to the oxygen atom of C=O group lead the formation of $CH_3\cdots O{=}C$ hydrogen bond. The shortest H···O distance exhibits in the C–H···O=C hydrogen bonds is found to be 2.62 Å which shorter than the expected value of normal van der Waals distance (see Figure 3). Moreover, the direction of these C–H···O=C hydrogen bonds is proposed to be almost parallel to the direction of the chain folding along the *a*-axis. Therefore, the presence of these hydrogen bonds may responsible for stabilizing the chain folding in the lamellae structure of PHB. Figure 4 displays the model of lamella structure with intermolecular hydrogen bond interactions of PHB crystal proposed by Sato et al.

PHB has physical and mechanical properties similar to those of commercial plastics of isotactic polypropylene (*i*PP),[18,19] as tabulated in Table 1. However, PHB is rigid, brittle and thermally unstable due to highly crystallinity and narrow processability temperature that caused difficulty in the conventional processing.[20-22] In order to modify those unfavorable properties and improve the physical and mechanical properties, copolymerization and blending approaches often used to obtain the desired properties of PHB. The unit and composition of comonomer greatly affect the physical and biodegradability properties of PHB-copolymers.[23-25] Several PHB copolymers that have

been developed are poly(hydroxybutyrate-*co*-hydroxyvalerate) [P(HB-*co*-HV)],[26-31] poly(hydroxybutyrate-*co*-hydroxyhexanoate) [P(HB-*co*-HHx)][32-36] and poly(hydroxybutyrate-*co*-hydroxypropionate) [P(HB-*co*-HP)].[37-39]

On the other hand, blending technique is more convenient and low cost for creating new materials by combining two or more polymers. The important characteristic in polymer blends is miscibility. According to thermodinamical behavior and compatibility between two polymers, miscible blend refers to a single phase system (homogeneous phase) which is equivalent with polymer-polymer solution (mix on a molecular level), whereas, immiscible blend refers to separate phase (inhomogenous system) that do not mix on a molecular level.[40] PHB was reported to be miscible by blending with poly(vinyl acetate) (PVAc),[41-43] poly(vinyl alcohol) (PVA),[44-47] poly(ethylene oxide) (PEO),[48-51] cellulose acetate butyrate (CAB),[52-55] poly(epichlorohydrin) (PECH),[56-59] and poly(ethylene glycol) (PEG).[60] PHB formed immiscible systems by blending with polylactic acid (PLA),[61-65] poly(methylene oxide) (PMO),[66] poly(butylene succinate) (PBS)[67] and polycaprolactone (PCL).[68]

2.2 Chitin

Chitin is the second most abundant polysaccharide in the nature after cellulose that widely exists in the nature as arthropod exoskeletons (especially shrimps and crabs),

insects and the internal shells of cephalopods. It is also a biodegradable and biocompatible polymer with excellent absorbability and non-toxicity. The chemical structure of chitin is similar with cellulose, except a $NHCOCH_3$ group replaces the hydroxyl group, as displays in Figure 5a. Moreover, the infrared spectra of chitin and cellulose is also similar since their chains conformation are same.[69,70]

Chitin naturally exhibits three crystalline allomorphs as α-, β- and γ-chitin. The most abundant and stable one is α-chitin which packed in the orthorhombic space group $P2_12_12_1$ with a = 0.474, b = 1.032 and c = 1.886 nm.[71] The α-chitin has excessive intramolecular and intermolecular hydrogen bonds that causes difficulty to dissolve in many solvents, see figure 5b.[72] The α-chitin crystal consists of two antiparallel molecules per unit cell where its chains arranged in sheets tightly held by a number of intra-sheet hydrogen bonds along the a parameter of unit cell dominated by C=O···NH hydrogen bond. The inter-sheet hydrogen bonds exist along the b parameter of the unit cell.[73] Chitin has amide and hydroxyl groups which can be expected to form intermolecular hydrogen bonding with carbonyl or methyl groups of PHB. Therefore, chitin is beneficial to improve the properties of PHB. Chitin and its derivatives has been reported in a wide variety of biomedical applications, such as tissue engineering,[74] suture,[75] wound dressing,[76] drug delivery,[77] wastewater treatment,[78,79] cosmetics and pharmaceutical fields,[80] agriculture and food processing.[81]

2.3 PLA

Poly(lactic acid) [PLA] is a biodegradable aliphatic polyester that can be produce from renewable resources, such as starch (from corn and potatoes) and sugar (from sugar cane and beets).[82-84] It can be readily broken down through a simple hydrolysis reaction into water and carbon dioxide. PLA has excellent mechanical properties which is comparable or even superior than those of petroleum-based polymers, especially the biocompatibility, high strength, high elasticity modulus, thermoplastic, molding capability, and printability.[84-88] However, PLA is rigid, brittle, and thermally unstable because it deforms at temperatures in excess of its glass transition temperature.[88] Therefore, several modification methods are often applied to improve those drawbacks aim to suit the application purpose, including blending,[89-91] copolymerization[92,93] and using plasticizers.[94-96] In addition, the change of molecular weight, crystallinity, chain orientation, and stereochemistry of PLA will also greatly affects the physical and mechanical properties of PLA.[88,97,98]

Depending on the stereochemistry and thermal history, PLA can be either semicrystalline or amorphous. PLA has two optically active seteroisomers, L (+)-LA and D(−)-LA (see Figure 6), but it also can exist as a racemic mixture, DL. The arrangement of the stereochemical L- and D-lactic acid structures can control almost all the properties of PLA. It has been reported that these two pure PLA stereoisomers, poly(L-lactic acid)

[PLLA] and poly(D-lactic acid) [PDLA] are semicrystalline, whereas the racemic poly(DL-lactic acid) [PDLLA] is amorphous.[99,100] The highly crystalline PLA can be obtained by the addition of low D or L content (< 2 %), while the presence of relatively high D or L content (> 20%) yields the amorphous one.[101,102]

The semicrystalline PLLA has three polymorphism forms, α, β, and γ depending on the method of preparation. The α-form is the most common type which can be prepared by melt or cold crystallization. Its crystals are packed into an orthorhombic $P2_12_12_1$ space group with a = 10.66 Å, b = 6.16 Å and c = 28.88 Å containing two antiparallel chains in 10_3 helix conformation.[103] The β-form can be obtained at a high draw ratio and high drawing temperature. The β-form crystal is considered to have a frustrated structure packing of three 3_1 helices in a trigonal unit cell with $a = b$ = 10.52 Å and c = 8.8 Å, space group $P3_2$.[104] The third type, γ-form was produced by epitaxial crystallization on hexamethylbenzene substrate, containing two antiparallel helices which packed in an orthorhombic unit cell of parameters a = 9.95 Å, b = 6.25 Å= and c = 8.8 Å.[105]

In the practical application, PLA has been widely used for a long time in biomedical field due to its excellent bioresorbability and biocompatibility in the human body, such as suture and orthopaedic fixation.[106-111] Since the PLA production cost can be reduced and the technique to improve the properties of PLA is also developed tremendously, PLA has been considered as a promising alternative material to substitute petroleum-based material.

Currently, PLA has been commercially used in many applications, as packaging material,[112,113] fiber/textile,[114,115] coating,[116] drug delivery,[117] and foamed article.[118,119]

3. Polymer Thin and Ultrathin Films

Recently, polymer thin and ultrathin films have attracted increasing interest in both research and application points of view. The confinement effect from the surface and interface in polymer thin and ultrathin films greatly affected their physical properties, which is considerably differ compare to their bulk form. Therefore, investigation of polymer films under spatial confined environment will certainly provide a new insight in the field of polymer science. On the other hand, the preferred characteristic of current devices that is lighter, smaller, and thinner, also contributed to the increase of polymer thin and ultrathin films technology.

The term of thin films is commonly used to refer to the films having a thickness of up to 1000 nm, however, sometimes it also used to address the ultrathin films. In order to distinguish the use of these terms, Ma et al.[120] roughly classified the films thickness into three categories: The first category includes the films with thicker than several hundred nanometers (usually labeled as thin films). The second category includes the films with the thickness close to the polymer coil size but less than 100 nm (termed as ultrathin films). The third category designed for the films with thickness below the polymer coil size that

approaching a quasi-two-dimensional state (the so-called monolayer).[121] Those confined films with restricted geometries can be considered to be the quasi two-dimensional (2D) system with one-dimensional (1D) confinement normal to the substrate. Along 1D confinement on the substrate, the lamellae have preferential orientation that can be either edge-on lamellae with the chain axis parallel to the substrate or flat-on lamellae with the chain axis normal to the substrate. Figure 7 shows the illustration of edge-on and flat-on lamellae. The free surface is generally dominated by edge-on lamellae that form at low temperature,[122,123] whereas the flat-on lamellae predominantly form at the interface at high temperature.[124,125] In thin films, edge-on lamellae are usually observed as the free surface effect is predominant. Further decreasing the film thickness, both edge-on and flat-on lamellae can be found in ultrathin films. In monolayer films, a typical diffusion-limited crystal usually grow because the interface effect plays major role to control the growth of the crystal, so flat-on lamellae is more favorable.[120-122, 126-128] Actually, many factors can control the lamellae orientation in the thin films, however, the thickness of the films, crystallization temperature, and surface chemistry of the substrate are the most important factors.[121]

As mentioned above, except for the lamellae orientation, the confinement and surface/interface effects can affect almost all the physical properties of polymer thin and ultrathin films, such as crystallization behavior,[126,129] degree of crystallinity,[130,131]

mobility,[132,133] glass transition temperature (T_g),[134,135] morphology and phase behavior,[136-138] etc. The crystallinity and the kinetic of crystallization of semicrystalline polymers were found to decrease in thin and ultrathin films. It seems the main reason is that the polymer chains hardly to fold in thermodynamically stable nucleus or the lamellae thickness is close to the films thickness, associated with a possible slowdown of the diffusion of polymer chains in the melt of thin films.[139] For example, the crystallinity of poly(di-*n*-hexylsilane) is decreased when the film thickness is less than 50 nm, in fact, the crystallization is almost inhibited when the thickness below 15 nm as the critical dimensions of nuclei is difficult to develop with decreasing the film thickness.[130,131] The mobility of polymer chains in the thin and ultrathin films may be differ at its surface and interface. The mobility of polymer chains is usually increased near the free surface region, especially for the lower molecular weight polymers, but no obvious change is observed for higher molecular weight polymers.[140,141] In contrast, the mobility of polymer chains at interface become limited due to the existence of interactions between polymer and solid substrate. The difference mobility of polymer chains at surface and interface is also closely related with the shifting of the T_g in thin and ultrathin films.[142,143]

Recent measurements have been developed to study the behaviors of polymer thin and ultrathin films. Among them, IR still to be a powerful tool to extract the information about molecular conformation and intermolecular interaction in the polymer thin and ultrathin

films. IR has several measurement techniques that are adjusted to the kinds of samples. For investigation of polymer thin and ultrathin films, IRRAS is the most suitable technique to characterize solid sample with nanometer scale. IRRAS is a surface sensitive technique where the electric field vector of light undergoes a phase change with the magnitude of each depends on the polarization of incident light.[144] Upon the reflection on the metal substrate, the electric vector of the light polarized parallel to the plane of incidence (*p*-polarized light) gives the signals of up to 90 degrees, whereas, the electric field of the light polarized perpendicular to the plane of incidence (*s*-polarized light) shift of 180 degrees which is negligible at all angle of incidence/theta (θ). The IRRAS reflection on metal substrate is illustrated in Figure 8. In short, this mechanism is known as the surface selection rule of IRRAS: vibration modes having transition dipole perpendicular to the surface substrate will appear with enhanced intensity. Therefore, IRRAS is very useful to observe the conformation and orientation of molecules on the surface of polymer thin and ultrathin films.

In many experiments, IR technique is often combined with XRD technique to investigate the structural properties of materials. Similar with IRRAS, one of GIXD techniques with surface sensitive that suitable for investigation of polymer thin and ultrathin films is called GIXD. GIXD uses a very small angle of incidence that reflects the crystalline near the surface region. Using the GIXD technique, the crystalline structure

along normal and parallel to the substrate can be obtained by measuring both in-plane and out-of plane geometries. Moreover, the depth of X-ray penetration into the film can be control by varying the angle of incidence around the critical angle for total reflection (θ_c).[145,146] Therefore, the specific crystalline information along out-of plane and in-plane directions within different depth can be observed.

The study of PHB thin and ultrathin films has been conducted using the combination of IRRAS and GIXD techniques. It has been found that the (020) reflection along out-of plane direction is strongly observed using GIXD measurement. The appearance of out-of-plane (020) reflection indicated that the edge-on lamellae with *b*-axis normal to the substrate surface is the preferred lamellae orientation of PHB crystallites in thin and ultrathin films.[147,148] The formation of edge-on lamellae corresponds to the dominant of free surface effect with lower nucleation barrier. Furthermore, increasing the annealing temperature caused the buried interface effect increased, as a result, the lamellar orientation changed from *b*-axis normal to substrate surface to the *c*-axis normal to the substrate surface (flat-on lamellae).[147] Furthermore, the crystallization of PHB is inhibited when the film thickness decreased to tens of nanometer close to the polymer-substrate interface.[149] The weak intermolecular C−H···O＝C hydrogen bonds still observed at 3009 cm^{-1} in IRRAS spectra of PHB thin films along the *a*-axis.[150]

In chapter 2, we investigated the crystallization and crystal structure of PHB ultrathin

films (thickness ~52 nm) using the combination of IRRAS and GIXD. The important finding in this present study is the evident presence of intermediate state observed in the melt crystallization process and the crystals transformation from intermediate state into highly-ordered state with the assistance of thermal energy. Intermediate state is specially appeared at 1731 cm^{-1} in IR frequency. It is usually difficult to detect in bulk PHB because it only appears in the early stage and diminish after the crystallization is finished.[151-153] In chapter 3, the effect of a small amount of PLLA on the crystallization behavior of PHB ultrathin film is investigated using the various molecular weights of PLLA. In this study, we described the correlation between the film thickness and the molecular weights of PLLA from the crystallization of PHB point of view.

4. Outline of each chapter

This thesis consists of three chapters. The outline of each chapter will be described as follows.

Chapter 1 described the effect of intermolecular hydrogen-bonding interactions formed between PHB and chitin in the blends on the crystallization behavior and crystalline structure of PHB. The PHB/chitin blends were studied as a function of composition and temperature by DSC, WAXD, and IR. We observed the significant changes of the blends with PHB content ≤ 50 % wt from the composition dependent of

DSC curves, WAXD patterns and IR spectra. The temperature-dependent spectral variations in the C＝O stretching were further analyzed by calculating the intensity changes, full width at half maximum (FWHM) and wavenumber shift. It is found that a new band appeared at around 1710~1714 cm^{-1} which is known as the hydrogen bonded C ＝O band in many polymer blends. Therefore, the appearance of this band clearly reveals the formation of the intermolecular hydrogen bondings in the PHB/chitin blends. We proposed that the intermolecular interactions formed between C＝O groups of PHB and the O−H and N−H groups of chitin (C＝O···H−O and C＝O···H−N) in the amorphous phase. The formation of these intermolecular hydrogen bondings is crucially responsible for decreasing the crystallinity of PHB in the blends. However, we found that the crystalline structure of PHB is not much affected by the addition of chitin.

In Chapter 2, the crystallization behavior and crystalline structure of PHB were investigated as ultrathin films (thickness ~52 nm) using two surface sensitive techniques, IRRAS and GIXD through heating and melt-cooling processes. Two kinds of crystalline structures of PHB were observed at 1722 and 1731 cm^{-1} from the analysis of IRRAS spectra that correspond to the C=O stretching of highly-ordered and intermediate states, respectively. Increasing temperature caused the crystals in the intermediate state acquire sufficient thermal energy to overcome the energy barrier, as a result, the transformation from the intermediate state into the highly-ordered state occurred. The weak intermolecular

hydrogen bonds of PHB still exist in such ultrathin films along *a*-axis. Furthermore, the 2D-GIXD results show that the intermediate state was dominant in edge-on-lamellae configuration where the crystallographic *b*-axis is normal to the film surface. Meanwhile, the highly-ordered state was predominant in flat-on lamellae configuration where the *b*-axis is parallel to the film surface. Moreover, from a very shallow angle of incidence measurement which only penetrates ~8 nm deep from the surface reveals that the crystals in the surface region strongly tended to align in an edge-on lamellae configuration.

Chapter 3 reported the effect of a small amount of PLLA on the crystallization behavior of PHB ultrathin films studied by IRRAS and GIXD. In this study, the correlation between molecular weight of PLLA and the film thickness was investigated using PLLA having molecular weight ranging from 300,000~710 g mol^{-1} and two different film thicknesses, i.e. 30 and 13 nm. The PHB/PLLA ratio is fixed at 80/20 (w/w) for all blends. The crystallization of PHB has shown a strong dependency on the molecular weight of PLLA and film thickness. In the 30-nm-thick samples, the crystallization of PHB is significantly reduced in the blends with molecular weight PLLAs ranging from M_w 23,000 to 13,100 g mol^{-1}, however, the higher ($M_w \geq$ 50,000 g mol^{-1}) and lower ($M_w \leq$ 6,900 g mol^{-1}) molecular weight PLLAs do not significantly affect the crystallization. In contrast, in the 13-nm-thick films, the crystallization of PHB is remarkably inhibited in the blends having PLLAs $M_w \geq$ 6,900 g mol^{-1}. IRRAS showed that for the 30-nm-thick samples, a

small addition of PLLA ($M_w \geq 13{,}100$ g mol^{-1}) altered the crystalline structure of PHB only in the highly ordered state. However, such PLLAs greatly affect the PHB crystals in both intermediate and highly ordered states in the films with the thickness of 13 nm. Both GIXD and IRRAS results revealed some consistency that the lower molecular weights of PLLA ($M_w \leq 3{,}600$ g mol^{-1}) only slightly affect the crystallinity and crystalline structure of PHB. Furthermore, several factors such as the presence of free surface and interface effects, entanglement of PLLA chains and molecular size of PLLA must seriously be taken into account to comprehend the complex crystallization behavior of PHB in the PHB/PLLA ultrathin films, apart from the molecular weight and thickness dependences.

References

1. Hocking, P. J.; Marchessault, R. H. *In* Biopolymers from Renewable Resources; Kaplan, D. L. Ed.; Springer: Berlin, 1998; p 220.
2. Muller, H. M.; Seebach, D. *Angew. Chem*. **1993**, *32*, 477-502.
3. Anderson, A. J.; Dawes, E. A. *Microbiol. Rev.***1990**, *54*, 450-472.
4. Van der Walle, G. A. M.; de Koning, G. J. M.; Weusthuis, R. A.; Eggink G. *Adv. Biochem. Eng. Biotechnol.* **2001**, *71*, 263-291.
5. Byrom, D. *In* Plastic from Microbes: Microbial Synthesis of Polymers and Polymer Precursors, Hanser: Munich, 1994; p 5-33.
6. Valappil, S. P.; Misra, S. K.; Boccaccini, A. R.; Roy, I. *Expert Rev. Med. Devices* **2006**, *3*, 853-868.
7. Philip, S.; Keshavarz, T.; Roy, I. *J. Chem. Technol. Biotechnol*. **2007***, 82*, 233-247.
8. Chen, G. *Microbiol. Monogr*. **2010**, *14*, 17–37.
9. Lemoigne, M. *Ann. Inst. Pasteur* **1925**, *39*, 144-173.
10. Yokouchi, M.; Chatani, Y.; Todokoro, H.; Teranishi, K.; Tani, H. *Polymer* **1973**, *14*, 267-272.
11. Cornibert, I.; Marchessault, R. H. *J. Mol. Biol*. **1972**, *71*, 735-756.
12. Okamura, K.; Marchessault, R. H. *In* Conformation of Biopolymers; Ramachandran, G. M. Ed.; Academic Press: New York, vol 2, 1967; pp 709 -720.

13. Sato, H.; Murakami, R.; Padermshoke, A.; Hirose, F.; Senda, K.; Noda, I.; Ozaki, Y. *Macromolecules* **2004**, *37*, 7203–7213.

14. Sato, H.; Dybal, J.; Murakami, R.; Noda. I.; Ozaki, Y. *J. Mol. Struct*. **2005**, *744-747*, 35-46.

15. Sato, H.; Mori, K.; Murakami, R.; Ando, Y.; Takahashi, I.; Zhang, J.; Terauchi, H.; Hirose, F.; Senda, K.; Tashiro, K.; Noda, I.; Ozaki, Y. *Macromolecules* **2006**, *39*, 1525-1531.

16. Sato, H.; Sato, H.; Ando, Y.; Dybal, J.; Iwata, I.; Noda, I.; Ozaki, Y. *Macromolecules* **2008**, *41*, 4305-4312.

17. Wang, H.; Tashiro, K. *Macromolecules* **2016**, *49*, 581-594.

18. Zhao, Q.; Cheng, G. *In New Frontiers in Polymer Research*, R. K. Bregg, Ed.; Nova Science Publishers, Inc: New York, 2006; p 101.

19. Sudesh, K.; Abe, H.; Doi, Y. *Prog. Polym. Sci.* **2000**, *25*, 1503-1555.

20. de Koning, G.J.M.; Lemstra, P.J. *Polymer* **1993,** *34*, 4089-4094.

21. Barham, P.J. *J. Mater. Sci*. **1984**, *19*, 3826-3834.

22. El-hadi, A.; Schnabel, R.; Straube, E.; Mu, G.; Henning, S. *Polym. Test*. **2002**, *21*, 665-674.

23. Mitomo, H.; Morishita, N.; Doi, Y. *Macromolecules* **1993**, *26*, 5809-5811.

24. Mitomo, H.; Morishita, N.; Doi, Y. *Polymer* **1995**, *36*, 2573-2578.

25. Inoue, Y. *J. Mol. Struct*. **1998**, *441*, 119-127.

26. Bloembergen, S.; Holden, D. A.; Bluhm, T. L.; Marchessault, R. H. *Macromolecules* **1986,** *19*, 2865-2871.

27. Bluhm, T. L.; Hamer, G. K.; Marchessault, R. H.; Fyfe, C. A.; Veregin, R. P. *Macromolecules* **1986**, *19*, 2871-2878.

28. Inoue, Y.; Kamiya, N.; Yamamoto, Y.; Chujo, R.; Doi, Y. *Macromolecules* **1989**, *22*, 3800-3802.

29. Scandola, M.; Ceccoruli, G.; Pizzoli, M.; Gazzano, M. *Macromolecules* **1992**, *25*, 1405-1410.

30. Mansour, A. A.; Saad, G. R.; Hamed, A. H. *Polymer* **1999**, *40*, 5377-5391.

31. Yoshie, N.; Saito, M.; Inoue, Y. *Polymer* **2004**, *45*, 1903-1911.

32. Doi, Y.; Kitamura, S.; Abe, H. *Macromolecules* **1995**, *28*, 4822-4828.

33. Asrar, J.; Valentin, H. E.; Berger, P. A.; Tran, M.; Padgette, S. R.; Garbow, J. R. *Biomacromolecules* **2002**, *3*, 1006-1012.

34. Tsuge, T.; Kikkawa, Y.; Doi, Y. *Sci. Technol. Adv. Mater*. **2004**, *5*, 449-453.

35. Alata, H.; Aoyama, T.; Inoue, Y. *Macromolecules* **2007**, *40*, 4546-4551.

36. Hu, Y.; Zhang, J.; Sato, H.; Noda, I.; Ozaki, Y. *Polymer* **2007**, *48*, 4777–4785.

37. Shimamura, E.; Scandola, M.; Doi, Y. *Macromolecules* **1994**, *27*, 4429-4453.

38. Feng, L.; Watanabe, T.; He, Y.; Wang, Y.; Kichise, T.; Fukuchi, T.; Chen, G.; Doi, Y.; Inoue, Y. *Macromol. Biosci*. **2003**, *3*, 310–319.

39. Fukui, T.; Suzuki, M.; Tsuge, T.; Nakamura, S. *Biomacromolecules* **2009**, *10*, 700-706.

40. George, S. C.; Thomas, S. *In* Handbook of Multiphase Polymer Systems; Boudenne, A.; Ibos, L.; Candau, Y.; Thomas, S., Eds.; John Willey and Sons, Ltd.: United Kingdom, 2011; p 124.

41. Greco, P.; Martuscelli, E. *Polymer* **1989**, *30*, 1475-1483.

42. An, Y.; Dong, L.; Li, L.; Mo, Z.; Feng, Z. *Eur. Polym. J.* 1999, **35**, 365-369.

43. Madbouly, S. A.; Mansour, A. A.; Abdou, N. Y. *Eur. Polym. J.* **2007**, *43*, 3933-942.

44. Azuma, Y.; Yoshie, N.; Sakurai, M.; Inoue, Y.; Chûjô, R. *Polymer* **1992**, *33*, 4763-4767.

45. Yoshie, N.; Azuma, Y.; Sakurai, M.; Inoue, Y. *J. Appl. Polym. Sci*. **1995**, *56*, 17-22.

46. Ikejima, T.; Cao, A.; Yoshie, N.; Inoue, Y. *Polym. Degrad. Stab*. 1998, **62**, 463-469.

47. Ikejima, T.; Yoshie, N.; Inoue, Y. *Polym. Degrad. Stab*. **1999**, *66*, 263-270.

48. Kumagai, Y.; Doi, Y. *Polym. Degrad. Stab*. **1992**, *35*, 87-93.

49. Avella, M.; Martuscelli, E. *Polymer* **1988**, *29*, 1731-1737.

50. Avella, M.; Martuscelli, E.; Raimo, M. *Polymer* **1993**, *34***,** 3234-3240.

51. Di Lorenzo, M. L.; Silvestre, C. *Progr. Polym. Sci*. **1999**, *24*, 917-950.

52. El-Shafee, E.; Saad, G. R.; Fahmy, S. M. *Eur. Polym. J.*, **2001**, *37*, 2091-2104.

53. Scandola, M.; Ceccorulli, G.; Pizzoli, M. *Macromolecules* **1992**, *25*, 6441-6446.

54. Ceccoruli, G.; Pizzoli, M.; Scandola, M. *Macromolecules* **1993**, *26*, 6722-6726.

55. Pizzoli, M.; Scandola, M.; Ceccorulli, G. *Macromolecules* **1994**, *27*, 4755-4761.

56. Paglia, E. D.; Beltrame, P. L.; Canetti, M.; Seves, A.; Marcandalli, B.; Martuscelli, E. *Polymer* **1993**, *34*, 99-1001.

57. Finelli, L.; Sarti, B.; Scandola, M. *J. Macromol. Sci.-Pure Appl. Chem.* **1997**, *A34*, 13-33.

58. de Lima, J. A.; Felisberti, M. I. *Eur. Polym. J.* **2006**, *42*, 602-614.

59. Sadocco, P.; Canetti, M.; Seves, A.; Martuscelli, E. *Polymer* **1993**, *34*, 3368-3375.

60. Zhang, Q.; Zhang, Y.; Wang, F.; Liu, L. *Chinese J. Mater. Sci. Technol.* **1998**, *14*, 95-96.

61. Furukawa, T.; Sato, H.; Murakami, R.; Zhang, J.; Duan, Y. X., Noda, I.; Ochiai, S.; Ozaki, Y. *Maromolecules* **2005**, *38*, 6445-6454.

62. Zhang, J.; Sato, H.; Furukawa, T.; Tsuji, H.; Noda, I.; Ozaki, Y. *J. Phys. Chem. B* **2006**, *110*, 24463-24471.

63. Furukawa, T.; Sato, H.; Murakami, R.; Zhang, J.; Noda, I.; Ochiai, S.; Ozaki, Y. *Polymer* **2006**, *47*, 3132-3140.

64. Vogel, C.; Wessel, E.; Siesler, H. W. *Macromolecules* **2008**, *41*, 2975-2977.

65. Vogel, C.; Wessel, E.; Siesler, H. W. *Biomacromolecules* **2008**, *9,* 523-527.

66. Avella, M.; Martuscelli, E.; Orsello G., Raimo, M.; Pascucci, B. *Polymer* **1997**, *38*, 6135-6143.

67. Qiu, Z.; Ikehara, T.; Nishii, T. *Polymer* **2003**, *44*, 2503-2508.

68. Lovera, D.; Márquez, L.; Balsamo, V.; Taddei, A.; Castelli, C.; Müller, A. J. *Macromol. Chem. Phys*. **2007**, *208*, 924-937.

69. Tsai, C. S. Biomacromolecules: Introduction to Structure, Function and Informatics. John Willey and Sons, Inc: Hoboken, New Jersey, 2007; p 166.

70. Walton, A. G.; Blackwell, J. Biopolymers. Academic Press, Inc: New York, 1973; p 477

71. Minke, R.; Blackwell, J. *J. Mol. Biol.* **1978**, *120*, 167-181.

72. Kameda, T.; Miyazawa, M.; Ono, H.; Yoshida, M. *Macromol. Biosci.* **2005**, *5*, 103-106.

73. Rinaudo, M. *Prog. Polym. Sci.* **2006**, *31, 603-632.*

74. Jayakumar, R.; Prabaharan, M.; Nair, S. V.; Tamura, H. *Biotechnology Advances* **2010**, *28*, 142–150.

75. Nakajima, M.; Atsumi, K.; Kifune, K. *In* Chitin, Chitosan and Related Enzymes; Zikakis, J.P. Ed.; Harcourt Brace Janovich: New York, 1984; p. 407.

76. Madhumathi, K.; Kumar, P. T. S.; Abilash, S.; Sreeja, V.; Tamura, H.; Manzoor, K.;

Nair, S. V.; Jayakumar, R. *J. Mater. Sci. Mater. Med.* **2010**, *21*, 807–813.

77. Jayakumar, R.; Nwe, N.; Tokura, S.; Tamura, H. *Int. J. Biol. Macromolec.* **2007**, *40*, 175-181.

78. Aly, A. S.; Jeon, B. D.; Park, Y. H. *J. Appl. Polym. Sci.* **1997**, *65*, 1939–1946.

79. Crini, G. *Prog. Polym. Sci*. **2005**, *30*, 38-70.

80. Hirano, S.; Hirochi, K.; Hayashi, K.; Mikami, T.; Tachibana, H. *In* Cosmetic and Pharmaceutical Applications of Polymers; Gebelein, C. G.; Cheng, T. C.; Yang, V. C. Eds.; Springer: New York, 1991; p 95-104.

81. Kardas, I.; Struszczyk, M. H.; Kurcharska, M.; van den Broek, L. A. M.; van Dam, J. E. G.; Ciechańska, D. *In* The European Polysaccharide Network of Excellence (EPNOE): Research Initiatives and Result; Navard, P. Ed.; Springer: Verlag-Wien, 2012; p 329-364.

82. Kharas, G. B.; Sanchez-Riera, F.; Severson, D. K. *In* Plastics from Microbe; Mobley, D. P., Ed.; Hanser Publishers: New York, 1994; pp 93-137.

83. Xiao, L.; Wang, B.; Yang, G.; Gauthier, M. In Biomedical Science, Engineering and Technology; Ghista, D. N. Ed.; Intech, DOI: 10.5772/23927 , 2012; pp 247-282.

84. Garlotta, D. *J. Polym. Environ*. **2001**, *9*, 63-83.

85. Hartmann, M. H. *In* Biopolymers from Renewable Resources; Kaplan, D. L. Ed.; Springer: Verlag-Berlin Heridelberg, 1998; pp 395-399.

86. Raquez, J. M.; Habibi, Y.; Murariu, M.; Dubois, P. Polylactide (PLA)-based nanocomposites. *Prog. Polym. Sci.* **2013**, *38*, 1504-1542.

87. Kulkarni, R. K.; Moore, E. G.; Hegyeli, A. F.; Leonard, F. *J. Biomed. Mater. Res*. **1971**, *5*, 169-181.

88. Zhang, J-F.; Sun, X. *In* Biodegradable Polymers for Industrial Applications; Smith, R. Ed.; Woodhead Publishing Limited: Cambrige England, 2005: pp 251-281.

89. Wang, J.; Zhai, W.; Zheng, W. *J. Polym. Environ*. **2012**, *20*, 528-539.

90. Todo, M.; Takayama, T. *In* Biomaterials-Physics and Chemistry; Pignatello, R. Ed.; InTech 2011: pp 375-394.

91. Mohapatra, A. K.; Mohanty, S.; Nayak, S. K. *Polym. Compos*. **2014**, *35*, 283-293.

92. Plikk, P.; Målberg, S.; Albertsson, A-C. *Biomacromolecules* **2009**, *10*, 1259-1264.

93. Tyson, T.; Finne-Wistrand, A.; Albertsson, A-C. *Biomacromolecules* **2009**, *10*, 149-154.

94. Wang, R.; Wan, C.; Wang, S.; Zhang, Y. Polym. Eng. Sci. 2009, 49, 2414-2420.

95. Ljungberg, N.; Wesslén, B. *Polymer* **2003**, *44*, 7679-7688.

96. Martin, O.; Avérous, L. *Polymer* **2001**, *42*, 6209-6219.

97. Dorgan, J. R.; Braun, B.; Wegner, J. R.; Knauss, D. M. *In* Degradable Polymers and Materials; Khemani, K., Scholz, C. Eds.; American Chemical Society: Washington DC , 2006; pp 102-125.

98. Sin, L. T.; Rahmat, A. R.; Rahman, W. A. W. A. Polylactic Acid: PLA Biopolymer Technology and Applications. Elsevier: Oxford, United Kingdom, 2012; pp 109-131 and 177-215.

99. Jain, R. J. *Biomaterials 2000*, *21*, 2475-2490.

100. Urayama, H.; Kanamori, T.; Fukushima, K.; Kimura, Y. *Polymer* **2003**, *44*, 5635-5641.

101. Lunt, J.; Shafer, A. L. *J. Ind. Text*. **2000**, *29*, 191-205.

102. Groot, W.; Krieken, J. V.; Sliekersl, O.; Vos, S. D. *In* Poly(lactic acid): Synthesis, Structure, Properties, Processing, and Application; Auras, S., Lim, L-T., Selke, S. E. M., Tsuji, H. Eds.; John Wiley & Sons, Inc: Hoboken, New Jersey, 2010; pp 141-154.

103. Sasaki, S.; Asakura, T. *Macromolecules* **2003**, *36*, 8385-8390.

104. Puiggali, J.; Ikada, Y.; Tsuji, H.; Cartier, L.; Okihara, T.; Lotz, B. *Polymer* **2000**, *41*, 8921-8930.

105. Cartier, L.; Okihara, T.; Ikada, Y.; Tsuji, H.; Puiggali, J.; Lotz, B. *Polymer* **2000**, *41*, 8909-8919.

106. Kulkarni, R. K.; Pani, K. C.; Neuman, C.; Leonard, F. Arch. Surg. 1966, 93, 839-843.

107. Cutright, D. E.; Hunsuck, E. E.; *J. Oral Surg*. **1971**, *31*, 134- 139.

108. Cutright, D. E.; Hunsuck, E. E.; Beasley, J. D. *J. Oral Surg*. **1971**, *29*, 393-397.

109. Albertsson, A-C.; Varma, I. K. *Biomacromolecules* **2003**, *4*, 1466-1486.

110. Ikada, Y.; Tsuji, H. *Macromol. Rapid Commun*. **2000**, *21*, 117-132.

111. Suzuki, S. Ikada, Y. *In* Poly(lactic acid) Synthesis, Structures, Properties, Processing, and Applications; Auras, R., Lim, L-T., Selke, S. E. M., Tsuji, H. Eds.; John Wiley & Sons, Inc.: Hoboken, New Jersey, 2010; pp 445-456.

112. Tawakkal, I. S. M. A.; Cran, M. J.; Miltz, J.; Bigger, S. W. J. Food Sci. 2014, 79, R1477-R1490.

113. Obuchi, S.; Ogawa, S. *In* Poly(lactic acid) Synthesis, Structures, Properties, Processing, and Applications; Auras, R., Lim, L-T., Selke, S. E. M., Tsuji, H. Eds.; John Wiley & Sons, Inc.: Hoboken, New Jersey, 2010; pp 457-467.

114. Henton, D. E.; gruber, P.; Lunt, J.; Randall, J. *In* Natural Fibers, Biopolymers, and Biocomposite; Mohanty, A. K., Misra, M., Drzal, L. T. Eds.; CRC Press: Boca raton, Florida, 2005; pp 527-578.

115. Mochizuki, M. *In* Poly(lactic acid) Synthesis, Structures, Properties, Processing, and Applications; Auras, R., Lim, L-T., Selke, S. E. M., Tsuji, H. Eds.; John Wiley & Sons, Inc.: Hoboken, New Jersey, 2010; pp 141-154.

116. Whiteman, N. “2000 Polymers, Laminations and Coatings Conference”, Chicago, IL 2000, pp 631-635.

117. Kumari, A.; Yadav, S. K.; Yadav, S. C. *Coll. Surf. B. Biointerfaces* **2010**, *75*, 1-18.

118. Mikos, A. G.; Thorsen, A. J.; Czerwonka, L. A.; Bao, Y. Langer, R. *Polymer* **1994**, *35*, 1068-1077.

119. Fang, Q.; Hanna, M. A. *Creal Chem*. **2000**, *77*, 779-783.

120. Ma, Y.; Hu, W.; Reiter, G. *Macromolecules* **2006**, *39*, 5159-5164.

121. Liu, Y-X.; Chen, E-Q. *Coord. Chem. Rev*. **2010**, *254*, 1011-1037.

122. Wang, Y.; Ge, S.; Rafailovich, M.; Sokolov, J.; Zou, Y. Ade, H. Lüning, J.; Lustiger, A.; Maron, G. *Macromolecules* **2004**, *37*, 3319-3327.

123. Muratoğlu, O. K.; Argon, A. S.; Cohen, R. E. *Polymer* **1995**, *36*, 2413-2152.

124. Lovinger, A. J.; Keith, H. D. *Macromolecules* **1979**, *12*, 919-924.

125. Kovacs, A. J.; Starupe, C. *Faraday Discuss* **1979**, *68*, 225.

126. Schönherr, H.; Frank, C. W.; *Macromolecules* **2003**, *36*, 1188-1198.

127. Wang, Y.; Chan, C-M.; Ng, K-M.; Li, L. *Macromolecules* **2008**, *41*, 2548-2553.

128. Kikkawa, Y.; Abe, H.; Iwata, T.; Inoue, Y.; Doi, Y. *Biomacromolecules* **2001**, *2*, 940-945.

129. Frank, C. W.; Rao, V.; Despotopoulou, M. M.; Pease, R. F. W.; Hinsberg, W. D.; Miller, R. D.; Rabolt, J. F. *Science* **1996**, *273*, 912-915.

130. Despotopoulou, M. M.; Miller, R. D.; Rabolt, J. F. Frank, C. W. *J. Polym. Sci. Part B: Polym. Phys*. **1996**, *34*, 2335-2349.

131. Despotopoulou, M. M.; Frank, C. W.; Miller, R. D.; Rabolt, J. F. *Macromolecules* **1996**, *29*, 5797-5804.

132. Frank, B.; Gast, A. P.; Russell, T. P.; Brown, H. R.; Hawker, C. *Macromolecules* **1996**, *29*, 6531-6534.

133. Lin, E. K.; Kolb, R.; Satija, S. K.; Wu, W. *Macromolecules* **1999**, *32*, 3753-3757.

134. Tsui, O. K. C.; Russell., T. P.; Hawker, C. J. *Macromolecules* **2001**, *34*, 5535-5539.

135. Yang, C.; Onitsuka, R.; Takahashi, I. *Eur. Phys. J. E*. **2013**, *36*, 66.

136. Abe, H.; Kikkawa, Y.; Iwata, T.; Aoki, H.; Akehata, T.; Doi, Y. *Polymer* **2000**, *41*, 867-874.

137. Taguchi, K.; Miyaji, H.; Izumi, K.; Hoshino, A.; Miyamoto, Y.; Kokawa, R. *Polymer* **2001**, *42*, 7443-7447.

138. Ludwigs, S.; Krausch, G.; Magerle, R.; Zvelindovsky, A. V.; Sevink, G. J. A. *Macromolecules* **2005**, *38*, 1859-1867.

139. Mareau, V. H.; Prud'homme, E. E. *In* Soft Materials Structure and Dynamics; Dutcher, J. R., Marangoni, A. G. Eds.; Marcel Dekker: New York, 2005; pp 39-48.

140. Reiter, G. *Europhys. Lett*. **1993**, *23*, 579-584.

141. Tanaka, K.; Taura, A.; Ge, S-R.; Takahara, A.; Kajiyama, T. *Macromolecules* **1996**, *29*, 3040-3042.

142. Roth, C. B.; Dutcher, J. R. *J. Electroanal. Chem*. **2005**, *584*, 13-22.

143. Inoue, R.; Kanaya, T.; Nishida, K.; Tsukushi, I.; Telling, M. T. F.; Gabrys, B. J.; Tyagi, M.; Soles, C.; Wu, W-I. *Phys. Rev. E* **2009**, *80*, 031802.

144. Finke, S. J. Infrared Reflection-Absorption Spectroscopy of Thin Film Structures. Iowa State University, 1988, a Ph.D dissertation.

145. Factor, B. J.; Russell, T. P.; Toney, M. F. *Macromolecules* **1993**, *43*, 3441-3446.

146. Saraf, R. F.; Dimitrakopoulus, C.; Toney, M. F.; Kowalczyk, S. P. *Langmuir* **1996**, *12*, 2802-2806.

147. Sun, X.; Guo, L.; Sato, H.; Ozaki, Y.; Yan, S.; Takahashi, I. *Polymer* **2011**, *52*, 3865-3870.

148. Mori, K.; Mukoyama, S.; Zhang, Y.; Sato, H.; Ozaki, Y.; Terauchi, H.; Noda, I.; Takahashi, I. *Macromolecules* **2008**, *41*, 1713-1719.

149. Capitán, M. J.; Rueda, D. R.; Ezquerra, T. A. *Macromolecules* **2004**, *37*, 5653-5659.

150. Sato, H.; Murakami, R.; Mori, K.; Ando, Y.; Takahashi, I.; Noda, I.; Ozaki, Y. *Vib. Spectrosc.* **2009**, *51*, 132-135.

151. Zhang, J.; Sato, H.; Noda, I.; Ozaki, Y.; *Macromolecules* **2005**, *38*, 4274-4281.

152. Padermshoke, A.; Katsumoto, Y.; Sato, H.; Ekgasit, S.; Noda, I.; Ozaki, Y. *Spectrochim. Acta, Part A* **2005**, *61*, 541-550.

153. Padermshoke, A.; Katsumoto, Y.; Sato, H.; Ekgasit, S.; Noda, I.; Ozaki, Y. *Polymer* **2004**, *45*, 6547-6554.

Table 1. Comparison of physical properties of PHB and *i*PP

Properties	PHB	*i*PP
Melting temperature, °C	175	170
Glass transition temperature, °C	4	-10
Crystallinity (%)	60	50
Young modulus (GPa)	3.5	1.7
Tensile strength, MPa	40	38
Elongation to break (%)	5	400
Density, g/cm^3	1.250	0.905
UV resistance	good	bad
Solvent resistance	bad	good

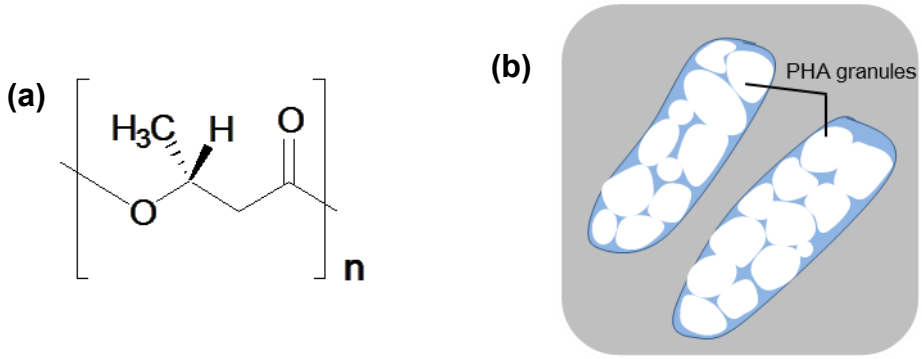

Figure 1. (a) Chemical structures of PHB and (b) accumulated PHAs in bacteria.

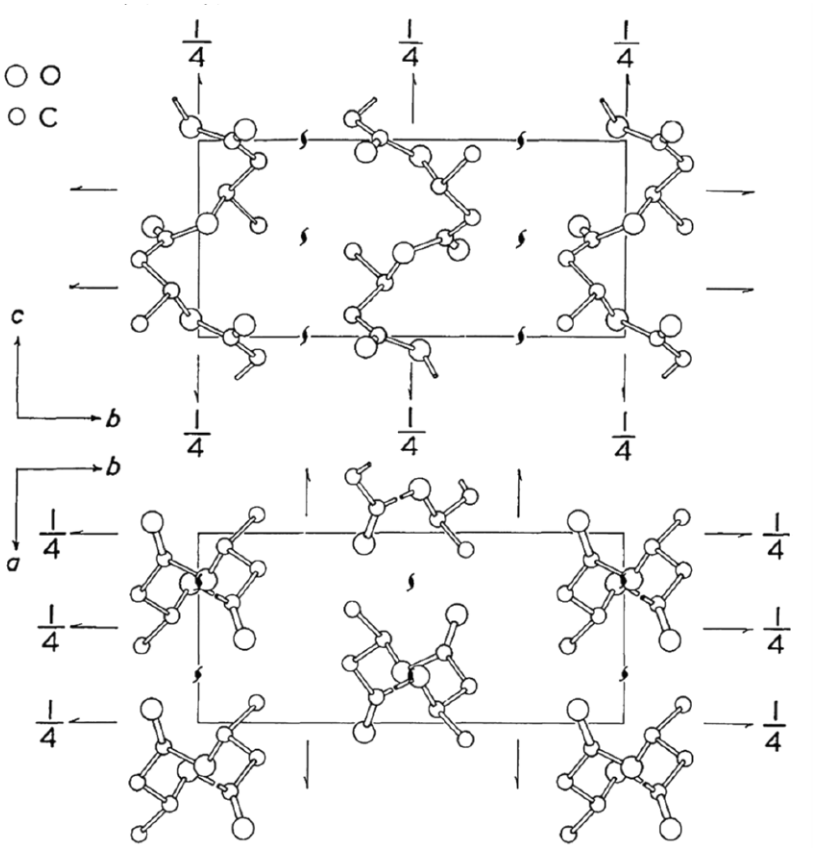

Figure 2. Crystal structure of PHB with a = 5.76 Å, b = 13.20 Å and c = 5.96 Å (fiber axis). Reproduced from Ref. 10

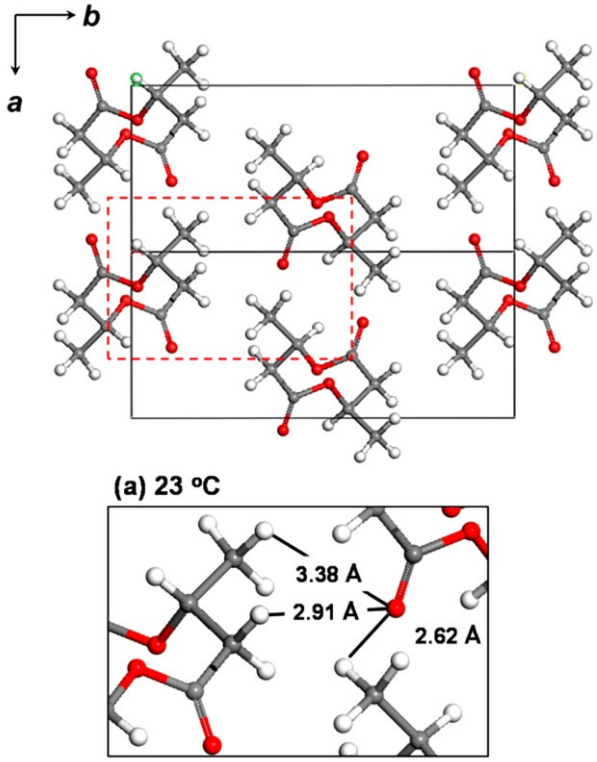

Figure 3. Intermolecular distance of PHB between O atom of C=O and H atom of CH_3 groups calculated at room temperature, reproduced from Ref. 17.

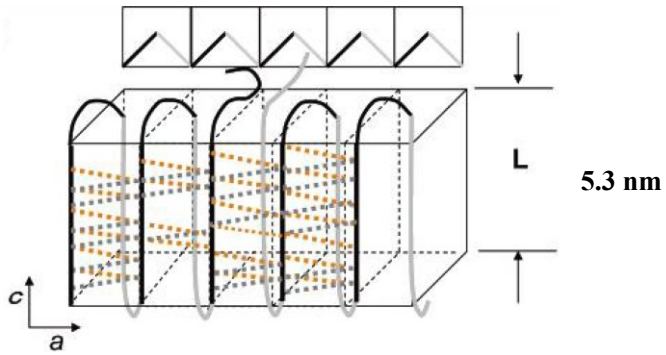

Figure 4. Intermolecular distance of PHB between O atom of C=O and H atom of CH_3 groups calculated at room temperature, reproduced from Ref. 15.

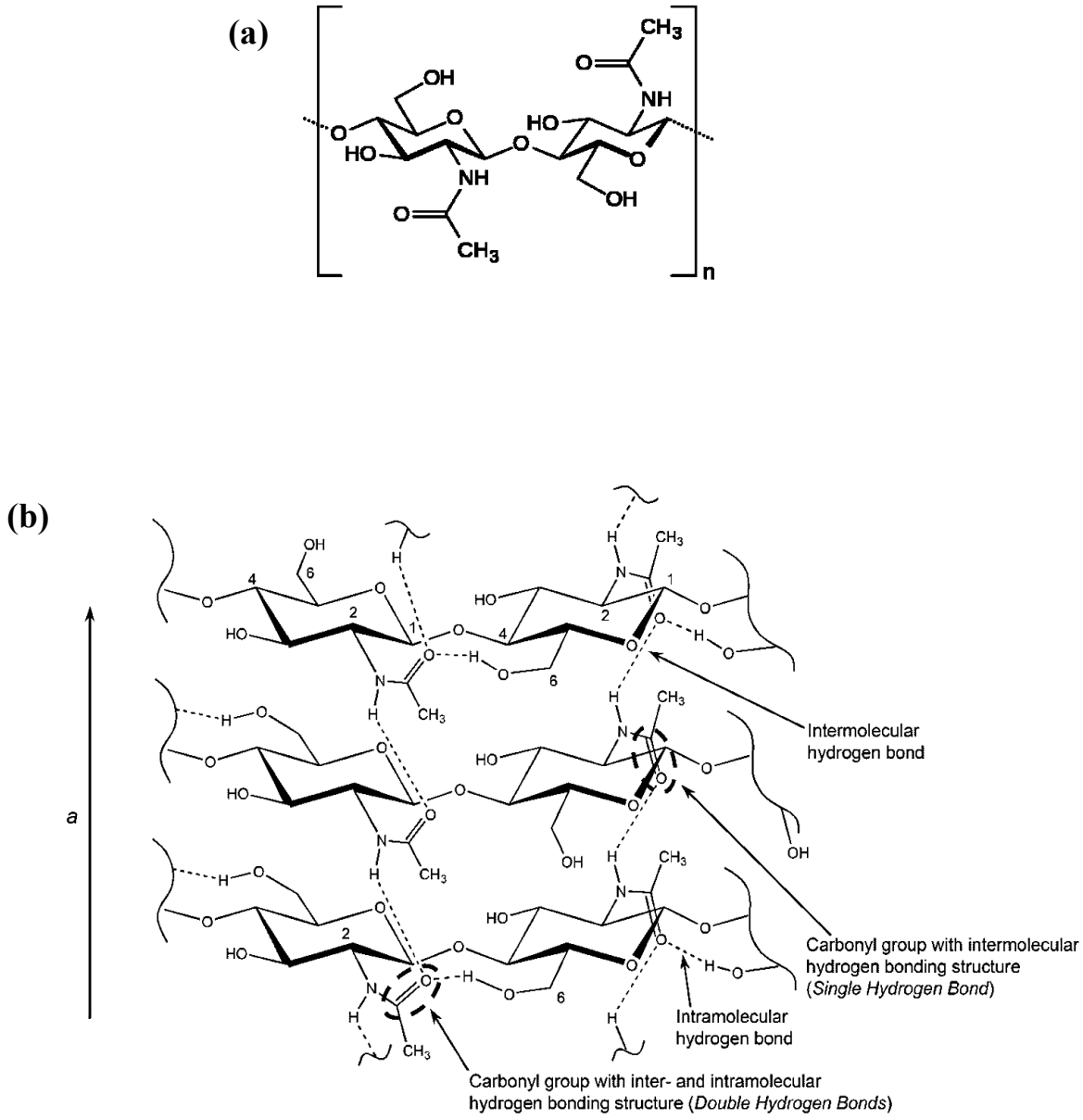

Figure 5. (a) Chemical structure of chitin, (b) diagram of the hydrogen bonding structure in the *ac* projection for α-chitin (reproduces from reference 72).

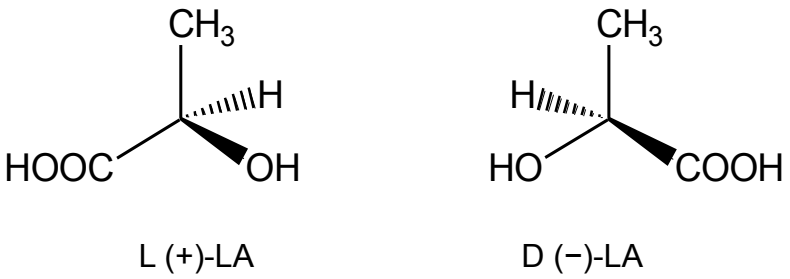

Figure 6. Two seteroisomers of lactic acid.

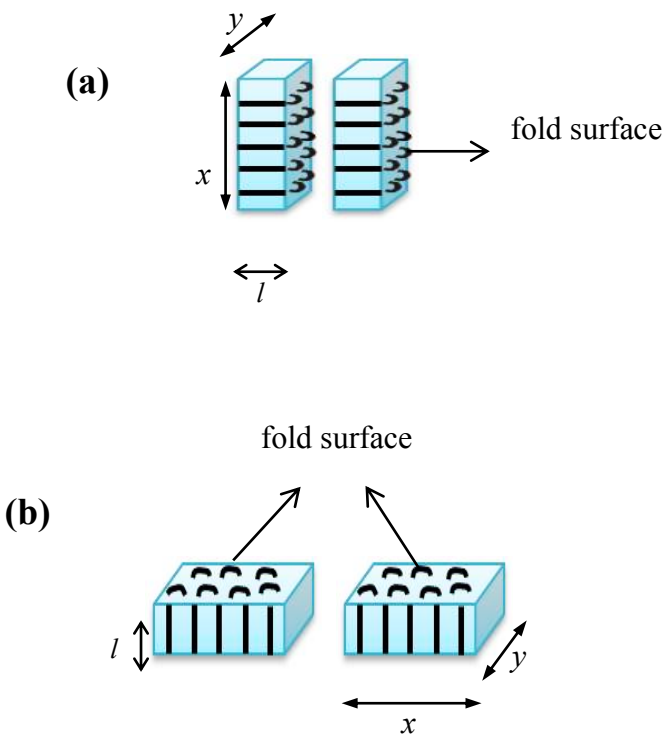

Figure 7. Illustration of (a) edge-on lamella and (b) flat-on lamellae. *x* and *y* indicated the two dimensional directions, while *l* indicated the lamellar thickness.

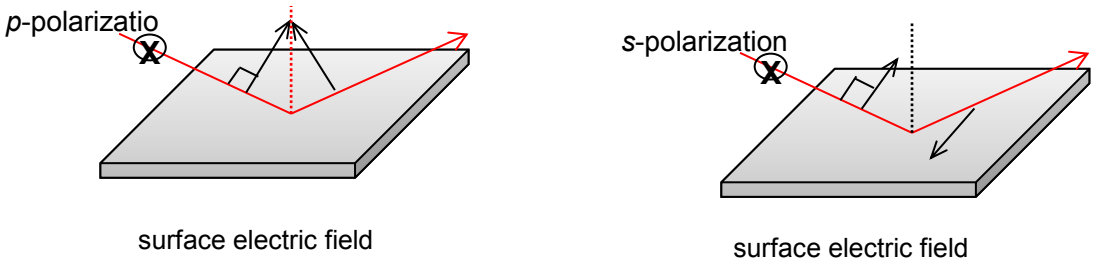

Figure 8. General schemes of IRRAS reflection on metal substrate

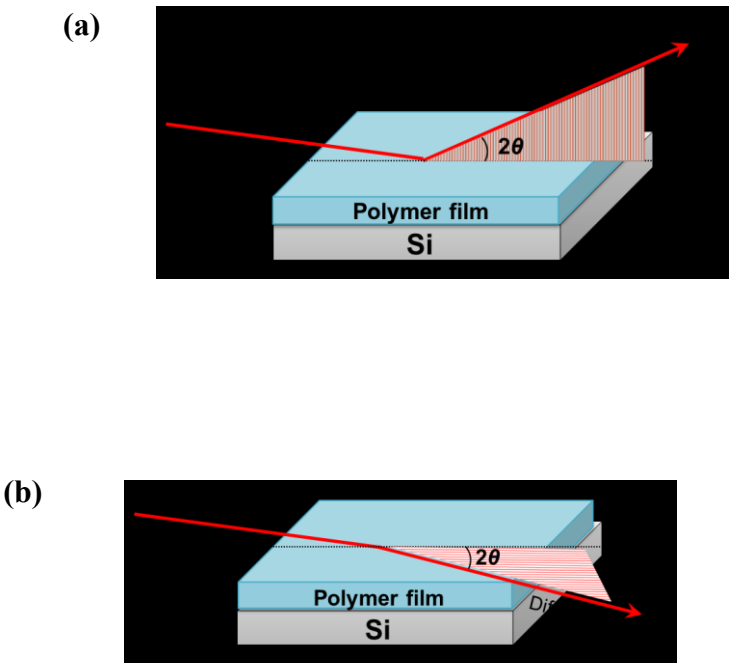

Figure 9. General schemes of (a) out-of plane and (b) in-plane GIXD measurements

Chapter 1

Intermolecular Hydrogen Bondings in the Poly(3-hydroxybutyrate) and Chitin Blends: Their Effects on the Crystallization Behavior and Crystal Structure of Poly(3-hydroxybutyrate)

ABSTRACT

Crystallization behavior and intermolecular hydrogen-bonding interactions of poly(3-hydroxybutyrate) (PHB)/chitin blends on as-solution cast films were studied as a function of composition and temperature by differential scanning calorimetry (DSC), wide-angle X-ray diffraction (WAXD) and infrared (IR) spectroscopy. The significant changes were observed in the DSC curves, WAXD patterns and IR spectra of the blends with PHB ≤ 50 wt %. We found that the crystallinity of PHB decreases in the blends, however, its crystal structure is not much affected by blending with chitin. The appearance of a new band at around 1710 ~ 1714 cm^{-1} clearly reveals the formation of intermolecular hydrogen bondings between the C=O groups of PHB and the O–H and N–H groups of chitin (C=O···H–O and C=O···H–N). It is very likely that these intermolecular C=O···H–N and C=O···H–O hydrogen bondings occur in the amorphous phase because of the reduction in the chain mobility in the blends with increasing chitin content, even above the melting temperature of PHB. The C=O···H–N and C=O···H–O hydrogen bondings are formed upon the cleavage of weak C=O···H_3C hydrogen bondings of PHB. Thus, the formation of the C=O···H–N and C=O···H–O hydrogen bondings is accompanied by the decrease in the crystallinity of PHB in the blends.

1. INTRODUCTION

Polyhydroxyalkanoates (PHAs) are bacterially synthesized polyesters that have attained great interest as promising biodegradable and biocompatible polymers for wide-range applications, such as biomedical, agricultural, packaging, pharmaceutical and paint industries.[1-3] Poly(3-hydroxybutyrate) or PHB (Figure 1a) is one of the most studied PHAs because its physical and mechanical properties are similar to those of commercial plastic derived from petrochemical, such as *isotactic* poly(propylene).[4-6] However, as a bacterially synthesized product, PHB has high-ordered stereoregularity that makes it highly crystalline and yields a narrow temperature window for processability. In addition, the secondary crystallization on the storage at ambient temperature[7] and the pre-existing crack within the spherulites result in the brittleness of PHB.[8,9] Therefore, these problems have decreased the potential applications of PHB.

Blending technique is one of the most convenient and more economical methods for making new materials based on the combination of two or more polymers to achieve the desired properties. Hence, PHB has been reported to be blended with various polymers, such as poly(vinyl acetate),[10,11] poly(l-lactic acid),[12,13] poly(ethylene oxide),[14] cellulose esters[15] and poly(vinyl alcohol).[16-18]

Our group has reported a series of studies on PHB, including its copolymers and blends from the structure, thermal and crystallization behavior points of view by

combination of various experimental techniques, such as infrared, near infrared, Raman and terahertz spectroscopy, X-ray diffraction (Wide-angle X-ray diffraction; WAXD and Small-angle scattering; SAXS), two-dimensional correlation spectroscopy and quantum chemical calculations.[12,13,16-32] One of the most important features in our findings is the existence of weak intramolecular interactions C–H···O=C hydrogen bonding between the CH_3 group of one helical structure and the C=O group of the other helical structure of PHB.[19-23] Furthermore, we reported the formation of intermolecular hydrogen-bonding interactions in the PHB blends. In the PHB/poly(4-vinylphenol) (PVPh) blends,[17] the intermolecular hydrogen bonds are formed between C=O groups of PHB and OH groups of PVPh. The exchange between intermolecular and intramolecular hydrogen bonds are found in those blends with PVPh content higher than the critical composition of ~50 wt %. In the PHB/cellulose acetate butyrate (CAB) blends,[27] the weak intermolecular hydrogen bonds between the OH groups in CAB and the C=O groups in the amorphous part of PHB (O–H···O=C) are formed in the blends with the high CAB content. These intermolecular interactions in the PHB/CAB blends highly depend on temperature and affect the crystallization kinetic of PHB in the blends.[28] Accordingly, the presence of these hydrogen bondings in the general polymer blends plays significant effects on the crystallinity, thermal properties, solubility and miscibility of the polymer blends.[33,34]

In the continuity of our interest, we broaden our investigation to a study of blend

systems of PHB and chitin (Figure 1b). Despite the studies on PHB/chitin blends are rare, chitin was chosen as a blend partner because it is the second most abundant polysaccharide in the nature after cellulose, which also has biodegradable and biocompatible properties.[35,36] Therefore, it is a highly potential blending source for large scale application in the future. On the other hand, chitin has hydroxyl and amide functional groups that may promote the formation of intermolecular hydrogen bondings with carbonyl groups of PHB. The intermolecular interaction, such as C=O···H−O and C=O···H−N hydrogen bonds, is an essential factor to reduce the crystallinity of PHB which further will improve the physical properties of PHB.[16,17,27,28] Therefore, the blending of PHB with chitin is expected to fabricate a good biodegradable and biocompatible polymer with more wide-range applications.

Previously, Lee et al.[37] reported that chitin can improve the mechanical properties of PVA with specific molecular interactions between C=O and OH. In related on another study on PHB blending systems, Ikejima et al.[38] studied thermal properties and crystallization behavior of PHB in the blends with chitin and chitosan. They reported that the crystallization of PHB was suppressed by blending with chitin and chitosan and suggested the formation of hydrogen bonds between carbonyl groups of PHB and amide NH groups of chitin from the results of ^{13}C NMR spectra. However, their suggestion was based only on evidences from the ^{13}C NMR study and not supported by other experimental

results. So far, the investigation of intermolecular hydrogen bondings in the PHB/chitin blends has not been fully explored yet.

The present study has aimed to investigate the intermolecular interactions and crystallization behavior of the PHB/chitin blends with the blend ratio of 100/0, 90/10, 80/20, 70/30, 60/40, 50/50, 40/60, 30/70, 20/80, 10/90 and 0/100 by combination of various techniques: differential scanning calorimetry (DSC), wide-angle X-ray diffraction (WAXD) and infrared (IR) spectroscopy. In this paper, our discussion focuses mainly on the following points: (1) the corroboration of the intermolecular hydrogen-bonding interactions in the PHB/chitin blends, particularly studies from IR spectra of the blends through the assignments in the regions of amide I, amide II and C=O stretching; (2) the evidences for the existence of these intermolecular hydrogen bondings in the amorphous phase; (3) the effects of intermolecular hydrogen bondings on the crystal structure and crystallization behavior of PHB in the PHB/chitin blends. The present study shows that the crystallinity of PHB decreases in the blends with chitin, particularly in the blends with PHB ≤ 50 wt % along with the formation of intermolecular C=O···H−N and C=O···H−O hydrogen bonds between PHB and chitin. Furthermore, these intermolecular hydrogen bonds were found to occur in the amorphous phase. The intermolecular interaction in the PHB/chitin blends is stronger than those in the PHB/CAB and PHB/PVPh.

2. EXPERIMENTAL SECTION

2-1. Materials and Sample Preparation

The bacterially synthesized PHB and chitin were purchased from Aldrich Japan Co. and Tokyo Chemical Industry Co., respectively, and were used without further purification. Samples of PHB/chitin blends were prepared by dissolving PHB and chitin in 1,1,1,3,3,3-hexafluoro-2-propanol (HFIP) with prescribed weight percentage. The films were prepared by casting the solution of blend samples on a perfluoroalkoxy (PFA) petri dish followed by evaporation at room temperature and continued by drying in a vacuum oven at 60°C for 12h.

2-2. Differential Scanning Calorimetry (DSC)

DSC measurements were performed with a Perkin-Elmer Pyris6 under nitrogen purge and a pure indium was used for calibration of the calorimeter. The DSC thermograms of PHB/chitin blends were measured over a temperature range of -40 to 200°C at heating and cooling rate of 10°C/min. The melting temperature and the heat of fusion of PHB were obtained from the first heating process. The samples were firstly melted at 190°C and maintained for one minute, then followed by cooling to -40°C.

The degree of crystallinity (X_c) of each blend was calculated from the enthalpy normalized to the actual weight fraction according to:

$$X_c = \frac{\Delta H_m}{\Delta H^\circ_{PHB}} \text{ x } \varphi \text{ x } 100$$

in which ΔH_m is the measured enthalpy in each blend, $\Delta H°_{PHB}$ is the enthalpy of the neat 100% PHB crystals (146 J g^{-1}) [39,40] and φ is the weight fraction (see also Table 1).

2-3. Wide-angle X-ray Diffraction (WAXD)

WAXD profiles of the blend films were measured at room temperature by using ULTIMA IV (Rigaku Co., Akishima, Japan) X-ray diffractometer equipped with a scintillation detector in the scattering range of $2\theta = 10^{\circ} - 30^{\circ}$. The X-ray beam of Cu Kα (wavelength 1.5406 Å) was employed at generator power of 40kV and 40 mA.

2-4. IR Spectroscopy

IR spectra of the blend films were measured by a Thermo Nicolet 6700 equipped with a liquid nitrogen cooled system and a mercury cadmium telluride (MCT) detector. The spectra were measured with 256 scans at a 2 cm^{-1} resolution in the region of 4000 to 650 cm^{-1}. The film samples were sandwiched by two KBr substrates, which were connected to a thermocouple to measure the precise temperature of film samples. The temperature was controlled by a temperature controller unit (CHINO, Model SU). The films were step wisely heated and cooled at a rate of 2°/min and maintained for three minutes before the measurement.

3. RESULTS AND DISCUSSION

3-1. Differential Scanning Calorimetry (DSC)

Figure 2a shows DSC thermogram of PHB/chitin blends with various compositions in the first heating process. PHB shows double endotherm peaks, i.e. a small peak appears because of the partial melting of imperfect crystals while a larger peak is caused by the melting of more perfect crystals and the recrystallized crystals during the heating process.[27] In contrast, chitin does not show any endotherm peak during the heating process as in the cases of previous studies of chitin blends.[37,38] Chitin most likely exists as the amorphous phase, and therefore, chitin does not show its thermal activity in DSC. The intensity of melting peaks of PHB decreases with increasing chitin contents in the blends, however the melting temperature (T_m) changes a little. A clear endotherm peak cannot be observed for the blends with PHB 50 wt % and eventually disappears when the PHB content becomes less than 40 wt %, signifying that the crystallinity of PHB substantially decreases by blending with chitin. However, it is noted that chitin does not much affect the T_m of the PHB crystals in the blend samples.

Figure 2b shows DSC thermograms obtained during the cooling process to investigate the effect of chitin matrix on the crystallization of PHB. It can be clearly seen that the intensity of the crystallization peak of PHB in the blends decreases with increasing chitin content, also indicating that the crystallizability of PHB decreases in the blends. Another

important point in Figure 2b is that the depression in the crystallization temperature (T_c) is higher than that of T_m. The increment of T_c in the blends with the chitin up to 10 wt % is caused by the nucleation effect of chitin. It clearly indicates that in the small loadings chitin act as a nucleating agent that promotes the rapid growth of the PHB crystals.[8,9,41] As a result, the temperature when PHB begins to crystallize is earlier in those blends. However, in the blends with higher chitin contents, the certain chitin chains interfere the crystallizability of PHB by forming intermolecular interactions and hinder the growth of the PHB crystal. Therefore, plot of T_c in Figure 2c is gradually decreased. The thermal characteristics of blends are summarized in Table 1.

The most important factor in the reduction of crystallinity is due to the formation of intermolecular interactions between PHB and chitin during the crystallization process, which would be caused by reduced mobility of PHB molecules peculiar in PHB/chitin blends. The intermolecular interactions which play a crucial role for reducing the crystallinity of PHB has also been observed in other blends, such as PHB/CAB blend[27] and PHB/chitosan blend.[38,42]

3-2. Wide-Angle X-ray Diffraction (WAXD)

Figure 3 shows X-ray diffraction patterns of PHB/chitin blends with various compositions collected at room temperature. PHB shows several sharp diffraction peaks in

the WAXD patterns, while chitin presents a simple broad diffraction peak (110) located around $2\theta = 19.6°$. It is important to highlight that chitin as a cast film from HFIP solution has crystalline volume fraction about 10%.[43] It gives us another evidence that chitin cast film reasonably exists in the amorphous phase.

The intensity of PHB diffraction peaks decreases gradually with increasing chitin content in the blends and eventually the peaks disappear for the blends with PHB ≤ 30 wt %. The diffraction peak position of PHB in the blends is almost the same as that of PHB, indicating that chitin little affects the crystalline structure of PHB. The WAXD results in Figure 3 indicate a similar trend as the DSC results that the significant changes are observed in the blends with PHB ≤ 50 wt %. Even though chitin suppresses the crystallinity of PHB, the WAXD results suggest that the crystalline structure of PHB does not change significantly by blending with chitin. It is noted that although DSC could not observe the melting peak for the blend with PHB 40 wt %, the crystalline diffraction due to (020) planes still appears in its WAXD pattern. This occurrence may be ascribed to the different sensitivity of the DSC and WAXD measurement techniques.

Figure 3 also suggests that the formation of intermolecular interactions between PHB and chitin occur in the amorphous phase. If the intermolecular interactions do not occur, the diffraction of crystalline peaks of PHB should be observed together with the diffraction of chitin.[42] However, with increasing chitin content in the blends only broad peak (consider

as a dominant amorphous phase)[27] is observed, indicating that the crystallizability of PHB is suppressed to impend a complete amorphous state because of the presence of strong interactions.[44]

The difference in the crystallization of the blends can be explained in terms of chain mobility. It is known that the adequate chain mobility towards the growth front is one of the major (kinetic control) factors in the crystallization of semicrystalline polymers. For example, in binary crystalline and amorphous blends, the amorphous chains reduce the mobility of the crystalline polymer chains to the growth front. As a result, the crystallization rate will be reduced with the increase of the amorphous component in the blends. However, if sufficient time is given to crystallize and there are no any interactions between the two blend components, then the crystallizable polymer chain should be able to crystallize. In another case, if the amorphous and crystalline polymer components are capable to form intermolecular interactions, the crystallizability of the crystalline polymer component should drastically drop with composition. The crystallizable chain mobility is almost quiescent (even the crystallization time is sufficient) due to intermolecular interactions. Therefore, the mobility of the crystallizable amorphous component is inadequate to reach the growth front and rearrange into the crystal lattice. For example, in the PHB/starch blends, the crystallinity and melting points of PHB are not altered by starch compositions, even up to 50 %. It indicates that the mobility of PHB chains is not affected

by the starch component due to hindrance. On the other hand, in the present study, the crystallinity of PHB drastically reduced with chitin composition as seen in the DSC and WAXD results. Furthermore, the present discussion suggests that the intermolecular interactions between PHB and chitin must be stronger than the PHB and starch blend system.[45,46] The detailed explanation and evidence of intermolecular hydrogen bond interactions will be discussed based on IR measurements in the following section.

3-3. Composition–Dependent IR Spectra

3-3-1. C=O stretching, Amide I and Amide II Region.

Figure 4a shows normalized IR spectra in the 1800-1500 cm^{-1} region and their second derivatives of PHB/chitin blends with various compositions collected at room temperature. All the IR spectra were normalized by dividing all the absorbance values by the highest absorbance value in one spectrum. The region of 1770-1680 cm^{-1} contains strong absorption bands due to the C=O stretching modes of PHB. A band at 1723 cm^{-1} is assigned to the C=O stretching mode of PHB in the crystalline phase and a broad band centered at 1747 cm^{-1} arises from the C=O stretching mode of PHB in the amorphous phase.[19-23] As aforementioned, a weak intramolecular hydrogen bonding between the C=O and CH_3 groups exists in the crystalline PHB. Therefore, the bands at 1723 and 1747 cm^{-1}, hereinafter, are referred to *intra* C=O and *free* C=O of PHB, respectively.[16,27]

As seen from Figure 4a, the intensity of *intra* C=O band decreases with decreasing the PHB content in the blends while that of *free* C=O band becomes predominant. The significant change of *intra* C=O occurs in the blend with PHB 50 wt % and the band eventually disappears with PHB ≤ 40 wt %, indicating that PHB remains in the amorphous phase in these blends. However, note that the position of *intra* C=O band in the blends is almost the same as that of neat PHB. These results confirm the similar position of T_m of PHB in the DSC and peak diffraction of PHB in the WAXD results described above. On the other hand, the position of *free* C=O band at 1747 cm^{-1} of neat PHB shifts by 7 cm^{-1} to a lower frequency with increasing chitin content in the blends (see the second derivative spectra). This indicates the existence of intermolecular hydrogen bondings between PHB and chitin in the amorphous phase. The detail of this evidence will be discussed later in the temperature-dependent IR spectra section.

The second derivatives spectra of the blends with PHB ≤ 50 wt % shown in the inset of Figure 4b indicate that a weak shoulder band starts to appear at around 1707 cm^{-1} in the blend with PHB 50 wt % and appears more obviously in the blends with PHB 40, 30 and 20 wt % at around 1710-1714 cm^{-1}. Neither the neat PHB spectrum nor the neat chitin spectrum exhibits this band. Therefore, this new band maybe ascribed to the C=O stretching of PHB with an intermolecular hydrogen bonding with the OH and NH groups of chitin (hereinafter defined as *inter* C=O). This assignment is reasonable because the

intensity of *inter* C=O band increases with increasing chitin content in the blends reciprocal to the predominant of *free* C=O and diminish of *intra* C=O. The similar characteristics have been discussed for the PHB/PVPh blends with PVPh ≥ 70 wt % in previous studies [16-18]. In addition, it is known that the hydrogen bonded C=O bands in many polymer blends which contain carbonyl groups appear around this frequency.[47,48]

In Figure 4a, there are three bands in the region of 1690-1500 cm^{-1} originated from chitin. Note that PHB does not show any absorption band in this region. In the chitin spectrum, this region consists mainly of amide I and amide II bands. Amide I band splits into two bands at 1661 and 1625 cm^{-1}; the splitting of amide I band is known as a special characteristic of α-chitin and has been interpreted as the existence of two types of hydrogen bonds formed by amide groups.[49,50] The C=O groups of amide groups being engaged in the intermolecular C=O···HN hydrogen bonds give rise to an Amide I band at 1661 cm^{-1}, while, a band at 1625 cm^{-1} arises from an Amide I mode of amide groups which have double hydrogen bonds, intermolecular C=O···HN hydrogen bond (defined as *inter* C=O chitin) and intramolecular C=O···HO hydrogen bond (defined as *intra* C=O chitin).[51-54] Another band at 1555 cm^{-1} is attributed to an Amide II mode.[37,50] Note that the relative intensity of the 1625 cm^{-1} band is weaker compared with that of 1661 cm^{-1} as depicted in Figure 4b.

3-3-2. C–H Stretching Region of PHB

Figure 5 exhibits composition-dependent IR spectra in the 3020-2900 cm^{-1} region and their second derivatives for the PHB/chitin blends at room temperature. A band at 3009 cm^{-1} has been assigned to the C–H stretching mode of the weak hydrogen bond between the C=O group and the CH_3 group in the crystal lamella of PHB.[19-23] The peak at 3009 cm^{-1} decreases with increasing chitin content in the blends and entirely disappears when PHB ≤ 50 wt %, indicating that the crystal lamella of PHB is disrupted. Therefore, the formation of PHB crystals is getting difficult in these blend samples, when the chitin content decreases. However, the position of this band does not change with decreasing the chitin content compared with that of neat PHB. This result gives further evidence that the crystalline structure of PHB does not change by blending with chitin. The detail assignment of IR bands is tabulated in Table 2.

3-4. Temperature-Dependent IR Spectra

3-4-1. C=O stretching Region

Figure 6 shows temperature-dependent IR spectra in the 1780-1670 cm^{-1} region of PHB/chitin blends with PHB: (a) 100, (b) 70, (c) 50 and (d) 30 wt % and their second derivatives measured during the heating process, respectively. It can be seen that the intensity of *intra* C=O at 1723 cm^{-1} decreases with temperature, while

the intensity of *free* C=O increases. However, plots of the normalized peak at 1723 cm^{-1} versus temperature in Figure 7a show that PHB crystals in the blends have similar melting behavior to the crystals in neat PHB. PHB crystals show the continuous-melting up to the T_m then decrease sharply above the T_m. This result further suggests that the PHB crystals are excluded from the chitin chains.

To discuss quantitatively about the confinement effect in the blends, the normalized full-width at half-maximum (FWHM) of the *free* C=O band of PHB versus temperature is plotted in Figure 7b. The FWHM calculation for the deconvoluted C=O amorphous band that are separated from the *intra*- and *inter* C=O bands was carried out by GRAMS software. The FWHM of the amorphous band reflects the degree of conformational distribution in the amorphous phase and the thermal mobility of the molecular chains. Generally, at room temperature, the chains of semicrystalline polymer in the amorphous region are constrained because they are packed in between the crystalline (lamellae structure) regions. As a result, the chain mobility at the T_g is almost quiescent and the thermal motion of polymer chains is hindered below the T_m during the heating process. It can be seen from Figure 7b that in the vicinity of the T_m, the FWHM of the *free* C=O band at 1747 cm^{-1} of PHB sharply increases, indicating that the mobility of the amorphous chains

increase significantly due to the melting of the crystals then followed by the marked reduction in the confinement.

In the case of blend samples, if there were no intermolecular interactions between PHB and chitin chains in the amorphous region, we could expect a similar abrupt change in the FWHM of the *free* C=O band during the heating process. However, as can be seen in Figure 7b, the FWHM of the *free* C=O band is reduced with the increase in the chitin content, implying the increase in the strong confinement in the amorphous region. Such strong confinement is probably due to the formation of intermolecular hydrogen-bonds between PHB and chitin molecules. Therefore, in the blend with PHB 50 wt %, the mobility of PHB chains in the amorphous phase is slightly increased with temperature, which shows a sharp contrast to the neat PHB where a drastic increase in mobility is suggested especially above 130°C. Note that the linear increment of each plot may be due to the thermal expansion during the heating process.

Figure 6c-d also shows the appearance of *inter* C=O band at around 1710 cm^{-1} in the spectra of the blends with PHB 50 and 30 wt % with temperature. Among these IR spectra, the spectrum of the blend with PHB 30 wt % shows a clear existence of this band at 1711 cm^{-1} (see the insert of Figure 6d). The appearance of *inter* C=O at around 1710 cm^{-1} suggests that the C=O groups of PHB are hydrogen bonded with the NH or OH groups of

chitin.

Figure 7c plots the wavenumber of the *inter* C=O band versus temperature for the blends with PHB: 40, 30 and 20 wt %. During the heating process, the *inter* C=O band gradually shifts to a higher wavenumber up to the T_m of PHB and further shows a distinct shift above the T_m of PHB, especially for the blend with PHB 40 wt %. Moreover, the *inter* C=O band shifts to a higher wavenumber with the increase in the chitin content in the blends. These results indicate that the intermolecular hydrogen bonding becomes weak with temperature and the increase in chitin content in the blends.

Compared to our previous studies on PHB blending systems such as PHB/CAB[27] and PHB/PVPh blends,[16] the results on the present PHB blends show some differences from previous ones. For example, in the PHB/CAB blend with the ratio of 50/50, crystalline PHB still exists in the amorphous matrix. During the heating process, the crystallinity of PHB is increased and followed by melting of the PHB crystals.[27] In the PHB/PVPh blend with 30 wt % PVPh, the intermolecular hydrogen bonds C=O···HO of PHB−PVPh are dissociated during the heating process, and then, PHB forms the weak intramolecular hydrogen bondings (CH_3···O=C).[16] In contrast, such exchanging behavior of intermolecular to intramolecular interactions in the PHB crystals was not observed in the present study for all the blends studied during the heating process. Although the intermolecular hydrogen bondings (C=O···H−O and C=O···H−N) of PHB-chitin become

weak with temperature, however, they are not dissociated during the heating to form intramolecular interactions ($CH_3\cdots O=C$) of PHB. Therefore, there is no increasing crystallinity of PHB in the blends and melting of PHB crystals in the blends with chitin ≥ 50 wt %. This strongly suggests that the intermolecular interactions in the PHB/chitin blends are significantly stronger than the intermolecular interactions in the PHB/CAB and PHB/PVPh blends.[16,17,27]

3-4-2. Amide I and Amide II Region

Figure 8 displays temperature-dependent IR spectra in the 1700-1500 cm^{-1} region of chitin and the blends with PHB 30 and 50 wt % (bottom) and their second derivatives spectra (up). In the chitin spectrum (Figure 8a), the intensity of amide I band at 1625 cm^{-1} shows a significant decrease with temperature, while, another peak of amide I band at 1661 cm^{-1} changes a little with temperature. These results suggest that the *inter* C=O chitin is strong and almost stable with temperature. In contrast, the *intra* C=O chitin is weak with temperature. Therefore, the peak at 1625 cm^{-1} gradually decreases with temperature. This result agrees with the conclusion by Kameda et al.[52] that the C=O···HO hydrogen bond is weaker than the C=O···HN hydrogen bond. The similar tendency of those two bands is also found for in the blends with PHB 30 and 50 wt % (Figure 8b and c).

Based on all the above results, we propose the structure change and the formation of intermolecular interactions in the PHB/chitin blends in Figure 9. In the blends with PHB

content ≤ 50 wt %, the C=O groups in the amorphous chain of PHB form the intermolecular hydrogen bondings with OH and NH groups of chitin (C=O···HN and C=O···HO) and small crystalline lamella of PHB may still exist. With increasing temperature, the crystalline lamella transforms into amorphous chain and associates with chitin to form intermolecular hydrogen bondings. The intermolecular hydrogen bondings are not exchanging to intramolecular C=O···H_3C of PHB with temperature. Above the T_m of PHB, these intermolecular hydrogen bondings still exist, even though they become weak.

4. CONCLUSION

In the present study, we have explored the crystallization behavior of PHB in the PHB/chitin blends in relation with intermolecular hydrogen bondings by using DSC, WAXD and IR spectroscopy. The crystallinity of PHB is reduced by blending with chitin, especially the crystallinity in the blends with PHB ≤ 50 wt %. However, the crystalline peaks at 1723 and 3009 cm^{-1} of PHB in the blends appear almost at the same positions as those of neat PHB, implying that the crystal structure of PHB is changed little by the presence of chitin molecules. The reduction of crystallinity of PHB is probably due to the formation of intermolecular hydrogen bondings between

the C=O groups of PHB and the NH and OH groups of chitin (C=O···HN and C=O···HO) in the amorphous region of the blends (Figure 9).

In the C=O stretching region of blends with PHB ≤ 50 weight %, the *intra* C=O band at 1723 cm^{-1} is diminished, the *free* C=O band at 1747 cm^{-1} becomes dominant, and a new band assigned to the *inter* C=O appears at around 1710 cm^{-1}. The presence of this new band highly depends on the blend composition. These results clearly reveal the existence of intermolecular hydrogen bondings between PHB and chitin molecular chains. The fact that the intermolecular hydrogen bondings occur in the amorphous phase, is further confirmed by the plot of FWHM of *free* C=O at 1740 cm^{-1} of PHB in the blends in Figure 8b. With temperature, these intermolecular hydrogen bondings become weak, however, they are not dissociated even up to the T_m of PHB to form intramolecular hydrogen bonds (CH_3···O=C) of PHB. Therefore, PHB cannot form crystals in the blends with PHB ≤ 50 wt %. This result suggests the presence of strong intermolecular hydrogen bondings in the PHB and chitin blends and it has been indicated that the intermolecular C=O···HN and C=O···HO in the PHB/chitin blends are significantly stronger than those of PHB/PVPh and PHB/CAB blends.

REFERENCES

1. Philip, S.; Keshavarz, T.; Roy I. *J. Chem. Technol. Biotechnol.* **2007**, *82*, 233–247.

2. Hazer, D. B.; Kılıçay**,** E.; Hazer, B. *Mater. Sci. Eng. C* **2012**, *32*, 637–647.

3. Chen, G-Q. *In* Plastics from Bacteria: Natural Functions and Applications. Chen, G-Q. Ed.; Springer: Heidelberg/ New York, 2010; p 17–37.

4. Zhao, Q.; Cheng, G. *In* New Frontiers in Polymer Research. Bregg, R. K. Ed.; Nova Science Publishers, Inc: New York, 2006; p 99–124.

5. Sudesh, K.; Abe, H.; Doi, Y. *Prog. Polym. Sci.* **2000**, *25*, 1503–1555.

6. Satkowski, M. M.; Melik, D. H.; Autran, J–P.; Green, P. R.; Noda, I.; Schechtman, L. A. *In Biopolymers*. Steinbüchel, A., Doi, Y. Eds.; Wiley-VCH: Weinheim, 2001; p 231.

7. de Koning, G. J. M.; Lemstra, P. J. *Polymer* **1993**, *34*, 4089–4094.

8. Barham, P. J. *J. Mater. Sci.* **1984**, *19*, 3826–3834.

9. El-hadi, A.; Schnabel, R.; Straube, E.; Mu, G.; Henning, S. *Polym. Test.* **2002**, *21,* 665–674.

10. Greco, P.; Martuscelli, E. *Polymer* **1989**, *30*, 1475–1483.

11. An, Y.; Dong, L.; Li, L.; Mo, Z.; Feng, Z. *Eur. Polym. J.* **1999**, *35*, 365–369.

12. Furukawa, T.; Sato, H.; Murakami, R.; Zhang, J.; Duan, Y.; Noda, I.; Ochiai, S.; Ozaki, Y. *Macromolecules* **2005**, *38*, 6445–6454.

13. Zhang, J.; Sato, H.; Furukawa, T.; Tsuji, H.; Noda, I.; Ozaki, Y. *J. Phys. Chem. B* **2006**, *110*, 24463–24471.

14. Avella, M.; Martuscelli, E. *Polymer* **1988**, *29*, 1731–1737.

15. Pizzoli, M.; Scandola, M.; Ceccorulli, G. *Macromolecules* **1994**, *27*, 4755–4761.

16. Guo, L.; Sato, H.; Hashimoto, T.; Ozaki, Y. *Macromolecules* **2011**, *44*, 2229–2239.

17. Guo, L.; Sato, H.; Hashimoto, T.; Ozaki, Y. *Macromolecules* **2010**, *43*, 3897–3902.

18. Huang, H.; Hu, Y.; Zhang, J.; Sato, H.; Zhang, H.; Noda, I.; Ozaki, Y. *J. Phys. Chem. B* **2005**, *109*, 19175–19183.

19. Sato, H.; Murakami, R.; Zhang, J.; Mori, K.; Takahashi, I.; Terauchi, H.; Noda, I.; Ozaki, Y. *Macromol. Symp.* **2005**, *230*, 158–166.

20. Sato, H.; Murakami, R.; Padermshoke, A.; Hirose, F.; Senda, K.; Noda, I.; Ozaki, Y. *Macromolecules* **2004**, *37*, 7203–7213.

21. Sato, H.; Mori, K.; Murakami, R.; Ando, Y.; Takahashi, I.; Zhang, J.; Terauchi, H.; Hirose, F.; Senda, K.; Tashiro, K.; Noda, I.; Ozaki, Y. *Macromolecules* **2006**, *39*, 1525–1531.

22. Sato, H.; Dybal, J.; Murakami, R.; Noda, I.; Ozaki, Y. *J. Mol. Struct.* **2005**, *744-747*, 35–46.

23. Sato, H.; Ando, Y.; Dybal, J.; Iwata, T.; Noda, I.; Ozaki, Y. *Macromolecules* **2008**, *41*, 4305–4312.

24. Sato, H.; Nakamura, M.; Padermshoke, A.; Yamaguchi, H.; Terauchi, H.; Ekgasit, S.; Noda, I.; Ozaki, Y. *Macromolecules* **2004**, *37*, 3763–3769.

25. Hu, Y.; Zhang, J.; Sato, H.; Futami, Y.; Noda, I.; Ozaki, Y. *Macromolecules* **2006**, *39*,

3841–3847.

26. Murakami, R.; Sato, H.; Dybal, J.; Iwata, T.; Ozaki, Y. *Polymer* **2007**, *48*, 2672–2680.

27. Suttiwijitpukdee, N.; Sato, H.; Zhang, J.; Hashimoto, T.; Ozaki, Y. *Polymer* **2011**, *52*, 461–471.

28. Suttiwijitpukdee, N.; Sato, H.; Zhang, J.; Hashimoto, T. *Macromolecules* **2011**, *44*, 3467–3477.

29. Suttiwijitpukdee, N.; Sato, H.; Unger, M.; Ozaki, Y. *Macromolecules* **2012**, *45*, 2738–2748.

30. Hoshina, H.; Ishii, S.; Yamamoto, S.; Morisawa ,Y.; Sato, H.; Uchiyama, T.; Ozaki, Y.; Otani, C. *IEEE Trans. Terahertz Sci. Technol.* **2013**, *3,* 248–258.

31. Zhang, J.; Sato, H.; Noda, I.; Ozaki, Y. *Macromolecules* **2005**, *38*, 4274–4281.

32. Unger, M.; Morita, S.; Sato, H.; Ozaki, Y.; Siesler, H. W. *Appl. Spectrosc.* **2009**, *63*, 1027–1033.

33. He, Y.; Zhu, B.; Inoue, Y. *Prog. Polym. Sci.* **2004**, *29*, 1021–1051.

34. Kuo, S-W. *J. Polym. Res.* **2008**, *15*, 459–486.

35. Ravi Kumar, M. N. V. *React. Funct. Polym*. **2000**, *46*, 1–27.

36. Rinaudo, M. *Prog. Polym. Sci.* **2006**, *31*, 603–632.

37. Lee, Y. M.; Kim, S.H.; Kim, S. J. *Polymer* **1996**, *37*, 5897–5905.

38. Ikejima, Y.; Yagi, K.; Inoue, Y. *Macromol. Chem. Phys.* **1999**, *200*, 413–421.

39. Barham, P. J.; Keller, A.; Otun, E. L.; Holmes, P. A. *J. Mater. Sci.* **1984**, *19*, 2781–2794.

40. Gunaratne, L. M. W. K.; Shanks, R. A.; Amarasinghe, G. *Thermochim. Acta* **2004**, *423*, 127–135.

41. Sun, X.; Tokuda, A.; Oji, Y.; Nakatani, T.; Tsuji, H.; Ozaki, Y.; Yan, S.; Takahashi, I. *Macromolecules* **2012**, *45*, 2485–2493.

42. Chen, C.; Zhou, X.; Zhuang, Y.; Dong, L. *J. Polym. Sci. Part B: Polym. Phys*. **2005**, *43*, 35–47.

43. González-campos, J. B.; Prokhorov, E.; Luna-Bárcenas, G.; Galván, A. M.; Sanchez, I. C.; Nuño Donlucas, S. M.; Garcia-Gaitan, B.; Kovalenko, Y. *J. Polym. Sci. Part B: Polym. Phys*. **2009**, *47*, 932–943.

44. Huang, I. H.; Chang, L.; Woo, E. M. *Macromol. Chem. Phys.* **2011**, *212*, 1155–1164.

45. Zhang ,M.; Thomas, N. L. *J. Appl. Polym. Sci.* **2010**, *116*, 688–694.

46. Zhang, M. Development of Polyhydroxybutyrate Based Blends for Compostable Packaging [dissertation]. Loughborough University: Leicestershire, UK, 2010.

47. Coleman, M. M.; Lichkus, A. M.; Painter, P. C. *Macromolecules* **1989**, *22*, 586–595.

48. Moskala, E. J.; Howe, S. E.; Painter, P. C.; Coleman, M. M. *Macromolecules* **1984**, *17*, 1671–1678.

49. Brugnerotto, J.; Lizardi, J.; Goycoolea, F. M.; Argüelles-Monal, W.; Desbrières, J.;

Rinaudo, M. *Polymer* **2001**, *42*, 3569–3580.

50. Cárdenas, G.; Cabrera, G.; Taboada, E.; Miranda, S. P. *J. Appl. Polym. Sci.* **2004**, *93*, 1876–1885.

51. Carlstrom, D. *J. Biophys. Biochem. Cytol.* **1957**, *3*, 669–683.

52. Focher, B.; Naggi, A.; Torri, G.; Cosani, A.; Terbojevich, M. *Carbohyd. Polym.* **1992**, *17*, 97–102.

53. Yamaguchi, Y.; Nge, T. T.; Takemura, A.; Hori, N.; Ono, H. *Biomacromolecules* **2005**, *6*, 1941–1947.

54. Kameda, T.; Miyazawa, M.; Ono, H.; Yoshida, M. *Macromol. Biosci.* **2005**, *5*, 103–106.

Table 1: Thermal properties of PHB/chitin blends obtained from DSC measurements

PHB/chitin (wt % / wt %)	T_m (°C)	T_c (°C)	φ	ΔH_f (J g^{-1})	X_c (%)
100/0	169.1	66.2	1.0	113	77
90/10	168.9	69.4	0.9	73	56
80/20	168.7	65.0	0.8	61	52
70/30	167.3	60.7	0.7	26	25
60/40	166.8	58.0	0.6	20	23
50/50	150.9	n.d.	0.5	16	22
40/60	n.d.	n.d.	0.4	–	–
30/70	n.d.	n.d.	0.3	–	–
20/80	n.d.	n.d.	0.2	–	–
10/90	n.d.	n.d.	0.1	–	–
0/100	n.d.	n.d.	0	–	–

n.d. = not detected

Table 2: Band assignments of IR spectra of PHB/chitin blends

No.	Wavenumber (cm^{-1})	Assignments	Components
1	1555	Amide II	chitin
2	1625	Amide I, C=O with double hydrogen bonds: *inter* C=O chitin, C=O···HN and *intra* C=O chitin, C=O···HO	chitin
3	1661	Amide I, C=O with single hydrogen bond: *inter* C=O chitin, C=O···HN	chitin
4	1710 - 1714	*inter* C=O, C=O···HO and C=O···HN	PHB−chitin
5	1723	*intra* C=O	PHB crystalline
6	1740 - 1747	*free* C=O	PHB amorphous
7	3009	*intra* C−H, C=O···H−C	PHB crystalline

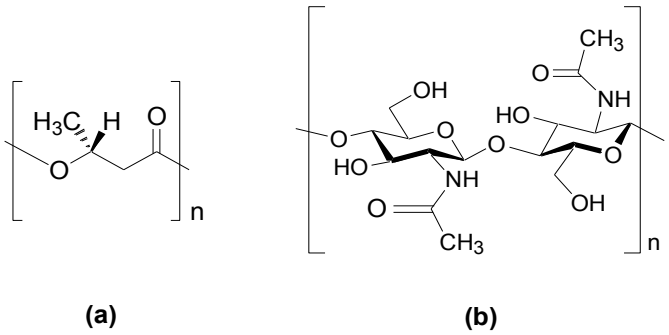

Figure 1. Chemical structures of (a) poly(3-hydroxybutyrate) (PHB) and (b) chitin.

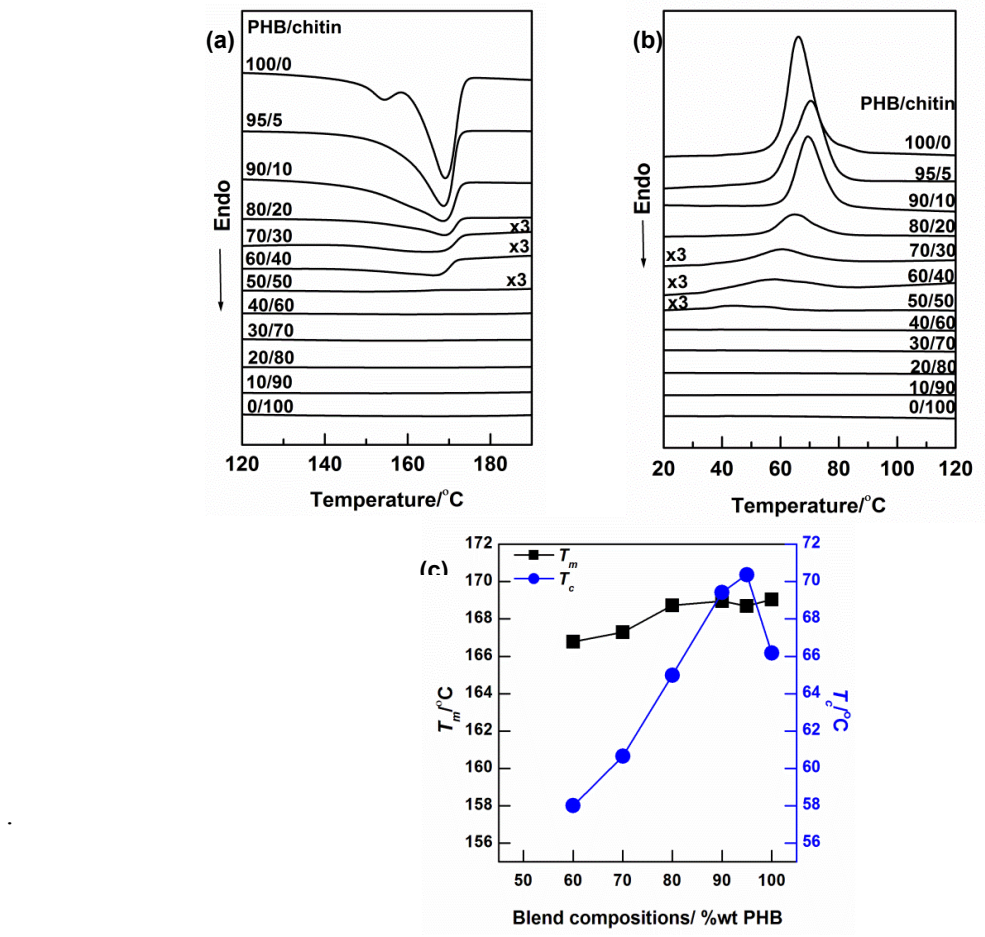

Figure 2. DSC thermograms of PHB/chitin blends with different blend ratios at a rate of 10°C/min in the (a) heating process and (b) cooling process (the peaks have been normalized relative to the mass of the sample) and (c) Plot of T_m and T_c for the blends versus the composition of PHB in the blends.

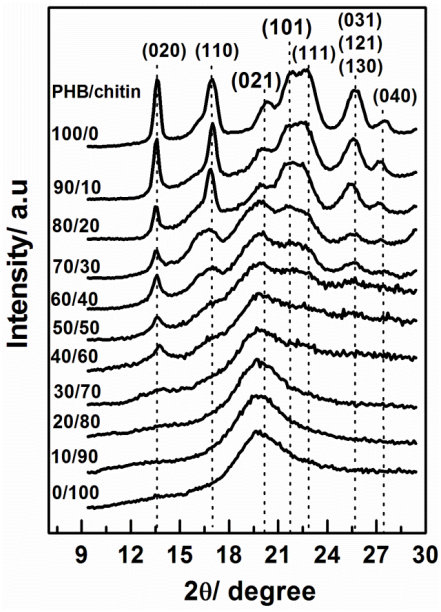

Figure 3. X-ray diffraction profiles of PHB/chitin blends with different ratios collected at room temperature.

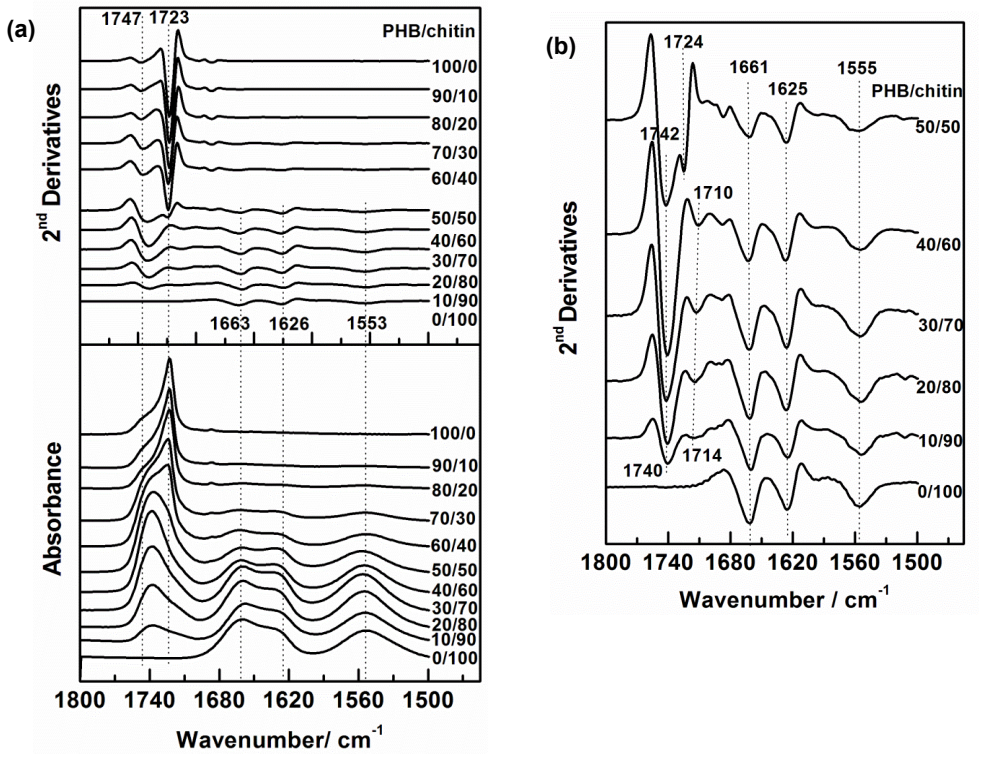

Figure 4. IR spectra in the 1800-1500 cm^{-1} region of (a) PHB/chitin blends with different ratios collected at room temperature (bottom) and their second derivatives (up), (b) the enlargement of the second derivative spectra of the PHB/chitin blends with PHB ≤ 50 wt %.

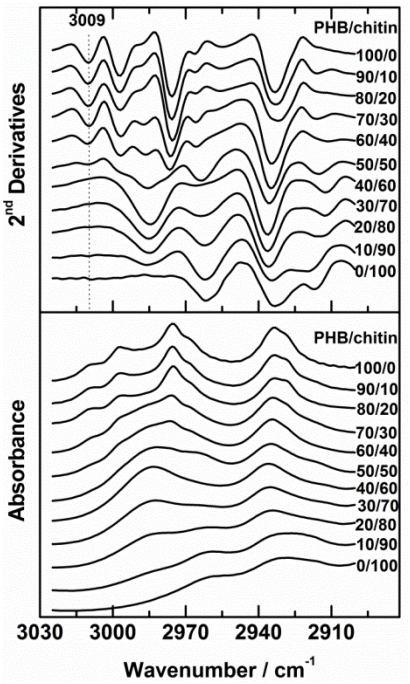

Figure 5. IR spectra in the 3020-2900 cm^{-1} region of PHB/chitin blends with different ratios collected at room temperature (bottom) and their second derivatives (up).

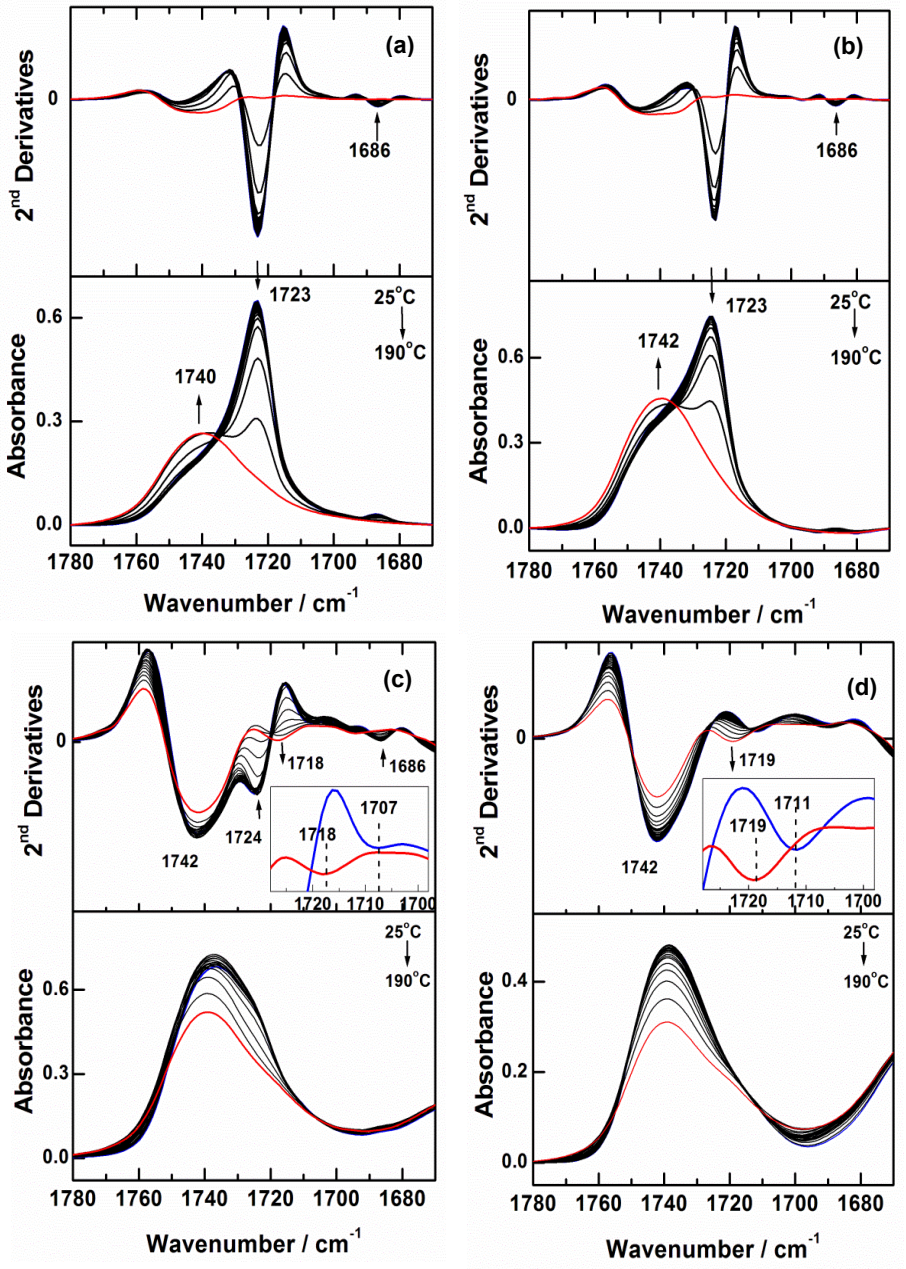

Figure 6. Temperature-dependent IR spectra (bottom) and their second derivatives (top) in the C=O stretching band region of PHB wt %: (a) 100, (b) 70, (c) 50 and (d) 30.

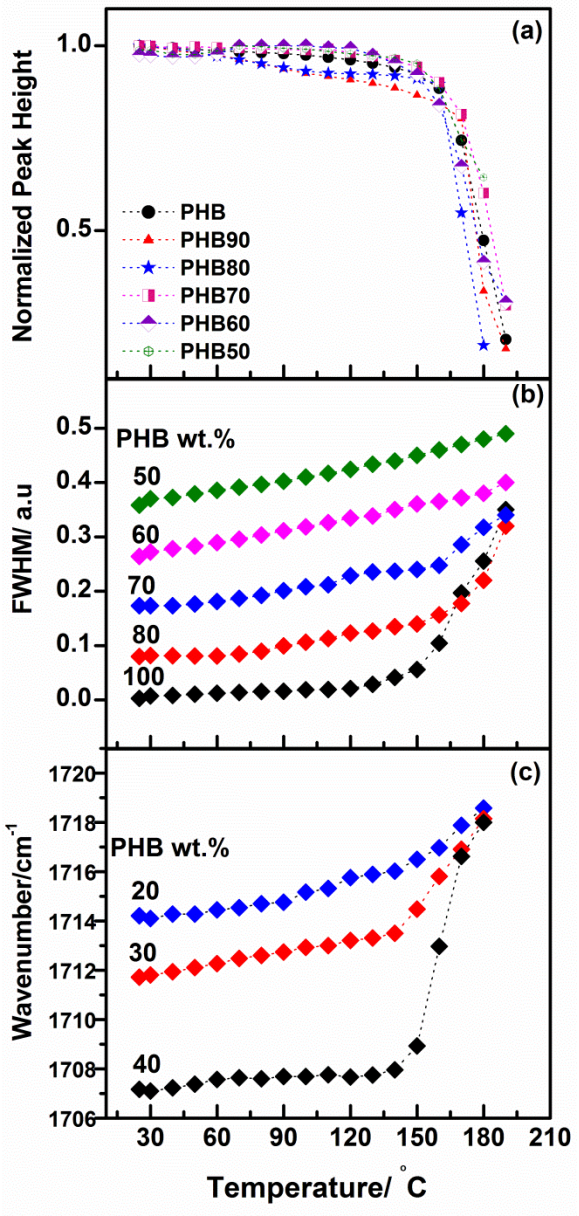

Figure 7. (a) Plots of the normalized peak height at 1723 cm^{-1} versus temperature, (b) plots of the full width at half maximum (FWHM) of *free* C=O band at 1747 cm^{-1} of PHB versus temperature, and (c) plots of wavenumber shift of *inter* C=O band versus temperature for blends with PHB: 40, 30 and 20 wt % (all during heating process).

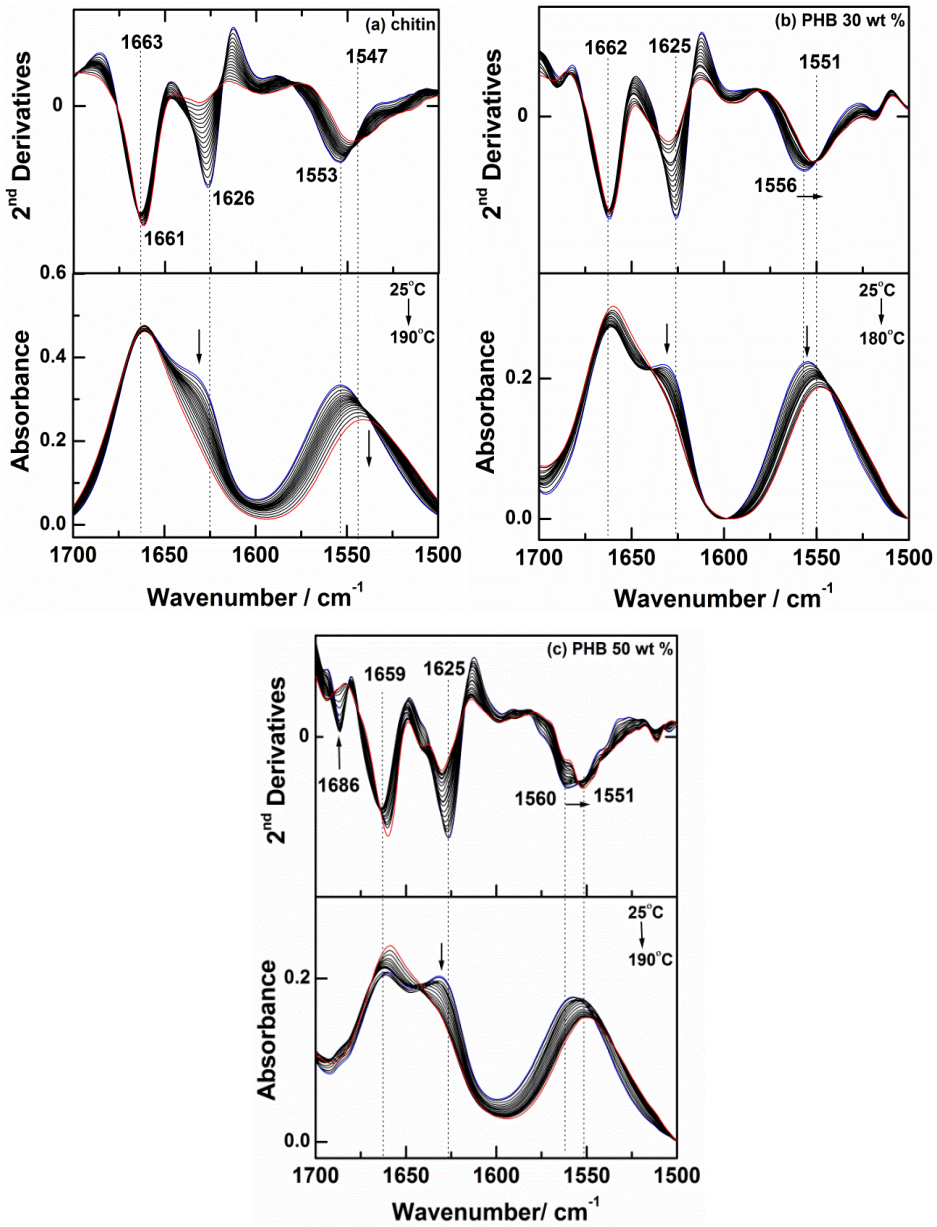

Figure 8. Temperature-dependent IR spectra (bottom) and their second derivatives (top) in the 1700-1500 cm^{-1} region of (a) chitin, (b) PHB 30 wt % and (c) PHB 50 wt %.

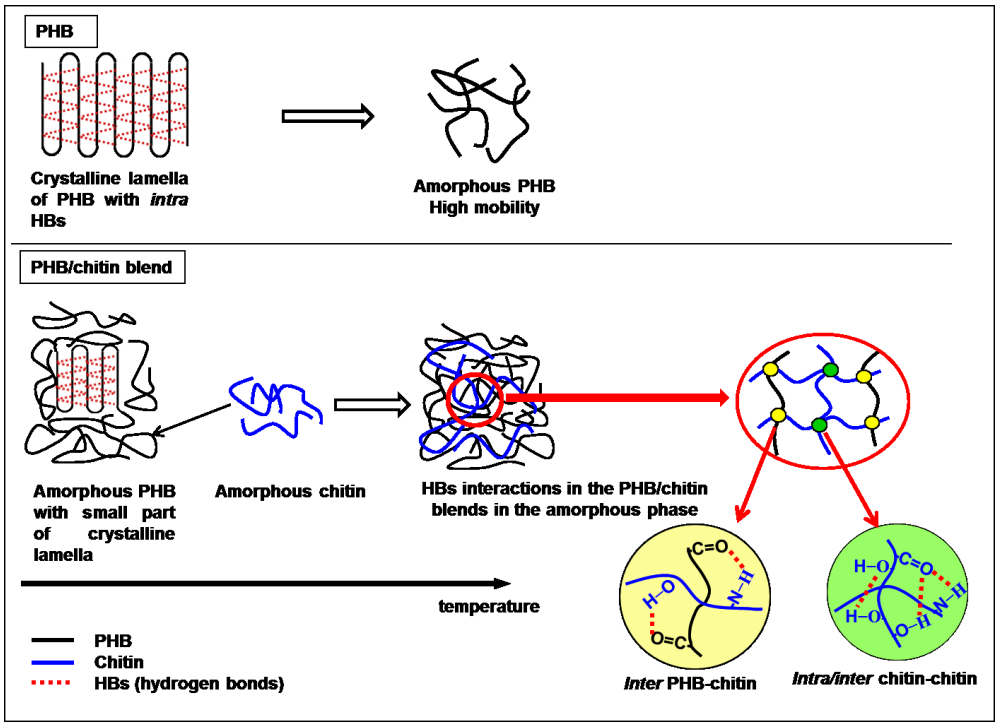

Figure 9. Sketch of the structure changes for PHB (up) and PHB/chitin blends with PHB ≤ 50 wt % (below) and the formation of intermolecular PHB-chitin hydrogen bonds in the amorphous phase.

Chapter 2

Evolution of Intermediate and Highly-ordered Crystalline States Under Spatial Confinement in Poly(3-hydroxybutyrate) Ultrathin Films

ABSTRACT

The crystallization behavior and crystalline structures of poly(3-hydroxybutyrate) (PHB) ultrathin films (~52 nm) under spatial confinement were investigated using infrared reflection-absorption spectroscopy (IRRAS) and two-dimensional grazing incidence X-ray diffraction (2D-GIXD). Intermediate and highly-ordered crystalline states were observed during heating and melt-cooling of these films. In the ultrathin films, the intermediate state was noticeably stable at lower temperatures, whereas the highly-ordered state was more stable at higher temperatures. A transformation from the intermediate state into the highly-ordered state occurred as the temperature increased, as the crystals in the intermediate state acquire sufficient thermal energy to overcome the energy barrier. 2D-GIXD results show that the intermediate state was dominant in edge-on-lamellae configuration where the crystallographic *b*-axis is normal to the film surface. Meanwhile, the highly-ordered state was predominant in flat-on lamellae configuration where the *b*-axis is parallel to the film surface. In the surface region, crystals strongly tended to align in an edge-on lamellae configuration.

1. INTRODUCTION

Ultrathin films of polymeric materials have become more and more desirable for use in a variety of current devices as criteria demand become lighter, thinner and smaller. Applications for such films include coatings, selective membranes, electronic sensors, solar cells, packaging, and biomedical materials.[1–4] The thickness of films < 100 nm (so-called ultrathin film) is comparable to the average polymer coil size and considered as a typical one-dimensional confinement system.[5–7] As such, their physical properties including morphology,[8,9] glass transition temperature (T_g),[10–12] mobility[13,14] and crystallization behavior[15–18] are appreciably different from those of the bulk material. In such thin films, the effects from surface/interface and confinement effects can be dominant factors for influencing the nucleation and preferred alignment of crystals during the crystallization process.

The terms “edge-on lamellae” and “flat-on lamellae” are often used for specific crystal orientations to indicate that the chain axis is parallel or normal to the surface substrate, respectively.[5] For example, dynamic Monte Carlo simulations of polymer thin films with thicknesses comparable to the polymer coil size show dominant edge-on lamellae formation on slippery walls and flat-on lamellae dominance on sticky walls, particularly at high temperatures.[6] Edge-on lamellae have also been observed in a high-density polyethylene (HDPE) film at a thickness < 100 nm.[19] Generally, it can be assumed that

dominant edge-on lamellae are formed at low temperatures in surface regions, while flat-on lamellae are mainly formed at high temperatures in substrate-interface regions.[20,21] On the other hand, oriented ultrathin films can be induced through recrystallization on oriented substrates, such as carbon-coated polyethylene.[22–23] Hence, understanding the crystallization and crystal structure under confined geometries is very crucial in the field of polymer science and nanotechnology engineering.

Poly(3-hydroxybutyrate) (PHB) is one of the most comprehensively studied biodegradable polymers, with physical properties similar to isotactic polypropylene (*i*PP),[24–26] and is considered a promising alternative material for a number of different applications. Crystalline PHB is orthorhombic with the space group $P2_12_12_1$ (a = 5.76 Å, b= 13.20 Å, and c = 5.96 Å (fiber axis)).[27] PHB is known to have unique weak hydrogen bonding (C–H···O=C) along the *a*-axis direction between CH_3 groups in one helical chain and C=O groups in another helical chain.[28–31] Since the direction of these hydrogen bonds is nearly parallel to the lamellae folding direction, this interaction may be responsible for stabilizing the lamella crystals.[31] PHB is also a good candidate for studying polymer crystallization from the melt because of the presence of low level heterogeneous nuclei, due in turn to its high stereoregularity and crystallinity.[32,33] Nevertheless, as in the case for many other polymeric materials, information about the crystalline structure and the crystallization behavior of PHB ultrathin films is still limited.

Mori et al.[34] reported two kinds of crystallites in P(HB-*co*-HHx) thin films (ca. 82.8 nm thick) with different *b*-axis dimensions from the split of the (020) Bragg reflections in grazing incidence X-ray diffraction (GIXD). A shorter *b*-axis arises from densely-folded lamellae corresponding to the stable state, while a longer axis indicates loosely-packed lamellae corresponding to the metastable state. Recently, Sun et al.[20] studied the crystallization behavior of PHB thin films on Si wafers using GIXD. They observed the change of lamellar orientation from the *b*-axis perpendicular to the surface to the *c*-axis perpendicular to the surface by changing the annealing temperature, due to the influence of free surface and buried interface effects, respectively. Furthermore, they reported that the melt-crystallization of PHB on poly(vinylphenol) (PVPh) layer was significantly inhibited due to the interdiffusion between PHB and PVPh.[35] Crystallization of PHB also significantly decreased after the addition of small amounts of high molecular weight poly($_{L}$-lactic acid) (PLLA).[36] A new band appears in the PHB/high molecular weight PLLA blends at 1731 cm^{-1}, corresponding to the intermediate state band. Unfortunately, information about the crystalline structure and behavior in the intermediate state was still incomplete in this study.

The findings by our group related to the intermediate state[37–40] are important points for understanding the crystallization behavior of PHB, although a widely-accepted definition of the intermediate state has not yet been established. Our group observed a weak feature at

1731 cm^{-1} during the crystallization of bulk PHB from the spectral variation of infrared (IR) spectroscopy and two-dimensional correlation spectroscopy (2DCOS) analysis. The 1731 cm^{-1} band is assigned to an intermediate state of the C=O stretching band that can be reconciled with the concepts proposed by Strobl.[41]

In the present study, we have explored the crystallization behavior and role of the intermediate state in the crystallization of PHB ultrathin films, which are expected to differ from those of the bulk, using several surface-sensitive techniques including infrared-reflection absorption spectroscopy (IRRAS), X-ray reflectivity (XRR), and two-dimensional grazing incidence X-ray diffraction (2D-GIXD). In particular, we have focused our study on the nucleation sites, growth, preferred orientation, and crystalline structure of the intermediate state and those of the highly-ordered crystalline state of PHB confined in ultrathin films during heating and melt-cooling processes. Moreover, we have meticulously studied the transformation from the intermediate state to the highly-ordered state assisted by thermal energy. A unique stable feature of the intermediate state was found after the melt-cooling process, which has not been previously observed in bulk PHB. In the GIXD study, the crystalline peaks measured in the out-of-plane and in-plane geometries with two different angles of incidence are discussed, indicating nucleation sites and preferred orientations that are strongly dependent on the films and thermal processes involved. To the best of our knowledge, this is the first IRRAS and X-ray study that

unambiguously demonstrates the anomalously stable intermediate structure and transformation to a highly-ordered structure in PHB ultrathin films.

2. EXPERIMENTAL SECTION

2-1. Materials and Sample Preparation

Bacterially synthesized PHB purchased from Aldrich Co., Ltd., was purified by being dissolved in hot chloroform, precipitated in methanol and vacuum dried at 60 °C. PHB was diluted in chloroform for use in spin coating, at rotating speeds and spin coating times of 4000 rpm and 45 s, respectively. Flat Au substrates were used for IRRAS, while Si (100) wafers were used for GIXD measurements. Prior to measurement, the films were dried and annealed under low vacuum at 60 °C for 12 h. The typical thickness of PHB ultrathin films was ca. 52 nm.

2-2. IRRAS Spectroscopy

Specular reflectance IRRAS spectra were measured using a Thermo Nicolet 6700 FTIR spectrometer equipped with a MCT detector. A reflection attachment (Spectra-Tech. FT80 RAS) with an incident angle of 80° was attached to the spectrometer together with a rotatable wire-grid polarizer of KRS5-substrate (ST Japan). The temperature was controlled using a temperature controller CHINO (model SU) and the spectra were collected at 2 cm^{-1} resolution with 256 scans. The film was heated and cooled at a rate of

2 °C/min and maintained at a constant temperature for 3 min prior to each measurement.

2-3. X-ray Diffraction

XRR profiles were collected at room temperature using a Rigaku SmartLab with CuKα radiation (Rigaku Co.) The thicknesses of the PHB thin films were determined by nonlinear least squares fitting of the XRR profiles with software developed in-house (Figure 1). The film thickness dependence is almost linear to the concentration, these values were confirmed to be reproducible. 2D-GIXD measurements were conducted with a multi-axis diffractometer installed at BL03XU of SPring-8, Japan, at a wavelength = 0.1 nm and critical angle for total reflection $\theta_c = 0.094°$. Out-of-plane and in-plane diffraction profiles were simultaneously collected using an image plate detector (R-AXIS IV, Rigaku Co.) The angle of incidence was set at 0.114° ($1.21\theta_c$) and 0.074° ($0.79\theta_c$) in order to obtain information about the crystallites in all regions of the film and in the narrow surface region, respectively.

3. RESULTS AND DISCUSSION

3-1. Temperature-dependent of IRRAS spectroscopy

C=O stretching region. Figure 2a shows IRRAS spectra and their second derivatives in the C=O stretching region of a PHB ultrathin film (52 nm thickness). Hereinafter, the blue curves in all IRRAS spectra indicate spectra measured at room temperature, while red

curves indicate spectra collected at an elevated temperature. The spectra in Figure 2a show two bands at 1726 and 1750 cm^{-1}. The intensity of the 1726 cm^{-1} band gradually decreases with temperature, eventually vanishing at 130 °C; conversely, the intensity of the 1750 cm^{-1} band increases with temperature. Although the band positions of these two modes are slightly different from the transmission spectra of bulk PHB (1723 and 1740 cm^{-1} for the C=O crystalline and amorphous mode, respectively),[42] we assigned the bands at 1726 and 1750 cm^{-1} to the C=O stretching crystalline and amorphous modes, respectively.

The relative intensity of the 1726 cm^{-1} band in the IRRAS spectra is lower than that of the corresponding C=O crystalline band at 1723 cm^{-1} in the transmission spectra of bulk PHB. IRRAS is sensitive to the configuration of molecules, especially for vibrational modes having transition moments perpendicular to the film surface, which become more intense.[43,44] The lower intensity of the 1726 cm^{-1} bands in the IRRAS spectra is likely to show that the C=O stretching of PHB in ultrathin films is aligned nearly parallel to the film surface, although we cannot unambiguously exclude the possibility of low crystallinity that is often observed for ultrathin films.[17,46] Since many PHB crystallites in ultrathin films grow along the *b*-axis normal to the surface[20,34] and the C=O bond is known to be perpendicular to the *c*-axis,[27,45] the C=O stretching should be preferentially oriented along the *a*-axis. The temperature at which the C=O crystalline band completely melts at 130 °C is much lower than the melting temperature of bulk PHB (~ 172 °C). This result indicates

that crystallization in confined environments is often inhibited, resulting in decreased crystallinity,[18,46–48] which is in accordance with the fact that the sample consists of many small crystallites that often have lower melting points.[18,49]

Figure 2b presents plots of wavenumbers for the amorphous and crystalline bands versus temperature, clearly shows a gradual shift of the C=O crystalline peak position to a lower frequency by approximately 4 cm^{-1} during the heating process. This sort of peak shift was not previously observed for bulk PHB. According to these observations, the C=O crystalline band contains a few different bands originating from the different crystalline structures with different IR frequencies. Based on the previous studies of bulk PHB,[37–40] it is likely that the PHB crystalline phase contains two kinds of crystalline structures, those being less ordered (imperfect) crystalline structure (presumably as the intermediate state) with a higher C=O frequency, and highly-ordered crystalline structure with a lower C=O frequency. Furthermore, a noticeable shift of the crystalline band from 1726 cm^{-1} to lower frequencies suggests a transformation of the intermediate state into the highly-ordered state as the temperature increases. In order to prove the existence of two kinds of crystalline structures and quantify their relative contents in the ultrathin films, we decomposed the IRRAS spectra shown in Figure 2a by Gaussian fitting into the amorphous, intermediate and highly-ordered crystalline fractions (Figures 3a–b), and the integrated intensity of each fraction is plotted in Figure 3c.

Figure 3a shows that the intermediate state is dominant prior to the heating process. During the heating process, the intensity of the intermediate state gradually decreases as depicted in Figure 3b–c. Figure 3c reveals that the decrease in the volume fraction of the intermediate state and the increase in that of the highly-ordered state occur simultaneously, with the most prominent variation present at around 70−100 °C. On the other hand, the intensity of the amorphous fraction increases only gradually up to 100 °C. These results indicate that the transformation of less ordered crystals (intermediate state) into highly-ordered crystalline structures at higher temperatures, which afford sufficient energies to overcome the activated energy needed for recrystallization into highly-ordered crystalline structures.

Figure 4 presents the IRRAS spectra in the C=O stretching region collected during the crystallization process terminated at room temperature; three obvious bands are present at 1750, 1731 and 1722 cm^{-1}. Initially, only a broad amorphous band was observed in the melt state, whose intensity decreases with decreasing temperature. Simultaneously, the two crystalline bands at 1731 and 1722 cm^{1} appear at approximately 80 °C, and for both peaks the intensity increases with decreasing temperature. However, the intensity of those two crystalline bands is much smaller than the C=O crystalline band at 1726 cm^{-1} as shown in Figure 2. This indicates that the melt-cooling process changes the direction of the dipole moments of C=O crystalline modes away from the surface normal direction. According to

previous reports, the 1750 cm^{-1} band corresponds to the C=O stretching amorphous mode, while the 1731 and 1722 cm^{-1} bands are the C=O stretching modes of the intermediate state and highly-ordered crystalline state, respectively.[37–40] The intermediate state in the PHB ultrathin film behaves quite differently from the intermediate state of bulk PHB. The intermediate state band at 1731 cm^{-1} is clearly detected in ultrathin films even after the crystallization process is finished, while in bulk PHB the corresponding band only appears during the crystallization process at a very small intensity, and is hardly present after the crystallization is finished.[37] Two speculations that can explain such a stable character of intermediate state observed in the melt-cooled ultrathin films: (1) Thermodynamically stability that the intermediate state acquires with substrate and/or free surface; (2) Slow kinetics as a result of the confined effects associated with an enhanced activation energy for the transformation to the stable state. To determine which factor is dominant in the PHB ultrathin films, the temperature scan rate dependence must be detected, which would be one of the measurements to be accomplished in the near future. Such a feature of intermediate state of PHB, peculiar to the ultrathin films, could be a factor for explaining the reduced crystallinity in the surface region.

For quantitative discussion, we decomposed the IRRAS spectra shown in Figure 4 using Gaussian fittings into highly-ordered and intermediate crystalline fractions, amorphous and another feature developed at 1737 cm^{-1} which overlaps with the band due

to the C=O intermediate state (typical result is depicted in Figure 5). Since the three-peak fitting successfully performed for the spectra collected during the heating process (Figures 2 and 3) had failed for the melt-cooling data, the fourth peak was added to see the proper fitting. The fourth peak corresponds to the 1737 cm^{-1} band was previously reported by Unger et al. and it was assigned as an amorphous with some structural order.[51-53] Hereinafter, the bands at 1737 and 1748 cm^{-1} were assigned as an ordered-amorphous band and a disordered amorphous band, respectively.

In the initial crystallization stage as depicted in Figure 5a, the amorphous phase is dominant, while the crystalline phase in the intermediate and highly-ordered states are only minor components. When the crystallization at room temperature finished after the melt-cooling process, the intensity of amorphous bands at 1748 and 1737 cm^{-1} decreased, whereas the 1722 and 1731 cm^{-1} bands became more intense and well-resolved (Figure 5b). The thermal behavior of the ordered-amorphous band at 1737 cm^{-1} is in contrast to that of the intermediate state band at 1731 cm^{-1}; the intensity of 1737 cm^{-1} band decreased while the intensity of 1731 cm^{-1} band increased simultaneously, as depicted in Figure 5c. This result implies that the crystals in the intermediate state are trapped and quiescent in the ordered-amorphous phase of thin films. This is may be another reason why the intermediate state is rather stable after crystallization from the melt.

Figure 5c shows that upon the cooling process at least until 70°C, the intensity of

intermediate state and both amorphous phases is decreased, whereas the intensity of the highly-ordered state band is slightly increased with decreasing temperature. The enhanced intensity of the highly-ordered band is in accordance with the behavior of the intermediate state band. The decreased intensity of the C=O intermediate state band is related to the enhanced intensity of the C=O highly-ordered state band above 70 °C. A drastic increase in the intermediate state from 70 °C to room temperature probably reflects the transformation from amorphous state to the intermediate state.

The C−H stretching region. Figure 6 shows IRRAS spectra of a PHB ultrathin film in the C−H stretching region during (a) heating and (b) melt-cooling processes. In the C−H stretching region, there is a band arising from a weak intermolecular C−H···O=C hydrogen bond of the asymmetric CH_3 stretching mode, which can be monitored from the unusual C−H stretching frequency at 3009 cm^{-1}.[28–31] Note that in Figure 6a, the weak hydrogen bonding band is observed as a shoulder band at 3009 cm^{-1}. Bands at 2996 and 2967 cm^{-1} are assigned to the CH_3 asymmetric stretching modes, and those at 2934 and 2873 cm^{-1} are the CH_2 antisymmetric stretching mode and the CH_3 symmetric stretching mode, respectively.[30,54] The appearance of the 3009 cm^{-1} band indicates that weak intermolecular C−H···O=C hydrogen bonding is still present in the PHB ultrathin film along the *a*-axis. Similar to bulk PHB,[42,54] the 3009 cm^{-1} band becomes weaker as the temperature increases and vanishes in the melting state. Presumably, the C−H bond of C−H···O=C

hydrogen-bonding aligned in the same direction as the C=O bond, which is nearly parallel to the substrate surface.

Figure 6b depicts the C−H stretching region of a PHB ultrathin film during the melt-cooling process. Six crystalline bands are present at 3007, 2994, 2976, 2931, 2872 and 2854 cm^{-1} after the crystallization process. Compared to the corresponding bands in Figure 5a, the positions of these bands are shifted by 2 cm^{-1} to lower wavenumbers. Since this shift is almost the same magnitude as the resolution of our IRRAS spectroscopy, it is difficult to determine whether the strength of the C−H···O=C hydrogen bonding is altered or not. However, it is reasonable for us to assume that the strength of the hydrogen bonds is altered during the crystallization, since we know that the strength can vary with temperature and may be different between the intermediate state and the highly-ordered state. The shift of the C−H stretching band from 2878 to 2872 cm^{-1} generally indicates the transition from disordered to ordered conformations during crystallization.[37] Another interesting feature in Figure 6b is that the 3007 cm^{-1} band becomes more prominent via the melt-cooling process compared with the heating process. This result indicates that the number of oriented hydrogen bonds nearly perpendicular to the film surface increases during the thermal process as well as in the highly-ordered and the intermediate states.

3-2. Temperature-dependent 2D-GIXD

Figure 7 shows 2D-GIXD images of a PHB ultrathin film with thickness ca. 52 nm collected at (a) 30 °C, (b) 120 °C and (c) 30 °C after cooling. Because the angle of incidence of the X-ray beam was set at 0.114° (corresponding to 1.21 times of the critical angle for total reflection, θ_c), the X-ray can fully penetrate the entire region of the film, giving structural information on crystallites in all the regions of the film. In Figure 7a, the (020) Bragg reflection observed in the out-of-plane direction (the vertical direction in Figure 7) is dominant, while the (020) Bragg reflection observed in the in-plane direction (the horizontal direction in Figure 7) is relatively weak, indicating that for almost all crystallites in the film, the *b*-axis is perpendicular (*a* and *c*-axis are parallel) to the film surface. Moreover, the weak (020) Bragg reflection observed in the in-plane direction indicates that crystallites in which the *b*-axis direction is parallel to the film surface are minor components in the film. Hereafter, we refer to the crystallites having (020) Bragg reflections in the out-of-plane direction and in the in-plane lamellae as “edge-on lamellae” and “flat-on lamellae”, as in Ref. 34.

Crystallinity in the films increases with increasing temperature, since other weak Bragg reflections, i.e. (040), (031), (021) and (111) Bragg reflections are observed to increase with temperature (Figure 7b). The 2D-GIXD image after cooling from 120 to 30 °C (Figure 7c) is very similar to the one collected before the thermal process (Figure 7a).

In order to analyze the edge-on lamellae and flat-on lamellae in more detail, diffraction profiles of the (020) Bragg reflections are constructed from the 2D-GIXD images (Figures 8 and 9). In comparison with the previous GIXD study on P(HB-*co*-HHx) thin films using a conventional scintillation detector,[34] the present 2D-GIXD results can reveal novel aspects of the intermediate and highly-ordered states.

Figure 8a shows the one-dimensional (1D) profiles of (020) Bragg reflection along the out-of-plane direction, representing the temperature evolution of edge-on lamellae in the film. The (020) peak profile, which is quite broad before the heating process, becomes narrower as the temperature increases. However, after being cooled from 120 °C, we obtained a broader profile at 30 °C, similar to the initial profile. As the temperature increases, the peak position shifts from a 2θ value of 8.7° to a higher 2θ value; both are shown by the two vertical dotted lines in Figure 8a. Figure 8b shows an example of the profile of a (020) Bragg reflection fitted by the sum of two Gaussians, demonstrating the reconstruction by two (020) reflections appearing at around 2θ= 8.8° and 9.0°. The (020) reflection at lower 2θ (hereinafter called $(020)_L$) is believed to arise from the crystallites in the intermediate state, since it was initially dominant but decreased with temperature (Figure 8c). Meanwhile, the (020) reflection at higher 2θ (hereinafter called $(020)_H$) is attributed to the highly-ordered structure of the thermodynamically favorable state.

Figure 8c unambiguously indicates the thermal-energy-assisted transformation of the

intermediate state, since the volume of each state is proportional to the intensity of $(020)_L$ and $(020)_H$. It is interesting to see the recovery of the $(020)_L$ reflection after cooling (the blue curve in Figure 8a), presumably related to the stability of the intermediate state in ultrathin films observed in the present IRRAS data.

Figure 9a shows the 1D-profiles of (020) Bragg reflection along the in-plane direction, representing the temperature evolution of flat-on lamellae in the film. Since the intensity of the (020) reflection observed in the in-plane direction is about half that of the out-of-plane direction, PHB crystallites in ultrathin films are largely formed as edge-on lamellae. Interestingly, the flat-on lamellae also exhibit the two types of crystallites whose peak positions are shown by the two vertical dotted lines in Figure 9a. Figure 9b depicts the fitted profile of the (020) reflection along the in-plane direction, in which the $(020)_L$ and $(020)_H$ reflections are centered at around $2\theta = 8.59°$ and 8.79°, respectively. To the best of our knowledge, this is the first study on two types of PHB crystallites of flat-on lamellae in thin films. It is worth highlighting here that in flat-on lamellae, the stable state was already dominant in pristine film at 30 °C (Figure 9b) and showed a slight increase with temperature (Figure 9c), in sharp contrast to the behavior of the edge-on-stable state lamellae shown in Figure 8. Furthermore, we must acknowledge that the stable character of the intermediate state in flat-on lamellae (which gives the $(020)_L$ intensity in Figure 9c), especially below 50 °C, shows a striking contrast with that of the intermediate state in

edge-on lamellae shown in Figure 8c, where the monotonous decrease $(020)_L$ is seen with increasing temperature. Figure 9c shows that the intensity of $(020)_H$ gradually increases with temperature, presumably indicating that a small number of flat-on-intermediate crystallites have sufficient energy to transform into flat-on-highly-ordered crystallites, although the $(020)_L$ reflection steadily decreases above 50 °C. Such remarkable decrease in the $(020)_L$ intensity above 50 °C may indicate continuous melting of flat-on-intermediate state lamellae in the films.

Since the different thermal behavior of the (020) reflections along the out-of-plane and in-plane directions is expected to reflect the distribution of edge-on lamellae and flat-on lamellae in the thin films, we collected 2D-GIXD images at a very shallow incidence angle of 0.074° ($0.079\theta_c$) which only affords the Bragg reflection from crystallites in the surface region approximately 8 nm deep from the film surface (Figure 10). In Figure 10a, we can see a strong (020) reflection in the out-of-plane direction and a very faint (020) reflection in the in-plane direction. This indicates that the edge-on lamellae mainly form in the surface region, while flat-on the lamellae likely grow in the interfacial region between the substrate and PHB.

Figure 11 illustrates selected results obtained from the 2D-GIXD images. At low temperatures, the intermediate state of the edge-on lamellae is dominant in the surface region, whereas in the interface region the highly-ordered state of flat-on lamellae also

form. By increasing the temperature, many edge-on lamellae as well as flat-on lamellae in the intermediate state transform into the highly-ordered state. On the other hand, only a few edge-on lamellae and flat-on lamellae of the intermediate state could be reduced by increasing the temperature, due to the pre-melting of very less-ordered small crystallites. In addition, the melting point of such small crystallites is greatly influenced by the size distribution of less-ordered nanocrystallites and the heterogeneous environment peculiar to ultrathin films, both of which would give rise to the observed continuous melting behavior.

4. CONCLUSION

The crystallization behavior and crystalline structure of PHB ultrathin films under spatial confinement were studied using IRRAS and GIXD. Unique PHB crystals in both the intermediate state and the highly ordered crystalline state were observed during the heating and melt-cooling processes. The crystals in the intermediate state transform into the highly-ordered structures after receiving sufficient thermal energy at high temperatures. A remarkably stable intermediate state trapped in the ordered amorphous matrix is observed after crystallization from the melt-cooling process. The formation of such an intermediate state can be one of the factors responsible for the reduced crystallinity of PHB thin films, apart from the thickness confinement effect. 2D-GIXD measurements confirmed that in PHB ultrathin films, the major crystals mainly form as edge-on lamellae

and a minor portion form as flat-on lamellae. Regardless of the lamellae type, the crystalline consists of both the intermediate state and the highly-ordered state. Edge-on-intermediate state lamellae transform into edge-on-highly-ordered state lamellae as temperature increases, which agrees with the IRRAS results. For flat-on lamellae, the highly-ordered state is dominant even in pristine films, whereas the intermediate state is dominant for edge-on lamellae. In the surface region, the edge-on lamellae formation is more favorable.

REFERENCES

1. Bertrand, P.; Jonas, A.; Laschewsky, A.; Legras, R. *Macromol. Rapid. Commun.* **2000**, *21*, 319–348.
2. Cao, Q.; Rogers. J. A. *Adv. Mater*. **2009**, *21*, 29–53.
3. Hong, J-M.; Anderson, P. E.; Qian, J.; Martin, C.R. *Chem. Mater*. **1998**, *10*, 1029–1033.
4. Vendra, V. K.; Wu, L.; Krishnan, S. *In* Nanomaterials for the Life Sciences Vol. 5: Nanostructured Thin Films and Surfaces; Kumar, C. S. S. R., Ed.; Willey-VCH: Weinheim, 2010; p 1–54.
5. Liu, Y.-X.; Chen, E.-Q. *Coord. Chem. Rev.* **2010**, *254*, 1011–1037.
6. Ma Y.; Hu, W.; Reiter G. *Macromolecules* **2006**, 39, 5159–5164.

7. Müller, A. J.; Arnal, M. L.; Lorenzo, A. T. *In* Handbook of Polymer Crystallization; Piorkowska, E., Rutledge, G. C., Eds.; Willey: New Jersey, 2013, p 367.

8. Abe, H.; Kikkawa, Y.; Iwata, T.; Aoki, H.; Akehata, T.; Doi, Y. *Polymer* **2000**, *41*, 867–874.

9. Taguchi, K.; Miyaji, H.; Izumi, K.; Hoshino, A.; Miyamoto, Y.; Kokawa, R. *Polymer* **2001**, *42*, 7443–7447.

10. Yang, C.; Onitsuka, R.; Takahashi, I. *Eur. Phys. J. E*. **2013**, *36*: 66.

11. Fryer, D. S.; Nealey, P. F.; de Pablo, J. J. *Macromolecules* **2000**, *33*, 6439–6447.

12. Forrest, J. A.; Mattsson, J. *Phys. Rev. E* **2000**, *61*, R53–56.

13. Frank, B.; Gast, A. P.; Russell, T. P.; Brown, H. R.; Hawker, C. *Macromolecules* **1996**, *29*, 6531–6534.

14. Lin, E. K.; Kolb, R.; Satija, S. K.; Wu, W. *Macromolecules* **1999**, *32*, 3753–3757.

15. Frank, C. W.; Rao, V.; Despotopoulou, M. M.; Pease, R. F. W.; Hinseberg, W. D.; Miller, R. D.; Rabolt, J. F. *Science* **1996**, *273*, 912–915.

16. Schönherr, H.; Frank, C. W. *Macromolecules* **2003**, *36*, 1188–1198.

17. Despotopoulou, M. M.; Frank, C. W.; Miller, R. D.; Rabolt, J. F. *Macromolecules* **1996**, *29*, 5797–5804.

18. Wang, Y.; Ge, S.; Rafailovch, M.; Sokolov, J.; Zou, Y.; Ade, H.; Lüning, J.; Lustiger, A.; Maron G. *Macromolecules* **2004**, *37*, 3319–3327.

19. Mellbring, O.; Kihlman Øiseth, S.; Krozer, A.; Lausmaa, J.; Hjerberg, T. *Macromolecules* **2001**, *34*, 7496–7503.

20. Sun, X.; Guo, L.; Sato, H.; Ozaki, Y.; Yan, S.; Takahashi, I. *Polymer* **2011**, *52*, 3865–3870.

21. Reiter, G.; Botiz, I.; Graveleau, L.; Grozev, N.; Albrecht, K.; Mourran, A.; Möller, M. *In* Lecture Notes in Physics: Progress in Understanding of Polymer Crystallization; Reiter, G., Strobl, G. R., Eds.; Springer-Verlag: Berlin, 2007, p 195.

22. Yan, S. *Macromolecules* **2003**, *36*, 339–345.

23. Chang, H.; Guo, Q.; Shen, D.; Li, L.; Qiu, Z.; Wang, F.; Yan, S. *J. Phys. Chem. B* **2010**, *114*, 13104–13109.

24. Zhao, Q.; Cheng, G. *In* New Frontiers in Polymer Research; Bregg R.K., Ed.; Nova Science Publishers Inc.: New York, 2006, p 99–124.

25. Sudesh, K.; Abe, H.; Doi, Y. *Prog. Polym. Sci*. **2000,** *25*, 1503–1555.

26. Satkowski, M. M.; Melik, D. H.; Autran J-P.; Green, P. R.; Noda, I. Schechtman, L. A. *In* Biopolymers: Polyesters II-Properties and Chemical Synthesis; Steinbuchel, A., Doi, Y., Eds.; Wiley-VCH: Weinheim, 2001, vol. 3b, p 231-263.

27. Yokouchi, M.; Chatani, Y.; Tadokoro, H.; Teranishi, K.; Tani, H. *Polymer* **1973**, *14*, 267–272.

28. Sato, H.; Ando, Y.; Dybal, J.; Iwata, T, Noda, I.; Ozaki, Y. *Macromolecules* **2008**, *41*,

4305–4312.

29. Sato, H.; Mori, K.; Murakami, R.; Ando, Y.; Takahashi, I.; Zhang, J.; Terauchi, H.; Hirose, F.; Senda, K.; Tashiro, K.; Noda, I.; Ozaki, Y. *Macromolecules* **2006**, *39*, 1525–1531.

30. Sato, H.; Murakami, R.; Padermshoke, A.; Hirose, F.; Senda, K.; Noda, I.; Ozaki, Y. *Macromolecules* **2004**, *37*, 7203–7213.

31. Sato, H.; Ando, Y.; Mitomo, H.; Ozaki, Y. *Macromolecules* **2011**, *44*, 2829–2837.

32. Barham, P. J.; Keller, A.; Otun, E. L.; Holmes, P. A. *J. Mater. Sci*. **1984**, *19*, 2781–2794.

33. Barham, P. J. *J. Mater. Sci*. **1984**, *19*, 3826–3834.

34. Mori, K.; Mukoyama, S.; Zhang, Y.; Sato, H.; Ozaki, Y.; Terauchi, H.; Noda, I.; Takahashi, I. *Macromolecules* **2008**, *41*, 1713–1719.

35. Sun, X.; Chen, Z.; Wang, F.; Yan, S.; Takahashi, I. *Macromolecules* **2013,** *46*, 1573–1581.

36. Sun, X.; Tokuda, A.; Oji, Y.; Nakatani, T.; Tsuji, H.; Ozaki, Y.; Yan, S.; Takahashi, I. *Macromolecules* **2012**, *45***,** 2485–2493.

37. Zhang, J.; Sato, H.; Noda, I.; Ozaki, Y. *Macromolecules* **2005**, 38, 4274–4281.

38. Padermshoke, A.; Katsumoto, Y.; Sato, H.; Ekgasit, S.; Noda, I.; Ozaki, Y. *Spectrochim. Acta, Part A*. **2005**, *61*, 541–550.

39. Padermshoke, A.; Katsumoto, Y.; Sato, H.; Ekgasit, S.; Noda, I.; Ozaki, Y. *Polymer* **2004**, *45*, 6547–6554.

40. Padermshoke, A.; Sato, H.; Katsumoto, Y.; Ekgasit, S.; Noda, I.; Ozaki, Y. *Vib. Spectrosc.* **2004**, *36*, 241–249.

41. Strobl, G. *Eur. Phys. J. E.* **2000**, *3*, 165–183.

42. Khasanah; Reddy, K. R.; Sato, H.; Takahashi, I.; Ozaki, Y. *Polymer* **2015**, *75*, 141–150.

43. Francis, S. A.; Ellison, A. H. *J. Opt. Soc. Am*. **1959**, *49*, 131–138.

44. Umemura, J. *In* Handbook of Vibrational Spectroscopy; Chalmers, J. M., Griffiths, P. R., Eds.; Wiley: Chichester UK, 2002, Vol. 2, p 982–998.

45. Sato, H.; Murakami, R.; Mori, K.; Ando, Y.; Takahashi, I.; Noda, I.; Ozaki, Y. *Vib. Spectrosc.* **2009**, *51*, 132–135.

46. Despotopoulou, M. M.; Miller, R. D.; Rabolt, J. F.; Frank, C. W. *J. Polym. Sci., Part B: Polym. Phys*. **1996**, *34*, 2335–2349.

47. Zhang, Q. M.; Xu, H.; Fang, F.; Cheng, Z.-Y.; Xia, F. *J. Appl. Phys*. **2001**, *89*, 2613–2616.

48. Urayama, K.; Tsuji, M.; Neher, D. *Macromolecules* **2000**, *33*, 8269–8279.

49. Ashraf, A.; Dissanayake, D. M. N. M.; Eisaman, M. D. *Phys. Chem. Chem. Phys*. **2015**, 17, 23326–23331.

50. DeMaggio, G. B.; Frieze, W. E.; Gidley, D. W.; Zhu, M.; Hristov, H. A.; Yee, A. F. *Phys.*

Rev. Lett. **1997**, *78*, 1524–1527.

51. Unger, M.; Morita, S.; Sato, H.; Ozaki, Y.; Siesler, H. W. *Appl. Spectrosc.* **2009**, *63*, 1027–1033.

52. Unger, M.; Morita, S.; Sato, H.; Ozaki, Y.; Siesler, H. W. *Appl. Spectrosc.* **2009**, *63*, 1034–1040.

53. Unger, M.; Sato, H.; Ozaki, Y.; Siesler, H. W. *Macromol. Symp.* **2011**, *305*, 90–100.

54. Sato, H.; Dybal, J.; Murakami, R.; Noda, I.; Ozaki, Y. *J. Mol. Struct.* **2005**, *744-747*, 35–46.

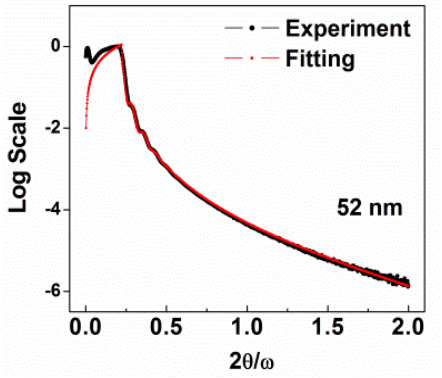

Figure 1. Typical X-ray reflectivity of PHB ultrathin film deposited on Si wafer.

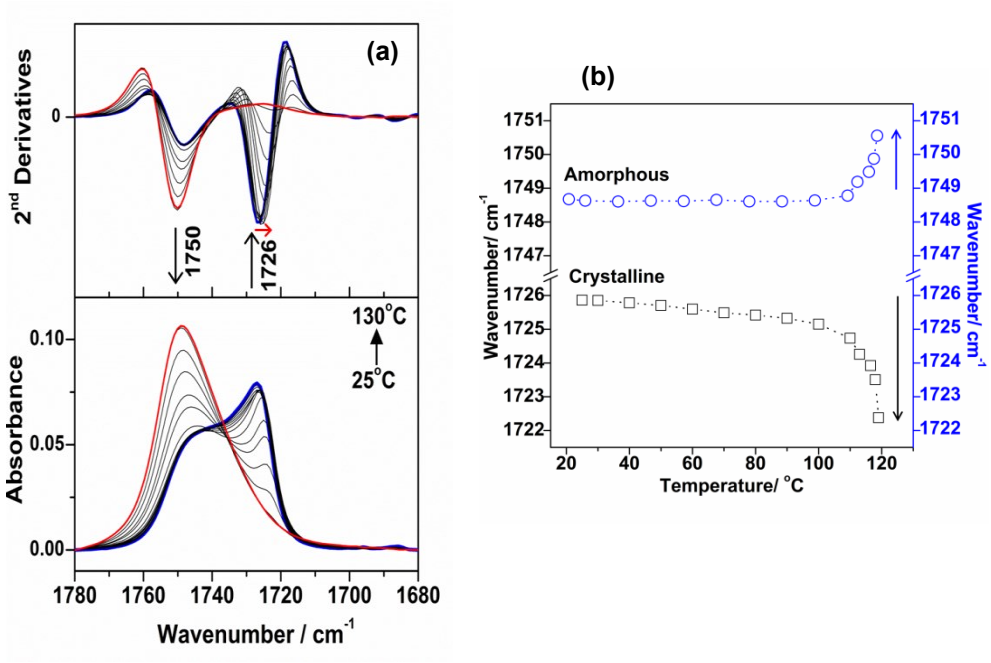

Figure 2. (a) IRRAS spectra (bottom) and their second derivatives (up) in the C=O stretching region of PHB ultrathin film collected during the heating process. (b) Shift plot of C=O crystalline and amorphous modes.

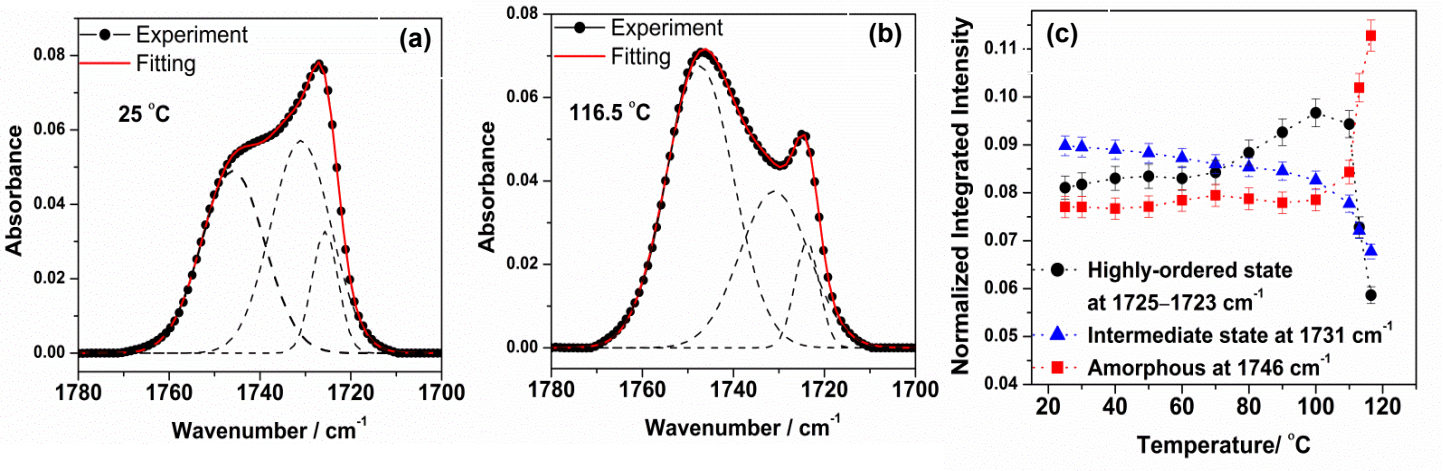

101

Figure 3. IRRAS spectra shown in Figure 2b fitted by sum of three Gaussians at (a) 25°C and (b) 116.5°C. (c) Plots of integrated intensity of amorphous, intermediate and highly-ordered states, each of which is normalized by the sum of integrated intensity of each fraction.

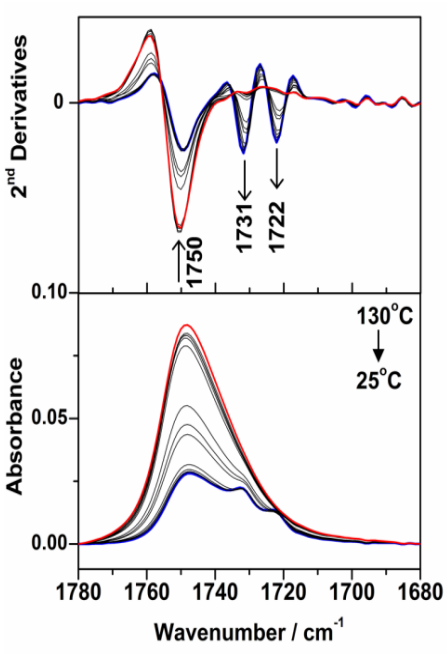

Figure 4. IRRAS spectra (bottom) and their second derivatives (up) in the C=O stretching region of PHB ultrathin film collected during the melt-cooling process.

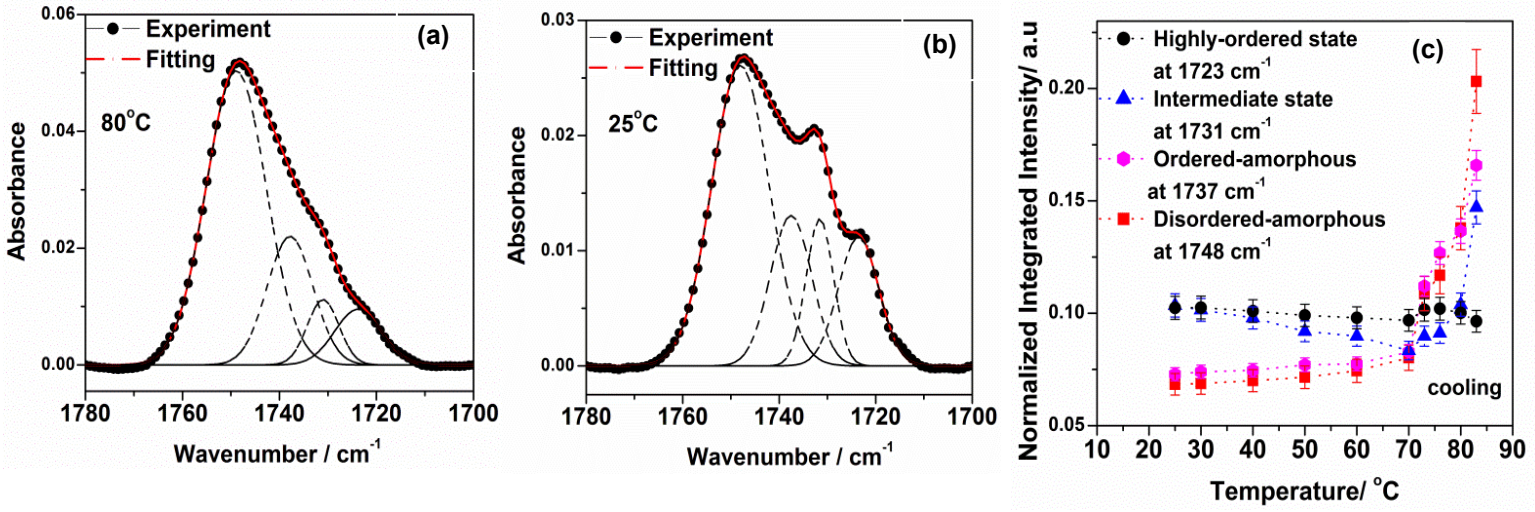

Figure 5. IRRAS spectra shown in Figure 4 fitted by sum of four Gaussians at (a) 80°C and (b) 25°C. (c) Plots of integrated intensity of amorphous, intermediate and highly-ordered crystalline states, each of which is normalized by the sum of integrated intensity of each fraction.

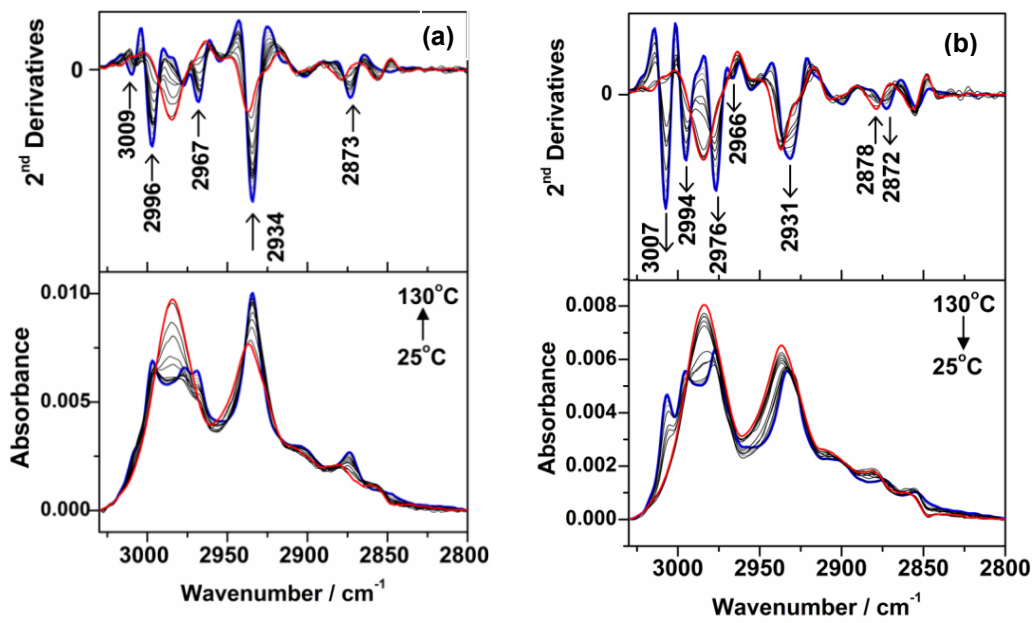

Figure 6. IRRAS spectra (bottom) and their second derivatives (up) in the C−H stretching region of PHB ultrathin film collected during (a) heating process and (b) melt-cooling process.

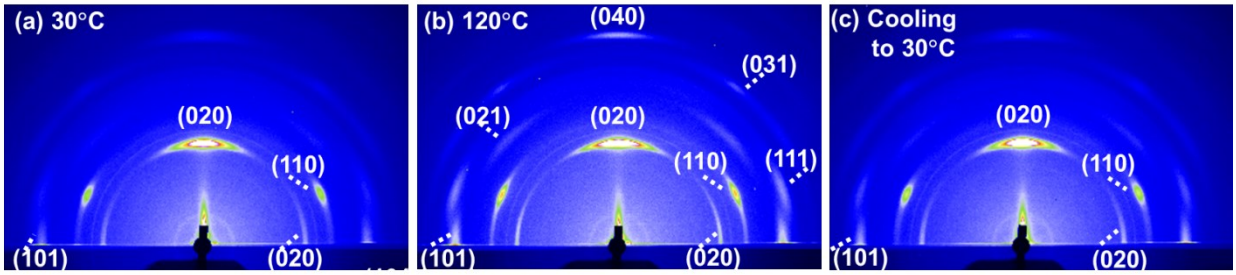

Figure 7. 2D-GIXD images of PHB ultrathin film collected at (a) 30°C, (b) 120°C and (c) after cooled down to 30°C, with the index of each reflection. The angle of incidence of X-ray beam is set at 0.114° (=1.21θ_c).

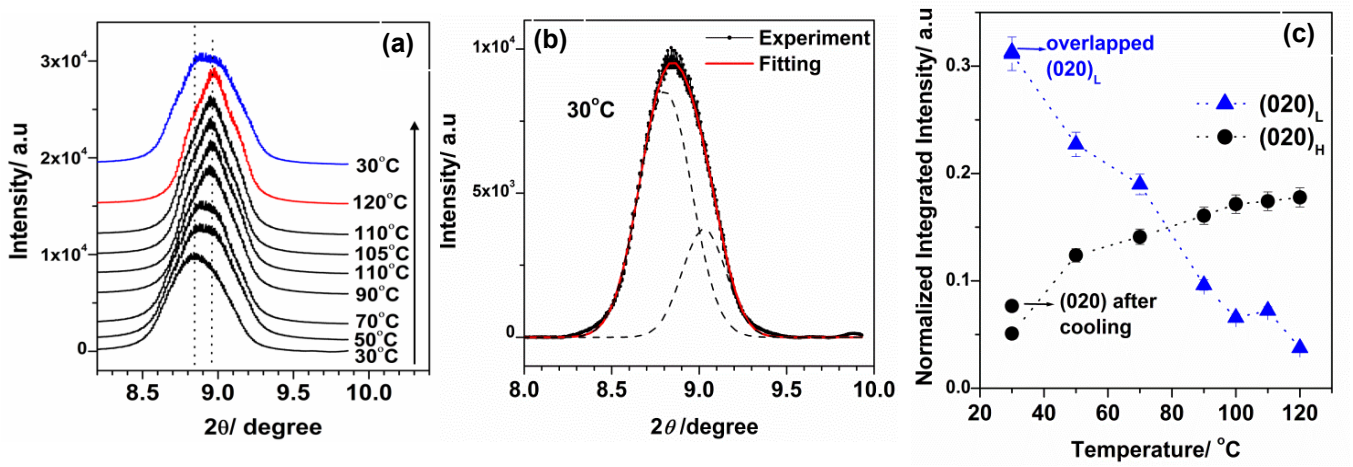

Figure 8. (a) Temperature dependence of "out-of-plane" (020) Bragg reflection profiles (from edge-on lamellae) constructed from the data shown in Figure 7. The vertical dotted lines indicate the peak positions of two (020) Bragg reflections. (b) Diffraction profile of out-of-plane (020) Bragg reflection at 30°C fitted by sum of two Gaussians, and (c) Plot of the fitted integrated intensity of intermediate and highly-ordered states, each of which is normalized by the sum of the overall integrated intensity.

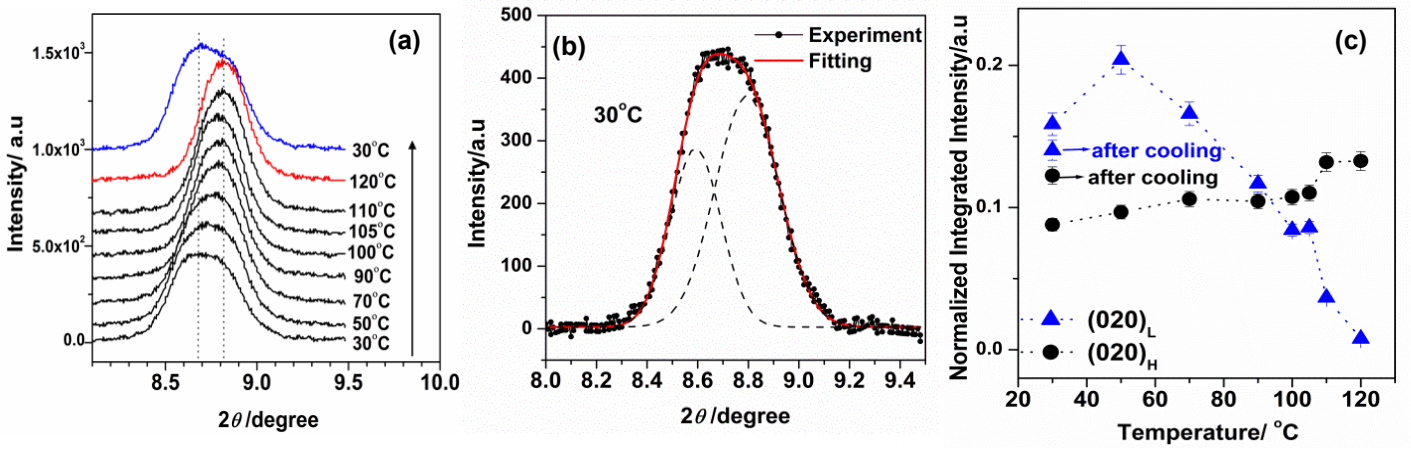

106

Figure 9. (a) Temperature dependence of "in-plane" (020) Bragg reflection profiles (from flat-on lamellae) shown constructed from the data shown in Figure 7. The vertical dotted lines indicate the peak positions of two (020) Bragg reflections. (b) Diffraction profile of in-plane (020) Bragg reflection at 30°C fitted by sum of two Gaussians. (c) Plots of fitted integrated intensity of intermediate and highly-ordered states, each of which is normalized by the sum of the overall integrated intensity.

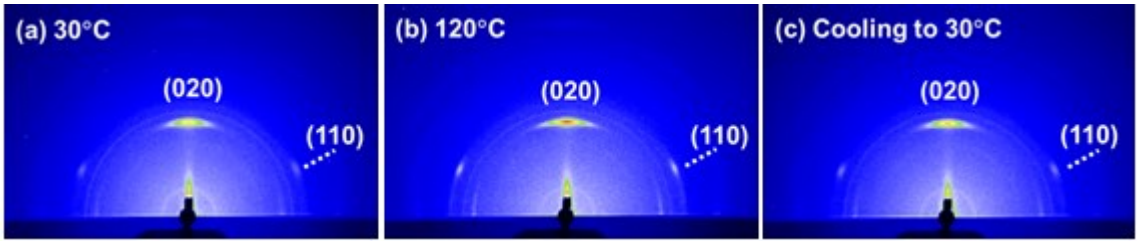

Figure 10. 2D-GIXD images of PHB ultrathin film collected at (a) 30°C, (b) 120°C and (c) after cooled down to 30°C with the index of each reflection. A very small angle of incidence of X-ray beam at 0.074° (=0.079θ_c) is applied, which affords structural information only in the narrow surface region.

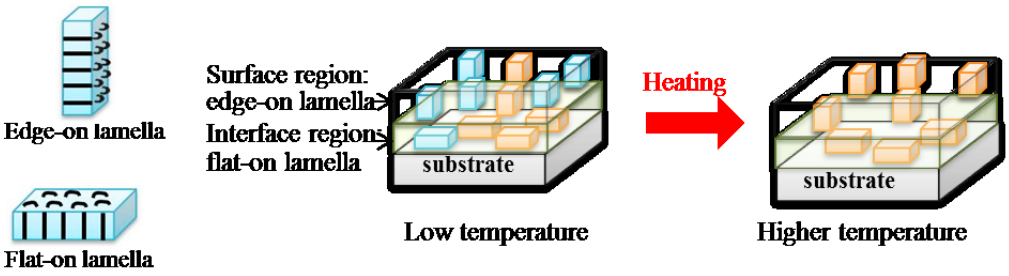

Figure 11. Illustration of the transformation of PHB crystallites from the intermediate state to highly-ordered state assisted by thermal energy in which their major locations are taken into account: blue bricks represent intermediate state and orange bricks represent highly-ordered state.

Chapter 3

Crystallization Behavior of Ultrathin Poly(3-hydroxybutyrate) Films in Blends with a Small Amount of Poly(L-lactic Acid): Correlation between Molecular Weight of Poly(L-lactic Acid) and Film Thickness

ABSTRACT

The crystallization behavior of poly(3-hydroxybutyrate) [PHB] ultrathin films in the blends with a small amount of poly(L-lactic acid)s [PLLAs] with different molecular weights was investigated using grazing incidence X-ray diffraction and infrared reflection absorption spectroscopy (IRRAS). Ultrathin films of PHB/PLLA with the same blend ratio of 80/20 (w/w) and two different film thicknesses, i.e. 30 and 13 nm, were prepared using PLLA having molecular weight ranging from 300,000~710 g mol^{-1} to explore the effects of the molecular weight of PLLAs on the crystallization of PHB under different confined environments. It was found that for the 30-nm-thick samples, the crystallization of PHB is significantly reduced in the blends with molecular weight PLLAs ranging from M_w 23,000 to 13,100 g mol^{-1}, however, the higher ($M_w \geq$ 50,000 g mol^{-1}) and lower ($M_w \leq$ 6,900 g mol^{-1}) molecular weight PLLAs do not significantly affect the crystallization. In contrast, in the 13-nm-thick films, the crystallization of PHB is remarkably inhibited in the blends having PLLAs $M_w \geq$ 6,900 g mol^{-1}. IRRAS showed that for the 30-nm-thick samples, a small addition of PLLA ($M_w \geq$ 13,100 g mol^{-1}) altered the crystalline structure of PHB only in the highly ordered state. However, such PLLAs greatly affect the PHB crystals in both intermediate and highly ordered states in the films with the thickness of 13 nm. These results showed that the ability of PLLAs for hindering the crystallization of PHB ultrathin films strongly depends on the molecular weight and film thickness. Both GIXD and

IRRAS results revealed some consistency that the lower molecular weights of PLLAs (Mw ≤ 3,600 g mol−1) only slightly affect the crystallinity and crystalline structure of PHB.

1. INTRODUCTION

Polymer blending has been well known as an effective way to create new desired physical properties of polymers.[1-3] Poly(3-hydroxybutyrate) [PHB], a thermoplastic polyester produced by bacteria, is a biodegradable and biocompatible polymer, and it is a promising alternative material of conventional plastics because its physical properties are similar to those of commercial isotactic polypropylene.[4-6] PHB has often been blended with other polymers to reduce its high crystallinity and modify its unfavorable properties, such as brittleness, low thermal stability and poor processability.[7–12] Poly(L-lactic acid) [PLLA] is also a biodegradable thermoplastic polyester. It is producible from renewable resources and has been used in many applications.[13-17] Blending of both biodegradable polymers should be very beneficial for sustainable and environmental-friendly materials to use in a wide range of applications. Therefore, PHB/PLLA blends have been one of the popular research topics in polymer blend studies. Their structure, morphology, miscibility and crystallization behaviors affecting physical properties have been extensively investigated with the aims of potential applications.[11,18-29]

PHB shows a biphasic separation in the blends with high molecular weight PLLA (M_w > 18,000), but it is miscible over the whole composition range of low molecular weight PLLA (M_w < 18,000) in the melt.[26-28] Similarly, high molecular weight PLLA (M_w = 680,000) was reported to be miscible in the melt with low molecular weight atactic-PHB

(M_w = 9,400).[24,25] Moreover, the miscibility of PHB and PLLA in their blends also greatly depends on the concentrations and crystallization dynamics of PLLA and PHB.[11,23] Most of the studies of PHB/PLLA blends has been carried out using bulk samples, while the investigations of PHB/PLLA ultrathin blend films have still been very limited.[11,18-29,46]

In general, the properties of polymers in thin and ultrathin films are considerably different from those in the bulk, such as glass transition (T_g),[30-32] morphology,[33,34] mobility,[35,36] and crystallization,[37-40] due to the confinement effects as well as the surface and interface effects. Preferred orientation of molecular chains is another phenomenon peculiar to crystalline polymer thin films, which often brings useful anisotropic features.[41-44] Therefore, investigations of thin and ultrathin polymer films can be very important for exploring the specific crystallization phenomena at the surface and interface region.

Previously, we found that PHB ultrathin films (thickness ~52 nm) formed two kinds of crystalline structures, i.e. highly ordered structure and less ordered structure (the latter has been recognized as the intermediate state), which yield IR bands at 1723 and 1731 cm^{-1}, respectively.[45] The band at 1731 cm^{-1} due to the intermediate structure appears during the melt-crystallization process, which is usually hard to be detected in bulk PHB. Similarly, the corresponding band shows up in the miscible PHB/PLLA (M_w PLLA = 13,100 g mol^{-1}) ultrathin films with similar thicknesses.[46] In addition, crystallization of PHB was extremely

reduced with the addition of ≥ 22 wt % PLLA. This result showed that the addition of another component, even by a small amount, can be quite effective to inhibit the crystallization of polymer thin films. Since the miscibility of PHB and PLLA depends on the molecular weight, varying the molecular weight of PLLA in the PHB/PLLA blends would result in different crystallization process of PHB.

In the present study, we investigate molecular weight dependence of a small amount of PLLA on the crystallization of ultrathin PHB films and its correlation with film thickness, using a wide-range of molecular weights of PLLAs (300,000~710 g mol^{-1}). In order to achieve the goal, the blend ratio was fixed at 80/20 (w/w). For distinguishing the effect of geometrical confinement and molecular weight dependence of PLLA on the crystallization of PHB, we prepared blend films with two different thicknesses, i.e., 30 nm and 13 nm. Two surface-sensitive techniques were employed to observe the crystallization behavior of PHB in the ultrathin blend films: grazing incidence X-ray diffraction (GIXD) and infrared-reflection absorption spectroscopy (IRRAS). It has been found in the present study that at the 30 nm thickness, the crystallization of PHB is significantly reduced in the blends having PLLAs with molecular weight ranging from M_w 23,000 to 13,100 g mol^{-1}, however, the higher ($M_w \geq 50{,}000$ g mol^{-1}) and lower ($M_w \leq 6{,}900$ g mol^{-1}) molecular weight PLLAs little affect the crystallization of PHB. Interestingly, in the 13-nm-thick films, the crystallization of PHB is remarkably inhibited in the blends with PLLAs of $M_w \geq 6{,}900$ g

mol^{-1}. The measurement of IRRAS revealed that the addition of PLLAs did not alter the crystalline structure of PHB in the intermediate state, but altered the crystalline in the highly ordered state in the 30-nm-thick films. On the other hand, a small addition of PLLAs has greatly affected the crystalline structure in both intermediate and highly ordered states for the films with the thickness of 13 nm. Apart from the thickness confinement, phase separation due to the presence of free surface effect, entanglement of PHB and aggregation of small molecules of PLLA, both of which are strongly molecular weight dependent phenomena, also become important factors that influence the ability of a small amount of PLLAs in inhibiting the crystallization of PHB. Although a small amount of biodegradable PLLA may not be so effective to control the crystallinity of bulk PHB, controlling the crystallinity of PHB films using a small addition of another polymer may be a great advance for thin film technology that will greatly expand the range of applications of PHB.

2. EXPERIMENTAL SECTION

2-1. Materials and Sample Preparation

Bacterially synthesized PHB with a weight-averaged molecular weight (M_w) of 650,000 g mol^{-1} purchased from Aldrich Co., Ltd., was dissolved in hot chloroform, precipitated in methanol, and vacuum-dried at 60 °C for several days to remove impurities.

Eight kinds of PLLAs with different molecular weight were obtained from Polysciences Inc. (M_w: 300,000; 100,000; and 50,000 g mol^{-1}) and Polymer Source Inc. (M_w: 23,000; 13,100; 6,900; 3,600 and 710 g mol^{-1}). Blends of PHB/PLLAs were prepared by dissolving PHB and PLLA in hot chloroform with prescribed amount.

Ultrathin films were deposited on flat-Au and Si (100) substrates for IRRAS and GIXD measurements, respectively, by spin-coating technique for 45s. The films were dried under low vacuum at 60 °C for 12 h. Annealing was carried out by keeping the films in a vacuum dry oven at 120 °C for 5 h, and then temperature was slowly cooled down to room temperature before the measurement of GIXD. Two types of film thicknesses: 30 ± 3 nm and 13 ± 2 nm, were produced by changing the concentration of solutions and rotating speeds.

2-2. Infrared Spectroscopy

All IRRAS spectra were measured using a Thermo Nicolet 6700 FTIR spectrometer equipped with a MCT detector at a 2 cm^{-1} resolution over 256 scans to ensure a high signal-to-noise ratio. A reflection attachment (Spectra-Tech. FT80 RAS) with an incident angle of 80° was attached to the spectrometer together with a rotatable wire-grid polarizer of KRS5-substrate (ST Japan).

2-3. X-ray Diffraction

GIXD profiles were collected using a Rigaku Ultima IV X-ray diffractometer

(Rigaku Co., Japan) where CuKα (λ = 1.542 Å) radiation was generated at 40 kV, 40 mA. The system was equipped with a scintillation detector and cross beam optics (CBO) for automatic alignment coupled with a thin film attachment. The angle of incidence was set at 0.19° (corresponding to $1.14\theta_c$) for the incident X-ray to fully penetrate the films. GIXD profiles were collected at room temperature with scanning speed of 0.3°/min and interval of 0.1°. Film thicknesses were determined from the X-ray reflectivity (XRR) profiles, after analyzed with an in-house developed nonlinear curve fitting software.

3. RESULTS AND DISCUSSION

3-1. Crystallinity and crystallization behavior of PHB studied GIXD.

Figure 1a shows out-of-plane GIXD profiles collected at room temperature of 30-nm-thick films of neat PHB and PHB/PLLA blends (80/20) where PHB was blended with eight kinds of PLLAs having different molecular weight (M_w = 300,000~710 g mol^{-1}). An obvious Bragg reflection centered at 2θ = 13.6° originates from the crystallites of PHB in the films and has been indexed as (020) reflection.[42,47] Two other weak reflections also appear at around 2θ = 16.6° and 20.3° in Figure 1a (1)–(5) that are (200/110) and (203) reflections of crystalline PLLA, respectively.[46] However, several diffraction profiles in Figure 1a (6)−(8) do not exhibit any reflections from PLLA, indicating that those PLLAs do not crystallize in those films. The molecular weight of those PLLAs (≤ 6,900 g mol^{-1})

should be below the critical molecular weight for crystallizable PLLA. Moreover, the results displayed in Figure 1a reveal that PHB and several kinds of PLLA ($M_w \geq 13{,}100$ g mol^{-1}) separately crystallize in those blends.

The appearance of only (020) reflection of PHB indicates that the *b*-axis of PHB crystallites is almost aligned normal to the film surface (the *ac* planes are parallel to the film surface).[42,45,47] This alignment also fixed the type of PHB lamellae as the edge-on lamellae. The fact that the (020) reflection of PHB appears in all PHB/PLLA blends means that the preferred alignment of PHB crystallites in the blends is the same as that of the neat PHB. Even though PLLA does not disturb the alignment and lamellae type of PHB in the blends, the intensity of (020) reflection of PHB shows a distinct variation as the molecular weight of PLLA is varied. The (020) peak, which is sharp, strong and not overlapped with other peaks, has often been used to characterize the degree of crystallinity of PHB thin films. Since the blend ratio and illuminated area of X-ray beam are fixed in this study, the intensity variation of (020) reflection would simply indicates a change in the crystallinity of PHB in the blends. Figure 1b shows a plot of the degree of crystallinity of PHB in the PHB/PLLA ultrathin blend films as a function of log of the ratio of M_w PHB to that of PLLA. The crystallinity of PHB in the blends was calculated by:

$$\%\ crystallinity = \frac{I_i}{I_{PHB}} \text{x } 100\%,$$

where I_i is the integrated intensity of (020) peak in the blends and I_{PHB} is that of neat PHB

calculated from GIXD profiles in Figure 1a. As can be seen from Figure 1b, the crystallinity of PHB slightly decreases with decreasing molecular weight of PLLA (M_w = 300,000~50,000 g mol^{-1}, hereinafter called higher molecular weight PLLAs) in the blends. The dramatic decrease in the crystallinity of PHB occurs in the blends with PLLA M_w = 23,000~13,100 g mol^{-1} (hereinafter called middle molecular weight PLLAs). Furthermore, the plot is increased again in the blends where PLLA of $M_w \leq$ 6,900 g mol^{-1} (hereinafter called lower molecular weight PLLAs). These results clearly reveal that the inhibition of crystallization of PHB by the addition of a small amount of PLLA strongly depends on the molecular weight of PLLA. It is quite probable that the higher molecular weight of PLLAs are also immiscible with PHB even in the thin films and that the origin of the moderate decrease in crystallinity in those films might be common in bulk PHB/PLLA blends. The lower molecular weight PLLAs slightly altering the crystallization of PHB, demonstrating a sharp contrast to the behavior of those in bulk samples in which noticeable change is usually observed.[26-28] Several factors would affect the crystallization behavior of PHB in the PHB/PLLA ultrathin blend films. Before we discuss those possible factors, we should investigate the effect of thickness confinement by using the thinner (13 nm) PHB/PLLA blend films.

Figure 2 displays out-of-plane GIXD profiles of 13-nm-thick films of neat PHB and PHB/PLLA blends (80/20) with various molecular weights of PLLA. PHB is still able to

crystallize in the film as the (020) reflection was clearly observed for the neat PHB, although the intensity of this (020) peak is much lower than that of the 30-nm-thick film. It has widely been accepted that the degree of crystallinity of a polymer often decreases by reducing the thickness.[40,48-50] As shown in the GIXD profiles of (1)–(5) in Figure 2, no (020) reflection of PHB is observed in the blends with higher and middle molecular weight of PLLAs ($M_w \geq 13{,}100$ g mol^{-1}), indicating that the crystallization of PHB ultrathin films is fully inhibited by the addition of high and middle molecular weight PLLAs. The (020) reflection also shows up in the blends with the lower molecular weight PLLAs as depicted in (7) and (8), which may be similar to the results observed in the corresponding films depicted in Figure 1a. However, the (020) reflection profile of (6) in Figure 2 is found to be very weak if we compare it to that of (6) in Figure 1a. The results shown in Figures 1 and 2 indicate that the lower molecular weight PLLAs do not significantly affect the crystallization of PHB. Reducing the film thickness seems to enhance the ability of higher and middle molecular weight PLLAs in inhibiting the crystallization of PHB.

Furthermore, it is noticed that the higher molecular weight PLLAs still crystallize as the (200/110) reflection shows up in Figure 2 (1)–(5). The very weak (200/110) indicates that only a tiny fraction of PLLA chains are able to crystallize in those blends. Similar to the results in Figure 1a (6)–(8), the lower molecular weight PLLAs in Figure 2 (6)–(8) do not exhibit any reflection peaks of PLLA, suggesting that the lower molecular weight of

PLLAs do not crystallize irrespective with the thickness confinement. Additionally, thermal annealing cannot induce the crystallization of PHB in those blends in the 13-nm-thick films as shown in Figure 3, indicating the strong inhibition on the crystallization of PHB by a small amount of PLLAs in these blend films.

The crystallization behavior of PHB in the PHB/PLLA ultrathin films shown in Figures 1 and 2 demonstrates a striking contrast with the behavior observed in bulk PHB/PLLA blends. Furthermore, the results of 30-nm-thick films and those of 13-nm-thick films also showed some differences as explained above, indicating a strong dependency of the crystallization of PHB in the PHB/PLLA ultrathin blend films on the molecular weight of PLLA and the film thickness. Several factors which would explain the results of Figures 1 and 2 can be summarized below. It would be worth considering those factors to understand the complex behavior of the crystallization in the ultrathin PHB/PLLA films:

1. Phase separation caused by the presence of free surface effect.

In thin polymer films, a free surface effect on phase separation would possibly be more dominant than an effect from the interface between a polymer and a substrate.[36] The presence of free surface can induce the phase separation of two polymers in the blends as the mobility of molecular chain is increased.[51] Phase separation may thus occur between PHB and higher molecular weight PLLAs in the 30-nm-thick films. Therefore, PHB and higher molecular weight PLLA may crystallize separately from each other. In contrast,

reducing the thickness is likely to enhance the interface effect. The mobility of molecules would be very restricted in the interface region as the intensive interaction between molecules and the substrate. In other words, PHB and PLLA are forced to be miscible in ultrathin films where the interface effect would be dominant.

2. Entanglement of PLLA molecular chains

It was reported that PLLA has a critical molecular weight for entanglement at around 16,000 g mol^{-1}.[52,53] The entangled chains of PLLAs would effectively trap PHB molecules and do not allow the PHB chains to be crystallized. The PLLA chains with $M_w \geq 13{,}100$ g mol^{-1} may be adequate for the entanglement with PHB molecules to inhibit the crystallization. On the other hand, the chain length of lower molecular weight PLLAs ($M_w \leq 3{,}600$ g mol^{-1}) are insufficient for the entanglement. Moreover, in the 13-nm-thick films, no phase separation would be expected due to the limited mobility.

3. Size of PLLA molecules

Since the crystallization of PHB has revealed to have the complex thickness dependence, the relationship with the molecular size of PLLA should be considered; the molecular size of each PLLA is listed in Table 1. Someone might consider that small PLLA molecules (lower molecular weight PLLAs) would hinder the crystallization of PHB through interlamellar segregation, because such shorter PLLA molecules are expected to easily diffuse into PHB molecules as an effective obstacle for lamellae folding of PHB.

However, our GIXD results have proved that such small molecules are ineffective to hinder the lamellae folding. Thus, those small molecules of PLLAs most probably aggregate during the crystallization process, being unable to affect the crystallization of PHB. Similarly, big molecules of high molecular weight PLLAs would also be ineffective to reduce the crystallinity PHB if the phase separation (as mentioned in 1) between PHB and PLLA would occur. However, molecules, whose size are comparable, or exceed half of the thickness of films, may effectively inhibit the crystallization of PHB because the phase separation would not be expected owing to the interaction with the substrate.

According to the three factors discussed above, the inhibition process on the crystallization of PHB in the PHB/PLLA ultrathin films can be illustrated in Figure 4. This scheme also denotes that the inhibition on the crystallization of PHB by a small amount of PLLAs strongly depends on the molecular weight of PLLAs and the film thickness.

3-2. Conformation and crystalline structure of PHB studied by IRRAS.

In order to explore chain conformation and crystalline structure of PHB in the PHB/PLLA ultrathin films on a molecular scale, the IRRAS measurements were conducted for the films. Figure 5 shows the IRRAS spectra (bottom panel) and their second derivatives (upper panel) in the C=O stretching region of 30-nm-thick films of PHB and PHB/PLLA (80/20) blends with various molecular weights of PLLAs. PHB shows two

bands at 1726 and 1749 cm^{-1} assigned to crystalline and amorphous C=O stretching modes, respectively.[45] By addition of PLLAs, the intensity of the C=O crystalline band at 1726 cm^{-1} is significantly reduced in the spectra of the blends where the molecular weight of PLLAs ≥ 6,900 g mol^{-1} (see the spectra of the bottom panel of (1)–(6) in Figure 5). These results reveal that the presence of PLLA appreciably decreases the crystallization of PHB. According to the IRRAS selection rule,[60,61] the weak absorbance of C=O crystalline band of PHB in the IRRAS spectra of the blends indicates that the C=O group is aligned more parallel to the substrate's surface. In the previous studies, the crystalline C=O group of PHB in the ultrathin films was also reported to be nearly parallel to a substrate surface (along the *a*-axis).[45,54]

Further reduction of the molecular weight of PLLA (M_w ≤ 3,600 g mol^{-1}) in the blends yields the spectra that are more similar to that of the neat PHB as seen from Figure 5 (7)–(8). This result indicating that these lowest molecular weight PLLAs neither stop the crystallization nor change the preferred alignment of PHB crystallites. The result is consistent with the result obtained from the GIXD measurements (profiles (7) and (8) in Figure 1a and 2).

Two bands at 1765 and 1778 cm^{-1} in all the blends are ascribed to the amorphous and fairly structural defected C=O stretching of PLLA.[23,54] The intensity of amorphous band at 1765 cm^{-1} of PLLA also decreases in the blends with decreasing the molecular weight of

PLLAs and eventually become very weak as observed for the blend with the lowest molecular weight PLLA (see Figure 5 (8)). The appearance of PLLA amorphous band at 1765 cm^{-1} in Figure 5 (1)–(5) suggests that the long chains are sufficient for the entanglements, whereas the short chains of lowest molecular weight PLLAs are unable to be entangled as is evidenced by the fact that the amorphous band almost disappears (see (7) and (8) of Figure 5). The PLLAs of short chains eventually aggregate in the films as described above. Probably those entangled of PLLA chains would trap PHB molecules in their blends, causing the delay of crystallization of PHB, whereas the aggregated shorter PLLA chains are irrelevant with the crystallization. These results so far have proved that the entanglement of PLLA chains would be a key factor responsible for hindering the crystallization of PHB in ultrathin films.

Although the intensity of C=O crystalline band of PHB becomes disrupted in the PHB/PLLA blends, no shift or distinct band-splitting at 1726 cm^{-1} was observed in all the samples. In the previous study, we revealed the behavior of two crystalline structures with different structural orders, i.e. highly-ordered and less-ordered (intermediate) structures, by deconvolution of the IRRAS spectra of PHB ultrathin films, where several overlapped bands coexist in the C=O stretching region of PHB ultrathin films due to the coexistence of the two crystalline structures.[45] In this study, the C＝O stretching band region of IRRAS spectra shown in Figure 5 are decomposed into several component using GRAMS

software.

Figure 6a displays the result of decomposition showing the bands of the highly ordered crystalline (1724 cm^{-1}), the intermediate state (1731 cm^{-1}), two amorphous states arising from different conformations of PHB (1739 and 1748 cm cm^{-1}), one amorphous band of PLLA (1764 cm^{-1}) and another one arising from structural defect of PLLA (1778 cm^{-1}).[46] The integrated intensity of each crystalline structure at 1724 and 1731 cm^{-1} is plotted in Figure 6b after normalization by the sum of all fractions in each blend. In comparison with the intensity of the corresponding bands of neat PHB, intensity of both intermediate (1731 cm^{-1}) and highly-ordered crystalline (1724 cm^{-1}) bands becomes weaker in the blends, suggesting that the presence of PLLAs suppresses the formation of PHB crystals in the blends. While the integrated intensity of intermediate state looks almost unchanged among the blend samples, the plot of highly ordered crystalline band shows a gradual increase in the blends with decreasing molecular weight of PLLA. It indicates that the variation in the molecular weight of PLLA does not affect the crystal formation of the intermediate state, but the higher molecular weight PLLAs disturb the crystal formation of the highly-ordered state.

Figure 7 exhibits IRRAS spectra (bottom) and their second derivatives (upper) in the C=O stretching region of 13-nm-thick film of PHB and PHB/PLLA (80/20) blends with various molecular weights of PLLAs. PHB still shows two bands due to the crystalline and

amorphous C=O bands at 1726 and 1749 cm^{-1}, respectively. However, the intensity of 1726 cm^{-1} band is lower than that of the 30-nm-thick films. Since a small amount of PLLAs ($M_w \geq 13{,}100$ g mol^{-1}) greatly suppresses the intensity and alters the band shape of C=O crystalline band of PHB as noticeably observed in Figure 7 (1)–(5), we conclude that those PLLAs disturbed both crystallinity and crystalline structure of PHB. The higher and middle molecular weight PLLAs were able to make the C=O crystalline band of PHB at 1726 cm^{-1} split into two bands at 1723 and 1731 cm^{-1}, which presumably correspond to highly ordered and intermediate crystalline structures of PHB, respectively. However, the IRRAS results would be inconsistent with the GIXD profiles shown in Figure 2 (1)–(5) in which no reflection from PHB crystals is recognized in corresponding blend samples. The inconsistency between GIXD and IRRAS may arise from the different sensitivity of these techniques in detecting tiny crystallites.[46] In those samples, PHB crystals are probably too small and the amount is also too small to be detected by conventional GIXD. The intensity of C=O crystalline bands observed in the blends with lower molecular weight PLLAs is found to be rather similar to that of neat PHB at 1726 cm^{-1} (Figure 7 (7) and (8)). It clearly indicates that the lower molecular weight PLLAs are unable to alter the crystallization of PHB, which is independent from the film thickness. Furthermore, the intensity of amorphous band of PLLA at 1765 cm^{-1}, which can be used as an indicator of entanglement of PLLAs chains, decreased with decreasing the molecular weight of PLLAs, which agrees

with the scheme discussed above.

To explore the crystallization behavior in the intermediate and highly-ordered state, the spectra shown in Figure 7 were also decomposed. A typical result is shown in Figure 8a. It displays the deconvoluted IRRAS spectra in the C=O stretching region of 13-nm-thick film of PHB/PLLA (M_w = 300,000 g mol^{-1}), and plots of integrated intensity of the 1724 cm^{-1} (highly ordered) and 1731 cm^{-1} (intermediate) bands normalized by the sum of the integrated intensity in each blend are depicted in Figure 8b. Similar to Figure 6b, the intensity of both intermediate and highly-ordered crystalline structures decreases markedly after the addition of PLLAs. However, the intensity of the intermediate state (1731 cm^{-1}) shows a small increase with decreasing molecular weight of PLLA. Furthermore, the intensity of highly ordered crystalline state (1724 cm^{-1}) greatly reduces at first and subsequently increases with decreasing molecular weight of PLLA. These results suggest that the molecular weight dependence of PLLA on the crystallization of PHB is greater for thinner films.

In the C−H stretching region, weak intermolecular hydrogen bonding between carbonyl and methyl groups (CH_3···O=C) of PHB was found at anomalously high frequency region.[56-59] The weak hydrogen bonding bands of PHB are still recognized in those 30 nm and 13 nm thick films as shown in Figure 9. In the 30 nm thick film, the weak hydrogen bonding band appeared at 3011 cm^{-1} as a weak shoulder band, while in the 13 nm

thick film, it shifted to 3009 cm^{-1} and the peak become more apparent. This results may indicate that the hydrogen bonds in the 13 nm thick film are weaker than the hydrogen bonds formed in the 30 nm thick film. However, the slightly higher intensity of 3009 cm^{-1} bands indicated in Figure 9b would reflect that, in the 13-nm-thick film, the number of oriented bonds nearly perpendicular to the film surface seems to be larger than those in the 30 nm thickness.

4. CONCLUSION

We have investigated the crystallization behavior of PHB in the PHB/PLLAs ultrathin films with thicknesses of 30 and 13 nm as a function of molecular weight of PLLA using GIXD and IRRAS measurements. Eight kinds of PLLAs with different molecular weight ranging from 300,000 to 710 g mol^{-1} were added to explore the effect of a small amount of PLLAs on the crystallization behavior of PHB in their ultrathin films. The PHB/PLLA ratio is fixed at 80/20 (w/w) for all blends. The crystallization of PHB has shown a strong dependency on the molecular weight of PLLA and film thickness. In the 30-nm-thick films, a phase separation occurs between PHB and higher molecular weight PLLAs ($M_w \geq$ 50,000 g mol^{-1}) in the blends, and therefore, those PLLAs less affect the crystallization of PHB. The miscible PHB and PLLAs blends are obtained with the middle molecular weight PLLAs (M_w 23,000~13,100 g mol^{-1}), yielding a dramatic decreases in the crystallinity of

PHB. It is quite noteworthy that the crystallization of PHB is fully inhibited in the blends with PLLAs with wider-range molecular weights ($M_w \geq$ 6,900 g mol^{-1}) when the film thickness is reduced to 13 nm.

IRRAS results have demonstrated that for the 30-nm-thick films, the addition of a small amount of PLLAs significantly suppresses the intensity of the crystalline band of PHB at 1726 cm^{-1}. However, the PLLAs do not affect the crystalline structures of PHB significantly. Furthermore, for the 13-nm-thick films, both the intensity and thus the crystalline structures of PHB are remarkably altered by a small amount of PLLA ($M_w \geq$ 6,900 g mol^{-1}). Both GIXD and IRRAS results show a consistency in that the lower molecular weight PLLA ($M_w \leq$ 3,600 g mol^{-1}) does not affect the crystallinity and crystalline structures of PHB. Furthermore, several factors such as the presence of free surface and interface effects, entanglement of PLLA chains and molecular size of PLLA must seriously be taken into account to comprehend the complex crystallization behavior of PHB in the PHB/PLLA ultrathin films, apart from the molecular weight and thickness dependences.

REFERENCES

1. Utracki, L. A.; Mukhopadhyay, P.; Gupta, R. K. In *Polymer Blends Handbook Second Edition*; Utracki, L. A., Wilkie, C. A. Eds.; Springer: New York, 2014; pp 19-36.

2. Yu, L.; Dean, K.; Li, L. Polymer Blends and Composites from Renewable Resources. *Prog. Polym. Sci.* **2006**, *31*, 576-602.

3. Robeson, L. M. Applications of Polymer Blends: Emphasis on Recent Advances. *Polym. Eng. Sci.* **1984**, *24*, 587-597.

4. Zhao, Q.; Cheng, G. In *New Frontiers in Polymer Research*; Bregg, R. K., Ed.; Nova Science Publishers Inc.: New York, 2006; pp 99−124.

5. Sudesh, K.; Abe, H.; Doi, Y. Synthesis, Structure and Properties of Polyhydroxyalkanoates: Biological Polyesters. *Prog. Polym. Sci*. **2000**, *25*, 1503−1555.

6. Satkowski, M.M.; Melik, D.H.; Autran, J-P.; Green, P.R.; Noda, I.; Schechtman, L.A. In *Biopolymers*; Steinbüchel, A., Doi, Y., Eds.: Wiley-VCH:Weinheim, 2001; pp 231.

7. Avella, M.; Martuscelli, E. Poly-D-(−)(3-hydroxybutyrate)/poly(ethylene oxide) Blends: Phase Diagram, Thermal and Crystallization Behavior. *Polymer* **1988**, *29*, 1731-1737.

8. *Pizzoli, M.; Scandola, M.; Ceccorulli, G. Crystallization Kinetics and Morphology of Poly(3-hydroxybutyrate)/Cellulose Ester Blends. Macromolecules*, **1994**, *27*, pp 4755–4761.

9. Xing, P.; Dong, L.; An, Y.; Feng, Z.; Avella, M.; Martuscelli, E. Misicbility and Crystallization of Poly(*β*-hydroxybutyrate) and Poly(*p*-vinylphenol) Blends.

Macromolecules **1997**, *30*, 2726-2733.

10. An, Y.; Dong, L.; Li, L.; Mo, Z.; Feng, Z. Isothermal Crystallization Kinetics and Melting Behavior of Poly(β-hydroxybutyrate)/Poly(vinyl acetate) Blends. *Polymer* **1999**, *35*, 365-369.
11. Furukawa, T.; Sato, H.; Murakami, R.; Zhang, J.; Duan, Y.; Noda, I.; Ochiai, S.; Ozaki, Y. Structure, Dispersibility, and Crystallinity of Poly(hydroxybutyrate)/Poly(L-lactic acid) Blends Studied by FT-IR Microspectroscopy and Differential Scanning Calorimetry. *Macromolecules* **2005**, *38*, 6445–6454.
12. Kabe, T.; Tsuge, T.; Kasuya, K.; Takemura, A.; Hikima T.; Takata, M.; Iwata, T. Physical and Structural Effects of Adding Ultrahigh-Molecular-Weight Poly[(R)-3-hydroxybutyrate] to Wild-Type Poly[(R)-3-hydroxybutyrate]. *Macromolecules* **2012**, *45*, 4858-1865.
13. Tsuji, H. Poly(lactide) Streocomplexes: Formation, Structure, Properties, Degradation, and Applications. *Macromol. Biosci*. **2005**, *5*, 569-597.
14. Tsuji, H. In *Bio-Based Plastics: Materials and Applications*. Kabasci, S. Ed.; John Wiley & Sons, Ltd.: United Kingdom, 2014; pp 171-239.
15. Suzuki, S.; Ikada, Y.; Obuchi, S.; Ogawa, S.; Mochizuki, M.; Hiraishi, A. In *Poly(Lactic acid) Synthesis, Structures, Properties, Processing and Applications*. Auras, R., Lim, L-T., Selke, S. E. M., Tsuhi, H., Eds.; John Wiley & Sons, Inc.:

Hoboken, New Jersey, 2010; pp 445-486.

16. Dorgan, J. R.; Lehermeier, H. J.; Palade, L-I.; Cicero, J. Polylactides: Properties and Prospects of an Environmentally Benign Plastic from renewable Resources. *Macromol. Symp*. **2001**, *175*, 55-66.

17. Auras, R.; Harte, B.; Selke, S. An Overview of Polylactides as Packaging Materials. *Macromol. Biosci*. **2004**, *4*, 835-864.

18. Sheng, C.; Zhang, T.; Yuan, Y.; Zhou, L.; Duan, Y.; Zhang, J. Effect of a Small Amount of Poly(3-hydroxybutyrate) on Their Crystallization Behavior of Poly(L-lactic acid) in Their Immiscible and Miscible Blends During Physical Aging. *Polym. Int.* **2014**, *63*, 1270-1277.

19. Vogel, C.; Wessel, E.; Siesler, H. W. FT-IR Spectroscopic Imaging of Anisotropic Poly(3-hydroxybutyrate)/Poly(lactic acid) Blends with Polarized Radiation. *Macromolecules* **2008**, *41*, 2975-2977.

20. Hu, Y.; Sato, H.; Zhang, J.; Noda, I.; Ozaki, Y. Crystallization Behavior of Poly(L-lactic acid) Affected by the Addition of a Small Amount of Poly(3-hydroxybutyrate). *Polymer* **2008**, *49*, 4204-4210.

21. Furukawa, T.; Sato, H.; Murakami, R.; Zhang, J.; Noda, I.; Ochiai, S.; Ozaki, Y. Comparison of Miscibility and Structure of Poly(3-hydroxybutyrate-co-3-hydroxyhexanoate)/Poly(L-lactic acid) Blends with

Those of Poly(3-hydroxybutyrate)/ Poly(L-lactic acid) Blends Studied by Wide-Angle X-ray Diffraction, Differential Scanning Calorimetry, and FTIR Microspectroscopy. *Polymer* **2007**, *48*, 1749-1755.

22. Furukawa, T.; Sato, H.; Murakami, R.; Zhang, J.; Noda, I.; Ochiai, S.; Ozaki, Y. Raman Microspectroscopy Study of Structure, Dispersibility, and Crystallinity of Poly(hydroxybutyrate)/Poly(L-lactic acid) Blends. *Polymer* **2006**, *47*, 3132-3140.
23. Zhang, J.; Sato, H.; Furukawa, T.; Tsuji, H.; Noda, I.; Ozaki, Y. Crystallization Behaviors of Poly(3-hydroxybutyrate) and Poly(L-lactic acid) in Their Immiscible and Miscible Blends. *J. Phys. Chem. B* **2006**, *110*, 24463-24471.
24. Park, J. W.; Doi, Y.; Iwata, T. Uniaxial Drawing and Mechanical Properties of Poly[(*R*)-3-hydroxybutyrate]/Poly(L-lactic acid) Blends. *Biomacromolecules* **2004**, *5*, 1557- 1566.
25. Ohkoshi, I.; Abe, H.; Doi, Y. Miscibility and Solid-state Structures for Blends of Poly[(*S*)-lactide] with Atactic Poly[(*R,S*)-3-hydroxybutyrate]. *Polymer* **2000**, *41*, 5985-5992.
26. Yoon, J-S.; Lee, W-S.; Kim, K-S.; Chin, I-J.; Kim, M-N.; Kim, C. Effect of Poly(ethylene glycol)-*block*-Poly(L-lactide) on the Poly[(*R*)-3-hydroxybutyrate]/Poly(L-lactide) Blends. *Eur. Polym. J.* **2000**, *36*, 435-442.

27. Koyama, N.; Doi, Y. Miscibility of binary blends of Poly[(*R*)-3-hydroxybutyric acid] and Poly([(*S*)-lactic acid]. *Polymer* **1997**, *38*, 1589-1593.

28. Blümm, E.; Owen, A. J. Miscibility, Crystallization and Melting of Poly(3-hydroxybutyrate)/Poly(L-lactide) Blends. *Polymer* **1995**, *36*, 4077-4081.

29. Zhang, L.; Xiong, C.; Deng, X. Miscibility, crystallization, and Morphology of Poly(β-hydroxybutyrate)/Poly(d,l-lactide) Blends. *Polymer* **1996**, *37*, 235-241.

30. Yang, C.; Onitsuka, R.; Takahashi, I. Confinement Effects on Glass Transition Temperature, Transition Breadth, and Linear Expansivity: An Ultraslow X-ray Reflectivity Study on Supported Ultrathin Polystyrene Films. *Eur. Phys. J. E: Soft Matter Biol. Phys.* **2013**, *36*, 66.

31. Fryer, D. S.; Nealey, P. F.; de Pablo, J. J. Thermal Probe Measurements of The Glass Transition Temperature for UltrathinPolymer Films as a Function of Thickness. *Macromolecules* **2000**, *33*, 6439−6447.

32. Forrest, J. A.; Mattsson, J. Reductions of the Glass Transition Temperature in Thin Polymer Films: Probing the Length Scale of Cooperative Dynamics. *Phys. Rev. E: Stat. Phys., Plasmas, Fluids, Relat. Interdiscip. Top*. **2000**, *61*, R53−56.

33. Taguchi, K.; Miyaji, H.; Izumi, K.; Hoshino, A.; Miyamoto, Y.; Kokawa, R. Growth Shape of Isotactic Polystyrene Crystals in Thin Films. *Polymer* **2001**, *42*, 7443−7447.

34. Abe, H.; Kikkawa, Y.; Iwata, T.; Aoki, H.; Akehata, T.; Doi, Y. Microscopic

Visualization on Crystalline Morphologies of Thin Films for Poly[(*R*)-3-hydroxybutyric acid] and its Copolymer. *Polymer* **2000**, *41*, 867−874.

35. Lin, E. K.; Kolb, R.; Satija, S. K.; Wu, W. Reduced Polymer Mobility near the Polymer/Solid Interfaces as Measured by Neutron Reflectivity. *Macromolecules* **1999**, *32*, 3753−3757.
36. Frank, B.; Gast, A. P.; Russell, T. P.; Brown, H. R.; Hawker, C. Polymer Mobility in Thin Films. *Macromolecules* **1996**, *29*, 6531−6534.
37. Wang, Y.; Ge, S.; Rafailovich, M.; Sokolov, J.; Zou, Y.; Ade, H.; Lüning, J.; Lustiger, A.; Maron, G. Crystallization in the Thin and Ultrathin Films of Poly(ethylene-vinyl acetate) and Linear Low-Density Polyethylene. *Macromolecules* **2004**, *37*, 3319−3327.
38. Schönherr, H.; Frank, C. W. Ultrathin Films of Poly(ethylene oxides) on Oxidized Silicon. 1. Spectroscopic Characterization of Film Structure and Crystallization Kinetics. *Macromolecules* **2003**, *36*, 1188−1198.
39. Frank, C. W.; Rao, V.; Despotopoulou, M. M.; Pease, R. F. W.; Hinsberg, W. D.; Miller, R. D.; Rabolt, J. F. Structure in Thin and Ultrathin Spin-Cast Polymer Films. *Science* **1996**, *273*, 912−915.
40. Despotopoulou, M. M.; Frank, C. W.; Miller, R. D.; Rabolt, J. F. Kinetics of Chain Organization in Ultrathin Poly(di-*n*-hexylsilane) Films. *Macromolecules* **1996**, *29*,

5797−5804.

41. Ma, Y.; Hu, W.; Reiter, G. Lamellar Crystal Orientations Biased by Crystallization Kinetics in Polymer Thin Films. *Macromolecules* **2006**, *39*, 5159−5164.

42. Sun, X.; Guo, L.; Sato, H.; Ozaki, Y.; Yan, S.; Takahashi, I. A Study on the Crystallization Behavior of Poly(β-hydroxybutyrate) Thin Films on Si Wafers. *Polymer* **2011**, *52*, 3865−3870.

43. Yan, S. Origin of Oriented Recrystallization of Carbon-Coated Preoriented Ultrathin Polymer Films. *Macromolecules* **2003**, *36*, 339−345.

44. Chang, H.; Guo, Q.; Shen, D.; Li, L.; Qiu, Z.; Wang, F.; Yan, S. Study on the Oriented Recrystallization of Carbon-Coated Polyethylene Oriented Ultrathin Films. *J. Phys. Chem. B* **2010**, *114*, 13104−13109.

45. Khasanah; Reddy, K. R.; Ogawa, S.; Sato, H.; Takahashi, I.; Ozaki, Y. Evolution of Intermediate and Highly Ordered Crystalline States under Spatial Confinement in poly(3-hydroxybutyrate) Ultrathin Films. *Macromolecules* **2016**, *49*, 4202-4210.

46. Sun, X.; Tokuda, A.; Oji, Y.; Nakatani, T.; Tsuji, H.; Ozaki, Y.; Yan, S.; Takahashi, I. Effects of Molar Mass of Poly(L-lactide acid) on the Crystallization of Poly[(*R*)-3-hydroxybutyrate] in Their Ultrathin Blend Films. *Macromolecules* **2012**, *45*, 2485−2493.

47. Mori, K.; Mukoyama, S.; Zhang, Y.; Sato, H.; Ozaki, Y.; Terauchi, H.; Noda, I.;

Takahashi, I. Crystalline Lamellae and Surface Morphology of Biodegradable Polyhydroxyalkanoate Thin Films: Thermal Behavior and Comparison between Poly(3-hydroxybutyrate-*co*-3-hydroxyhexanoate) and Poly(3-hydroxybutyrate). *Macromolecules* **2008**, *41*, 1713-1719.

48. Despotopoulou, M. M.; Miller, R. D.; Rabolt, J. F.; Frank, C. W. Polymer Chain Organization and Orientation in Ultrathin Films: A Spectroscopic Investigation. *J. Polym. Sci., Part B: Poly. Phys.* **1996**, *34*, 2335-2349.
49. Urayama, K.; Tsuji, M.; Neher, D. Layer-Thinning Efefcts on Ferroelectricity and the Ferroelectric-to-Paraelectric Phase Transition of Vinylidene Fluoride-Trifluoroethylene Copolymer Layers. *Macromolecules* **2000**, *33*, 8269-8279.
50. Zhang, Q. M.; Xu, H.; Fang, F.; Cheng, Z-Y.; Xia, F.; You, H. Critical Thickness of Crystallization and Discontinuous Change in Ferroelectric Behavior with Thickness in Ferroelectric Polymer Thin Films. *J. Appl. Phys*. **2001**, *89*, 2613-2616.
51. Farrance, O. E.; Jones, R. A. L.; Hobbs, J. K. The Observation of Rapid Surface Growth during the Crystallization of Polyhydroxybutyrate. *Polymer* **2009**, *50*, 3730-3738.
52. Cooper-White, J. J.; Mackay, M. E. Rheological Properties of Poly(lactides). Effect of Molecular Weight and Temperature on the Viscoelasticity of Poly(l-lactic acid). *J. Polym. Sci., Part B: Polym. Phys*. **1999**, *37*, 1803–1814.

53. Zhang, J-F.; Sun, X. In *Biodegradable Polymers for Industrial Applications*. Smith, R. Ed.; Woodhead Publishing Limited: England, 2005; p 255.

54. Sato, H.; Murakami, R.; Mori, K.; Ando, Y.; Takahashi, I.; Noda, I.; Ozaki, Y. Specific Crystal Structure of Poly(3-hydroxbutyrate) Thin Films Studied by Infrared Refelction-Absorption Spectroscopy. *Vib. Spectrosc*. **2009**, *51*, 132-135.

55. Zhang, J.; Tsuji, H.; Noda, I.; Ozaki, Y. Weak Intermolecular Interactions during the Melt Crystallization of Poly(L-Lactide) Investigated by Two-Dimensional Infrared Correlation Spectroscopy. *J. Phys. Chem. B* **2004**, *108*, 11514-11520.

56. Wang, H.; Tashiro, K. Reinvestigation of Crystal Structure and Intermolecular Interactions of Biodegradable Poly(3-hydroxybutyrate) α-Form and the Prediction of Its mechanical Property. *Macromolecules* **2015**, *49*, 581-594.

57. Sato, H.; Ando, Y.; Dybal, J.; Iwata, T.; Noda, I.; Ozaki, Y. Crystal Structures, Thermal Behaviors, and C−H···O=C Hydrogen Bondings of Poly(3-hydroxyvalerate) and Poly(3-hydroxybutyrate) Studied by Infrared Spectroscopy and X-ray Diffraction. *Macromolecules* **2008**, *41*, 4305−4312.

58. Sato, H.; Mori, K.; Murakami, R.; Ando, Y.; Takahashi, I.; Zhang, J.; Terauchi, H.; Hirose, F.; Senda, K.; Tashiro, K.; Noda, I.; Ozaki, Y. Crystal and Lamella Structure and C−H···O=C Hydrogen Bonding of Poly(3-hydroxyalkanoate) Studied by X-ray Diffraction and Infrared Spectroscopy. *Macromolecules* **2006**, *39*, 1525−1531.

59. Sato, H.; Murakami, R.; Padermshoke, A.; Hirose, F.; Senda, K.; Noda, I.; Ozaki, Y. Infrared Spectroscopy Studies of C−H···O Hydrogen Bondings and Thermal Behavior of Biodegradable Poly(hydroxyalkanoate). *Macromolecules* **2004**, *37*, 7203−7213.

60. Francis, S. A.; Ellison, A. H. Infrared Spectra of Monolayers on Metal Mirrors. *J. Opt. Soc. Am.* **1959**, *49*, 131−138.

61. Umemura, J. *In* Handbook of Vibrational Spectroscopy; Chalmers, J. M., Griffiths, P. R., Eds.; Wiley: Chichester, UK, 2002; Vol. 2, pp 982−998.

Table 1. Radius gyration (R_g) of PHB and PLLA

M_w (g mol^{-1})	R_g (nm)	$2R_g$ (nm)
PHB		
650,000	39.04	78.08
PLLAs		
300,000	29.76	59.52
100,000	15.85	31.7
50,000	10.65	21.3
23,000	6.82	13.64
13,100	5.57	11.14
6,900	4.94	9.88
3,600	3.42	6.84
710	2.60	5.2

M_w : molecular weight; R_g: radius of gyration

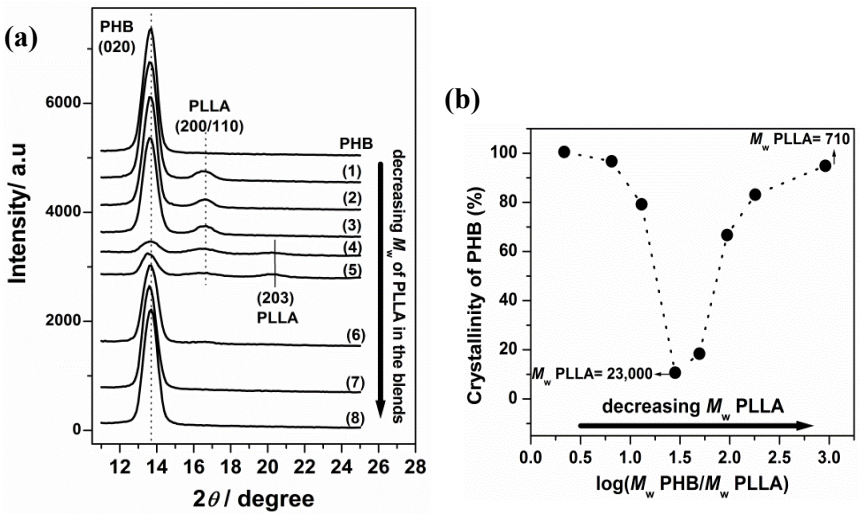

Figure 1. (a) Out-of-plane GIXD profiles of 30-nm-thick films of neat PHB and PHB/PLLAs blends (80/20) with different M_w of PLLA: (1) 300,000; (2) 100,000 (3) 50,000; (4) 23,000; (5) 13,100; (6) 6,900; (7) 3,600; (8) 710 g mol^{-1}. **(b)** Plot of crystallinity of PHB in the blends as a function of log (M_w PHB/M_w PLLA). The arrow

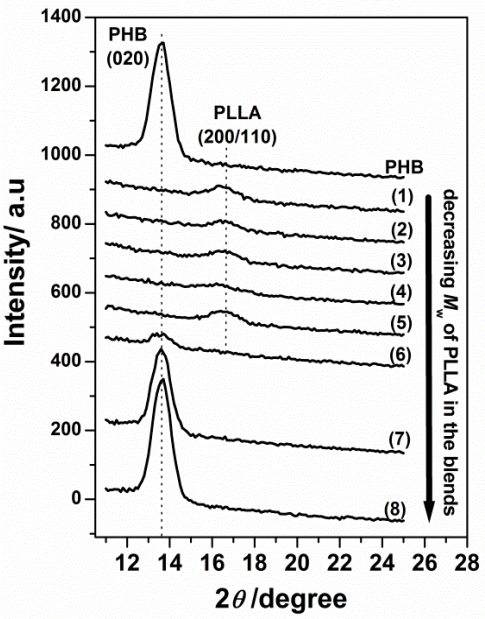

Figure 2. Out-of-plane GIXD profiles of 13-nm-thick films of neat PHB and PHB/PLLAs blends (80/20) with different M_w of PLLA: (1) 300,000; (2) 100,000 (3) 50,000; (4) 23,000; (5) 13,100; (6) 6,900; (7) 3,600; (8) 710 g mol^{-1}. The arrow direction shows the decreasing M_w of PLLA in the blends.

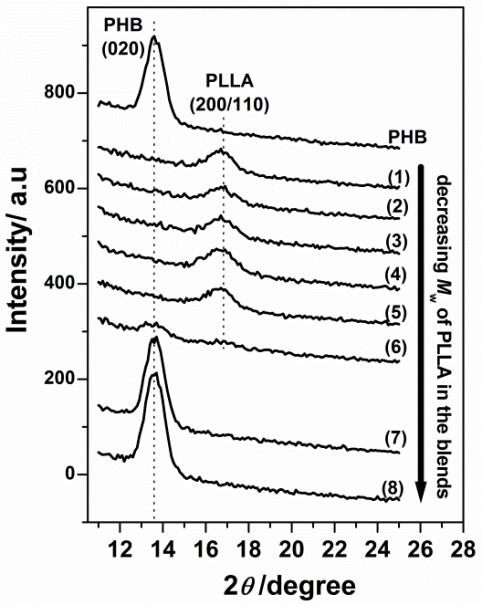

Figure 3. Out-of-plane GIXD profiles of annealed 13-nm-thick films of neat PHB and PHB/PLLA blends (80/20) with different M_w of PLLA: (1) 300,000; (2) 100,000 (3) 50,000; (4) 23,000; (5) 13,100; (6) 6,900; (7) 3,600; (8) 710 g mol^{-1}.

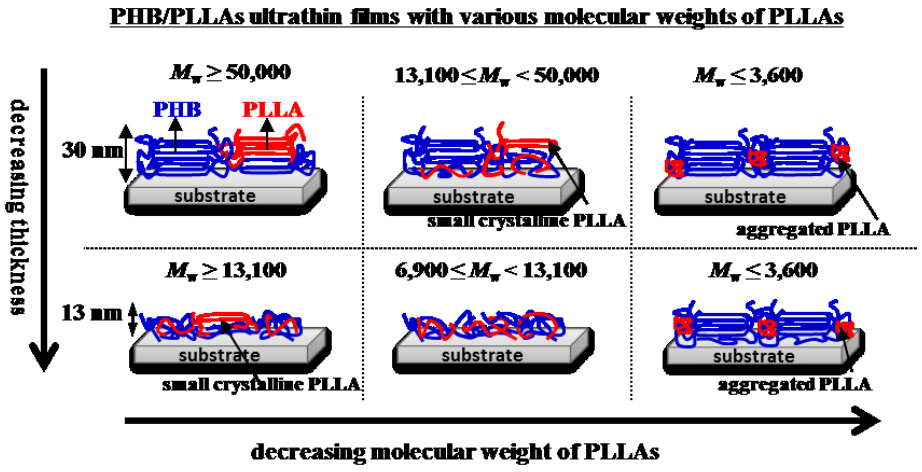

Figure 4. An illustration of the crystallization of PHB in the PHB/PLLA (80/20-w/w) ultrathin films (30 and 13-nm-thick films) with different molecular weights of PLLAs. Blue and red lines represent PHB and PLLA chains, respectively.

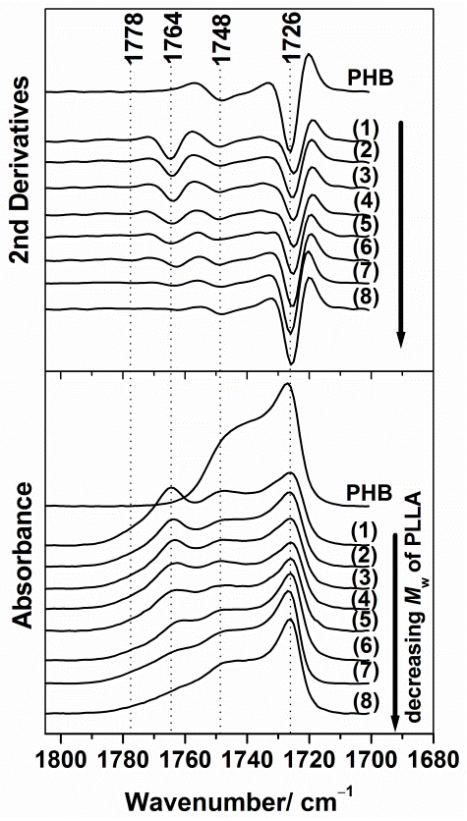

Figure 5. IRRAS spectra (bottom) and their second derivatives (upper) in the C=O stretching region of 30-nm-thick films of PHB and PHB/PLLAs (80/20) blends where M_w of PLLA are: (1) 300,000; (2) 100,000 (3) 50,000; (4) 23,000; (5) 13,100; (6) 6,900; (7) 3,600; (8) 710 g mol^{-1}. The arrow direction indicates the decreasing M_w of PLLA in the blends.

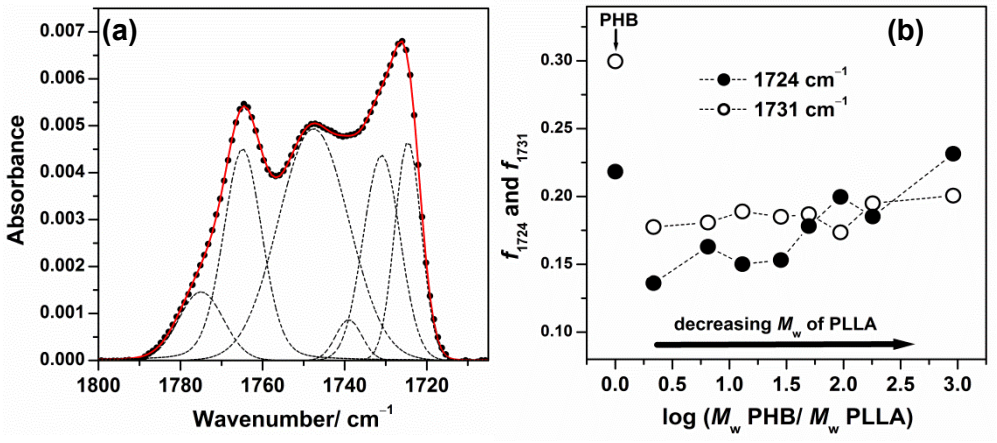

Figure 6 (a) Decomposition of an observed IRRAS spectrum in the C=O stretching region of the 30-nm-thick film shown in Figure 5(1) of PHB/PLLA blends with M_w PLLA = 300,000 g mol^{-1}. (b) Plots of integrated intensity of the 1724 cm^{-1} (highly-ordered) and 1731 cm^{-1} (intermediate) bands normalized by the sum of integrated intensity of all fractions in each blend. The arrow direction shows the decreasing M_w of PLLAs in the blends.

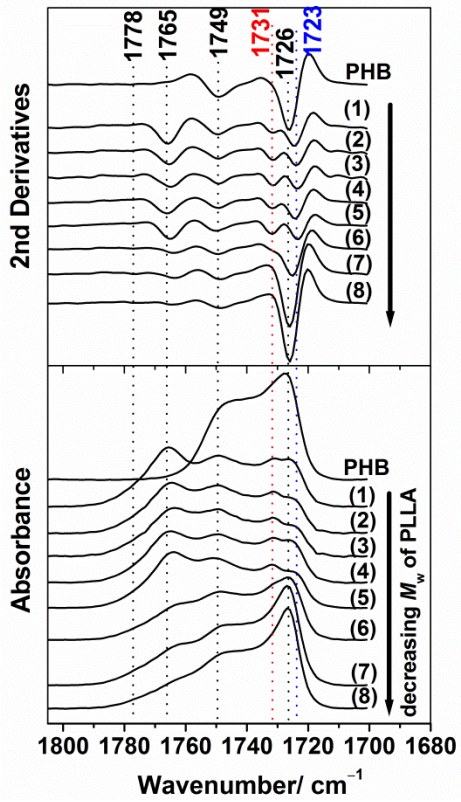

Figure 7. IRRAS spectra (bottom) and their second derivatives (upper) in the C=O stretching region of 13-nm-thick films of PHB and PHB/PLLAs (80/20) blends where M_w PLLA are: (1) 300,000; (2) 100,000 (3) 50,000; (4) 23,000; (5) 13,100; (6) 6,900; (7) 3,600; (8) 710 g mol^{-1}. The arrow direction shows the decreasing M_w of PLLA in the blends.

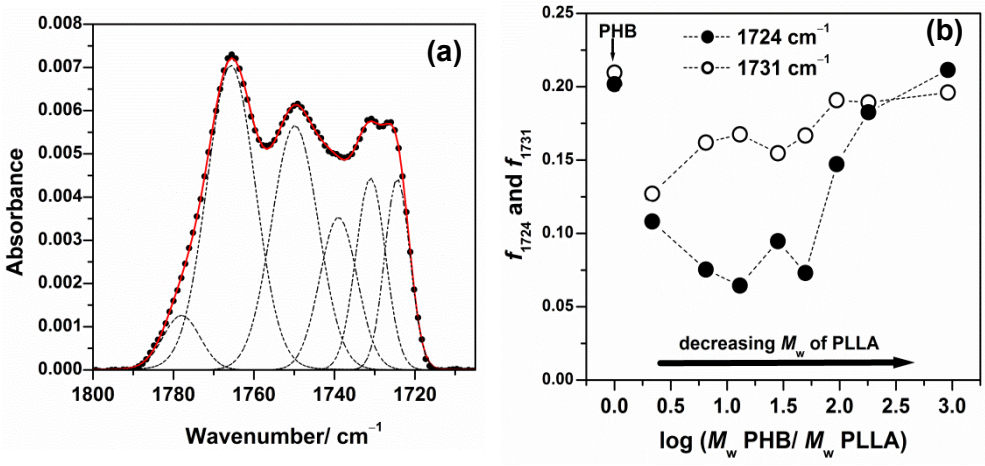

Figure 8. (a) Decomposition of an observed IRRAS spectrum in the C=O stretching region of the 13-nm-thick film shown in Figure 7(1) of PHB/PLLA blends with M_w PLLA = 300,000 g mol^{-1}. (b) Plots of integrated intensity of 1724 cm^{-1} (highly-ordered) and 1731 cm^{-1} (intermediate) bands normalized by the sum of integrated intensity of all fractions in each blend. The arrow direction shows the decreasing M_w of PLLAs in the blends.

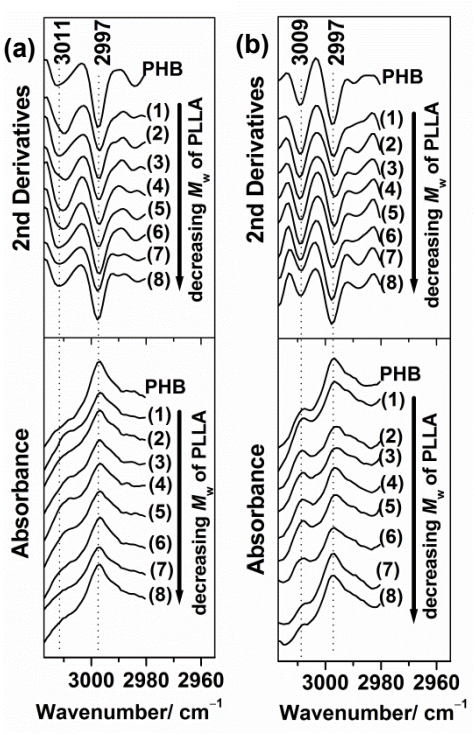

Figure 9. IRRAS spectra (bottom) and their second derivatives (upper) in the 3018-2980 cm^{-1} region of (a) 30-nm and (b)13-nm-thick films of PHB and PHB/PLLAs (80/20) blends where M_w PLLA are: (1) 300,000; (2) 100,000 (3) 50,000; (4) 23,000; (5) 13,100; (6) 6,900; (7) 3,600; (8) 710 g mol^{-1}. The arrow direction shows the decreasing M_w of PLLA in the blends.

Acknowledgments

The study presented in this thesis has been carried out at Graduate School of Science and Technology, Kwansei Gakuin University during April 2014-March 2017. My greatest gratitude and respect go first and foremost to Professor Yukihiro Ozaki, my supervisor, for his constant guidance and encouragement since I started my study in Kwansei Gakuin University five years ago. I have to thanks to Professor Ozaki for introducing me to the vibrational spectroscopy and polymer fields. His enthusiasm, perspective and achievements in scientific field have been enlightening my mind to be also enthusiasm on research life and pursuing my dream. He is one of powerful scientists I have ever known.

I am greatly indebted to Professor Isao Takahashi, for his generous guidance, help and valuable discussion to solve many problems in my research. I must thank Professor Takahashi for the X-ray experimental condition supported by him, especially the precious opportunity of synchrotron GIXD experiments at Spring8. Professor Takahashi also kindly provided all samples that I used in chapter 3. All of the guidance from Professor Takahashi will continuously influence and help me in the future.

I give my gratitude to Professor Harumi Sato (Kobe University, Japan) for her great help and valuable discussion in the analysis of polymers. She is an excellent collaborator and always helps me with her kind heart and nice smile. I also greatly thank to Dr. Kummetha Raghunatha Reddy (former Posdoctoral fellow in Ozaki group) for his

continuous guidance and valuable discussion. He is a kind person and excellent researcher. I owe him for teaching me the useful experimental techniques and analysis data that will continuously help me in the future.

I greatly thanks Japanese Government (Monbukagakusho) for the financial support of my doctoral course. Finally, I would like to thank to all past and current members of Ozaki Group, Department of Chemistry for their help, friendship and cooperation during my study in Japan.

This thesis is totally dedicated to my beloved parents and husband.

Khasanah
Graduate School of Science and Technology
Kwansei Gakuin University
March, 2017

List of Publication

Original Papers:

1. **Khasanah**, Kummetha Raghunatha Reddy, Harumi Sato, Isao Takahashi, Yukihiro Ozaki: Intermolecular Hydrogen Bondings in the Poly(3-hydroxybutyrate) and Chitin Blends: Their Effects on the Crystallization Behavior and Crystal Structure of Poly(3-hydroxybutyrate). ***Polymer*** 2015, *75*, 114-150.
2. **Khasanah**, Kummetha Raghunatha Reddy, Shigesaburo Ogawa, Harumi Sato, Isao Takahashi, Yukihiro Ozaki: Evolution of Intermediate and Highly Ordered Crystalline States under Spatial Confinement in Poly(3-hydroxybutyrate) Ultrathin Films. ***Macromolecules*** 2016, *49*, 4202-4210.
3. Mengfan Wang, **Khasanah**, Harumi Sato, Isao Takahashi, Jianming Zhang, Yukihiro Ozaki: Higher-order Structure Formation of a Poly(3-hydroxybutyrate) Film During Solvent Evaporation. ***RSC Advances*** 2016, *6*, 95021-95031.
4. **Khasanah**, Kummetha Raghunatha Reddy, Isao Takahashi, Yukihiro Ozaki: Crystallization Behavior of Ultrathin Poly(3-hydroxybutyrate) Films in Blends with a Small Amount of Poly(L-lactic Acid): Correlation between Molecular Weight of Poly(L-lactic Acid) and Film Thickness (*submitted*).
5. Morihisa Terasaki, **Khasanah**, Yukihiro Ozaki, Isao Takahashi, Harumi Sato: A Study

on Phase Separation in A Ultra-thin Film of Poly(methyl methacrylate)/Poly(4-vinyl phenol) by Infrared Reflection Adsorption Spectroscopy (*submitted*).

Oral Presentations:

1. **Khasanah**, Isao Takahashi, Kummetha Raghunatha Reddy, Shigesaburo Ogawa, Harumi Sato, Yukihiro Ozaki: The Evolution of Intermediate and Highly-ordered Crystalline States Under Spatial Confinement in Poly(3-hydroxybutyrate) Ultrathin Films. ***The 65th Society of Polymer Science Japan Annual Meeting***, May 25-27th 2016. Kobe, Japan.
2. **Khasanah**, Kummetha Raghunatha Reddy, Harumi Sato, Isao Takahashi, Yukihiro Ozaki: Study on the Crystallization Behavior, Intermediate State and Conformation Rearrangement of Poly(3-hydroxybutyrate) Ultrathin Film by Using IR-RAS and GIXD. ***The 64th Society of Polymer Science Japan Symposium on Macromolecules***, Sept. 15-17th, 2015. Sendai, Japan.
3. **Khasanah**, Raghunatha Reddy Kummetha, Isao Takahashi, Harumi Sato, Yukihiro Ozaki: Crystallization Behavior and Conformation Rearrangement of Poly(3-hydroxybutyrate) Ultrathin Film Investigated by Infrared Reflection Absorption Spectroscopy. ***The 61st Society of Polymer Science Japan Kansai Branch Meeting***, July 17th, 2015, Kobe, Japan.

4. **Khasanah**, Isao Takahashi, Kummetha Raghunatha Reddy, Harumi Sato, Yukihiro Ozaki: Confinement Effect of Chitin on the Crystallization Behavior of Poly(3-hydroxybutyrate) Thin Film Studied by Infrared-Reflection Absorption Spectroscopy and Grazing Incidence X-Ray Diffraction. ***The 64th Society of Polymer Science Japan Annual Meeting,*** May 27-29th **2015.** Sapporo, Japan.

Poster Presentations:

1. **Khasanah**, Isao Takahashi, Yukihiro Ozaki: Effect of a Small Amount of various Molar Mass Poly(L-lactide acid) on the Crystallization of Poly(3-hydroxybutyrate) Ultrathin Blend Films. ***Japan-Taiwan Medical Spectroscopy International Symposium (JTMSIS)/ 14th annual meeting of the Japan Association of Medical Spectroscop***y, Dec 4-7th 2016. Awaji Island, Japan.
2. **Khasanah**, Isao Takahashi, Yukihiro Ozaki: Effect of a Small Amount of Poly(L-Lactic acid) with Different Molecular Weight on the Crystallization Behavior of Poly(3-hydroxybutyrate) Ultrathin films in their Blends. ***The 65th Society of Polymer Science Japan Symposium on Macromolecules***, September 14-16th, 2016. Kanagawa, Japan.
3. **Khasanah**, Kummetha Raghunatha Reddy, Harumi Sato, Isao Takahashi, Yukihiro Ozaki: Crystallization and Chain Orientation in the Ultrathin Films of

Poly(3-hydroxybutyrate) Studied by IR-RAS and GIXD. ***The International Chemical Congress of Pacific Basin Societies 2015 (PACIFICHEM),*** Dec. 15-20th, 2015**.** Honolulu, Hawaii, USA.

4. **Khasanah**, Raghunatha Reddy Kummetha, Isao Takahashi, Harumi Sato, Yukihiro Ozaki: Structure and Crystallization Behavior of Poly(3-hydroxybutyrate) and Chitin Blends as Thin Films Studied by Reflection-Absorption Infrared Spectroscopy and Grazing Incidence X-ray Diffraction. ***The 63rd Society of Polymer Science Japan Symposium on Macromolecules,*** Sept. 24-26th, 2014**.** Nagasaki, Japan.
5. **Khasanah**, Raghunatha Reddy Kummetha, Nicolas Spegazzini, Harumi Sato, Yukihiro Ozaki: Structural Changes, Crystallization Behaviors and Intermolecular Interaction Between Poly(3-hydroxybutyrate) and Chitin Blends as Studied by Vibrational Spectroscopy and X-ray Diffraction Measurements. ***The 62nd Society of Polymer Science Japan Symposium on Macromolecules,*** Sept. 11-13th, 2013. Kanazawa, Japan.
6. **Khasanah**, Raghunatha Reddy Kummetha, Nicolas Spegazzini, Harumi Sato, Yukihiro Ozaki. Study on Crystallization Behavior and Intermolecular Interactions in Biodegradable Blend Between Poly(3-hydroxybutyrate) and Chitin. ***The 7th International Conference on Advanced Vibrational Spectroscopy (ICAVS 7),*** August 25-30th **2013.** Kobe, Japan.

7. **Khasanah**, Raghunatha Reddy Kummetha, Nicolas Spegazzini, Harumi Sato, Yukihiro Ozaki: Investigation of Intermolecular Interaction and Crystallization Behavior of poly(3-hydroxybutyrate) and Chitin Blends by Vibrational Spectroscopy and Wide-Angle X-ray diffraction. ***The 62nd Society of Polymer Science Japan Annual Meeting,*** May 29-31st, 2013. Kyoto, Japan.
8. **Khasanah**, Harumi Sato, Nicolas Spegazzini, Yukihiro Ozaki: Crystal Structure and Thermal Behavior of Biodegradable Polymer Blends of poly(3-hydroxybutyrate) and Chitin Studied by Infrared Spectroscopy and Wide Angle X-ray Diffraction. ***The 9th Society of Polymer Science Japan International Polymer Conference (IPC)***. Dec. 11-14th, 2012. Kobe, Japan.

Awards:

1. **Best Poster Award** in Japan-Taiwan Medical Spectroscopy International Symposium/14th Annual Meeting of Medical Spectroscopy, December 7th, 2016.
2. **Haruka Yamada Award** from Kwansei Gakuin University, December 21st, 2016.
3. **Nitta Memorial Award** from Kwansei Gakuin University, January 18th, 2017.